Report of Investigation 2022-1

PRELIMINARY LANDSLIDE INVENTORY OF PARTS OF THE FAIRBANKS NORTH STAR BOROUGH, ALASKA

Jaimy A. Schwarber, Margaret M. Darrow, Ronald P. Daanen, De Anne S.P. Stevens, and Peyton J. Presler

Photograph of the small head scarp of a landslide in colluvium adjacent to the Tanana River.

Published by
STATE OF ALASKA
DEPARTMENT OF NATURAL RESOURCES
DIVISION OF GEOLOGICAL & GEOPHYSICAL SURVEYS
2022

PRELIMINARY LANDSLIDE INVENTORY OF PARTS OF THE FAIRBANKS NORTH STAR BOROUGH, ALASKA

Jaimy A. Schwarber, Margaret M. Darrow, Ronald P. Daanen, De Anne S.P. Stevens, and Peyton J. Presler

Report of Investigation 2022-1

State of Alaska
Department of Natural Resources
Division of Geological & Geophysical Surveys

STATE OF ALASKA
Mike Dunleavy, Governor

DEPARTMENT OF NATURAL RESOURCES
Corri A. Feige, Commissioner

DIVISION OF GEOLOGICAL & GEOPHYSICAL SURVEYS
Steve Masterman, State Geologist and Director

Publications produced by the Division of Geological & Geophysical Surveys (DGGS) are available for free download from the DGGS website (dggs.alaska.gov). Publications on hard-copy or digital media can be examined or purchased in the Fairbanks office:

Alaska Division of Geological & Geophysical Surveys
3354 College Rd., Fairbanks, Alaska 99709-3707
Phone: (907) 451-5010 Fax (907) 451-5050
dggspubs@alaska.gov | dggs.alaska.gov

DGGS publications are also available at:
Alaska State Library,
Historical Collections & Talking Book Center
395 Whittier Street
Juneau, Alaska 99811

Alaska Resource Library and Information Services (ARLIS)
3150 C Street, Suite 100
Anchorage, Alaska 99503

Suggested citation:
Schwarber, J.A., Darrow, M.M., Daanen, R.P., Stevens, D.S.P., and Presler, P.J., 2022, Preliminary landslide inventory of parts of the Fairbanks North Star Borough, Alaska : Alaska Division of Geological & Geophysical Surveys Report of Investigation 2022-1, 80 p. https://doi.org/10.14509/30841

Contents

Figures

Tables

Appendices

Map Sheets

PRELIMINARY LANDSLIDE INVENTORY OF PARTS OF THE FAIRBANKS NORTH STAR BOROUGH, ALASKA

Jaimy A. Schwarber[1], Margaret M. Darrow[1], Ronald P. Daanen[2], De Anne S.P. Stevens[2], and Peyton J. Presler[1]

ABSTRACT

Landslides are geologic hazards that threaten human lives, property, and infrastructure. Effective landslide threat mitigation requires identifying, inventorying, and studying landslides; developing a detailed landslide inventory map is the beginning of this process. Here we present the first landslide inventory map of parts of the Fairbanks North Star Borough (FNSB), Alaska, along with supporting data and a qualitative analysis of the results. This research was funded by the U.S. Geological Survey (USGS) EDMAP program, which funds universities to train the next generation of geologic mappers. The map and geodatabase were developed using lidar-derived elevation data and satellite imagery, and supplemented with data from targeted fieldwork, which included field verification of landslides and a detailed field survey and series of laboratory soil tests on the large, informally named Tanana 440 landslide. We identified 1,679 landslides within the FNSB region, with 681 mapped within the focused EDMAP study area. These landslides occurred in bedrock and surficial loess deposits and vary widely in age, morphology, and material type. Most are prehistoric, but we did observe some historic and active landslides. Potential landslide triggers may include thawing permafrost, rain events, seismic events, and river erosion. Our goals with this work are to increase awareness of landslides as a potential geohazard and to aid state and local agencies and the general public in making informed land management decisions.

INTRODUCTION

Landslides pose serious geologic threats to human lives, private and public property, and infrastructure. Because slopes where landslides have occurred in the past may have higher risk of future landslides (Burns, 2007) inventory and evaluation of past events is critical to addressing these threats. Mitigation first requires a detailed landslide inventory map; but until this study there have been no published landslide inventory maps for any region within Alaska. The map accompanying this report represents the first systematic landslide inventory for the portion of the Fairbanks North Star Borough (FNSB; figs. 1, 2) that has lidar coverage—an area within Interior Alaska that includes the communities of Fairbanks, North Pole, Ester, and Fox.

This research was made possible with funding from the EDMAP program awarded by the USGS National Cooperative Geological Mapping Program (NCGMP). EDMAP partners a state geological survey with university geology professors to support undergraduate and graduate students at their college or university in a one-year mentored geologic mapping project.

REGIONAL SETTING

The FNSB, located in Interior Alaska, has a continental sub-Arctic climate (Wendler and Shulski, 2009). Continental climates are characterized by large temperature fluctuations, which in Interior Alaska are reflected by the record high (35.6˚C [96˚F] in June 1969) and low (-54.4˚C [-66˚F] in January 1934) temperatures recorded in Fairbanks (Alaska Climate Research Center, n.d.[b]). The mean annual snowfall and precipitation calculated for Fairbanks in a 30-year period (1981–2010) were 165 cm (65 in) and 27.5 cm (11 in), respectively (Alaska Climate Research Center, n.d.[b]). For the same 30-year period, the mean

[1]Alaska Division of Geological & Geophysical Surveys, 3354 College Rd., Fairbanks, Alaska 99709-3707.
[2] University of Alaska Fairbanks Arctic Coastal Geoscience Lab, P.O. Box 755780, Fairbanks, AK 99775

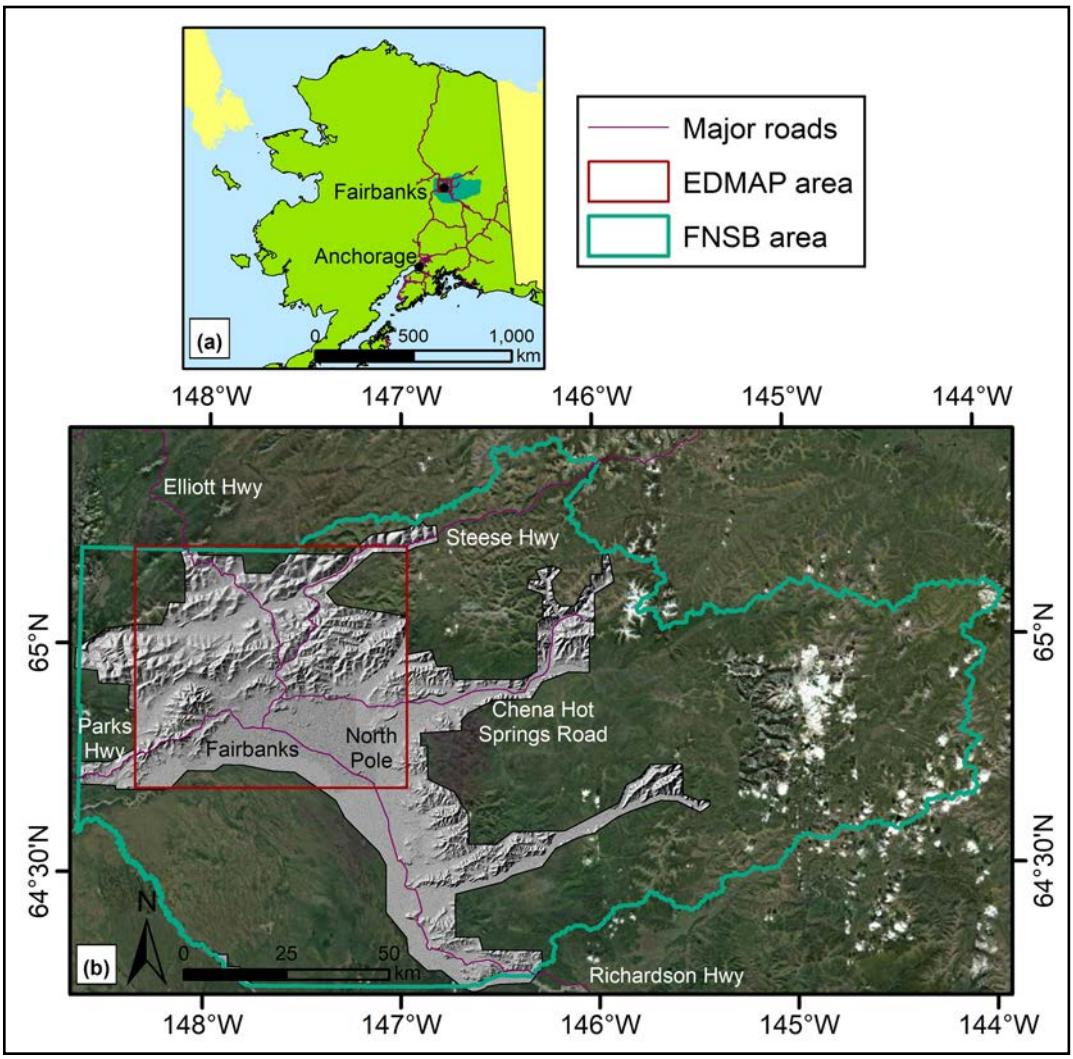

Figure 1. Location of EDMAP study area (inset map a) in relation to major Alaska roads and population centers, and (map b) with respect to the extent of the FNSB (outlined in green). The hillshade polygon in (shown in gray) is the area where QL1 and QL2 lidar data are available within FNSB (FNSB, 2020) and the background is high-resolution imagery (GeoNorth, 2021). The road data are from Alaska Department of Transportation and Public Facilities (AKDOT&PF; 2018). Landslides were mapped only for the area where lidar data were available.

annual air temperature (MAAT) in Fairbanks was -2.4°C (27°F; Alaska Climate Research Center, n.d. [a]), which supports a periglacial environment with permafrost (French, 2007). The borough is within the zone of discontinuous permafrost where 50–90 percent of the ground is underlain by permafrost (Jorgenson and others, 2008).

Fairbanks sits at the southern edge of the Yukon-Tanana Upland, which is characterized by rounded, even-topped ridges and gentle side slopes (Wahrhaftig, 1965). Ridges rise 152–914 m (500–3,000 ft) above adjacent valleys (Wahrhaftig, 1965). The bedrock of these uplands that surround Fairbanks to the north, east, and west is part of the Yukon-Tanana Terrane unit of Upper Paleozoic age and older metamorphic rocks that formed during regional metamorphism (Newberry and others, 1996). The EDMAP study area is almost entirely within the Newberry and others (1996) geologic map. Nearly 75 percent of the geologic map is underlain by the heterogeneous Fairbanks Schist (Newberry and others, 1996). This unit is nearly 90 percent quartzite and quartz muscovite schist but includes metamorphic rocks such as schist,

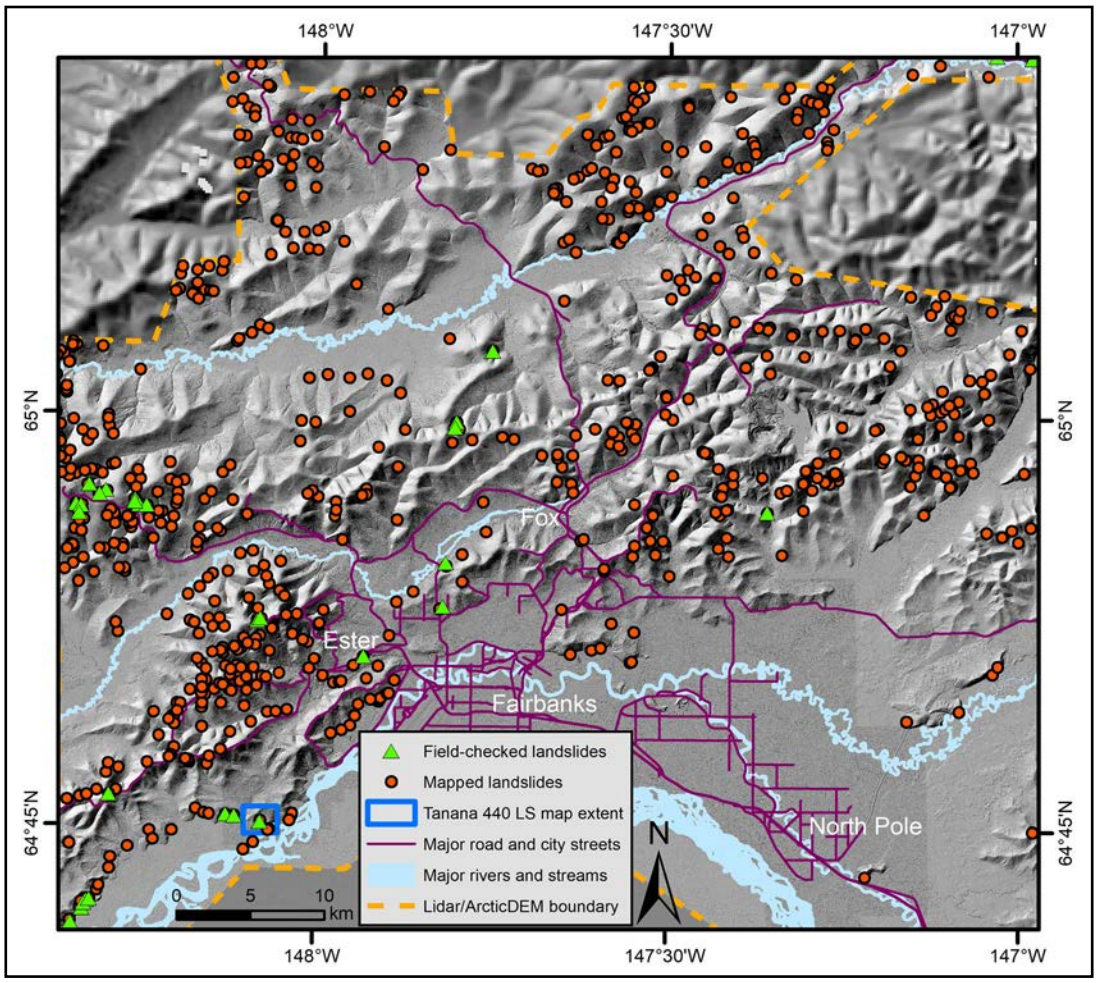

Figure 2 . EDMAP study area with locations of mapped and field-checked landslides , with lidar hillshade area outlined in dashed orange (FNSB, 2020) and ArcticDEM hillshade (Porter and others, 2018) as base layers. The road data are from AKDOT&PF (2018) and the hydrology data are from the Alaska Geospacial Council (AGC; 2020).

marble, quartzite, and amphibolite (Newberry and others, 1996).

Interior Alaska has not experienced glaciation during the Quaternary period, except for small cirque glaciers in localized mountainous areas (Briner and others, 2017; Péwé, 1975). Instead, much of Interior Alaska is blanketed by Quaternary loess—wind-blown silt transported from the outwash plains of the Tanana River by katabatic winds from the south and deposited during glacial cycles (Péwé, 1955; 1975). Other loess sources include fluvial deposits from the Yukon and Nenana Rivers and a minor contribution from the local schist bedrock (Muhs and Budahn, 2006). The history of loess deposition in Alaska extends from as long as 3 million years ago (Westgate and others, 1990). Péwé (1975) initially estimated that the loess surrounding Fairbanks was mainly deposited during the Illinoian and Wisconsinan glaciations, but newer data suggest that loess deposition may have begun 2 million years ago (Begét and others, 2008). The loess around Fairbanks ranges from 0.3–24.4 m (1–80 ft) thick on hilltops to 3–30.5 m (10–100 ft) thick on middle slopes, and retransported silt in the valley bottoms ranges from 30.5 to 91.5 m (10 to 300 ft) thick (Péwé, 1955). Loess deposits can offer insight into paleoclimates if they contain tephra layers or thermokarst features (Begét and others, 2008), unconformities (Westgate and others, 1990), or paleosol layers (Josephs, 2010). The presence of paleosols may indicate periods of decreased loess deposition rates due to

relative landscape stability (Josephs, 2010). It may be possible to determine absolute or relative ages of landslides if paleosols or tephra layers are 1) present and 2) able to be positively identified.

Interior Alaska is a seismically active region influenced by three main tectonic structural drivers: dextral strike-slip faults, seismic zones, and thrust faults in the Alaska Range foothills (Koehler and others, 2018). These structures range from the well-known Denali Fault—a large-scale dextral fault to the south of Fairbanks—to the Minto Flats fault zone, which is a small-scale set of north-northeast-trending sinistral faults (Koehler and others, 2018; Tape and others, 2015). Earthquake epicenters for the Denali Fault and Minto Flats fault zones are rarely deeper than 20 km or 40 km, respectively (Tape and others, 2015). The FNSB has a history of moderate- to large-magnitude earthquakes; for example, a 7.4M event in 1912, 6.3M and 6.5M events in 1929, and 7.3M events in 1937and 1947 (Péwé, 1982; St. Amand, 1948). The largest historic seismic event felt in Interior Alaska was the 7.9M Denali Fault earthquake in 2002 that triggered thousands of landslides along the rupture (Fuis and others, 2003). Although this event and associated landslides occurred south of our study area, it provides an example of seismically induced landslides. As another example, multiple rockslides along the Tanana River were reported after the 1947 earthquake, which had an epicenter near the intersection of the Nenana and Tanana river valleys (St. Amand, 1948).

METHODOLOGY

The EDMAP study area was chosen in coordination with the FNSB Emergency Manager to include the Borough's most populated areas (fig. 2). Jaimy Schwarber, University of Alaska Fairbanks (UAF) MS student, was the primary mapper for the smaller EDMAP study area and UAF researcher Dr. Margaret Darrow mapped the rest of the lidar area within the FNSB. Peyton Presler, an undergraduate student at UAF, assisted with the mapping by refining the landslide polygons within the EDMAP study area.

We followed the landslide mapping protocol that Slaughter and others (2017) developed for Washington State to create landslide deposit, scarp and flank, and scarp shapefiles. The protocol requires lidar data and its derivatives—digital terrain models (DTMs), hillshades, slope maps, and contour maps—for GIS-based mapping. In 2017, the FNSB released high-quality lidar data sets with two different resolutions and areal extents (table 1). The EDMAP study area encompassed all of the higher resolution USGS Quality Level 1 (QL1) lidar data and some of the lower resolution QL2 data (Heidemann, 2014). We made minor adjustments to the mapping protocol to accommodate arctic and periglacial conditions; for example, we changed the "historic" designation from 150 years to 100 years to more accurately reflect the time since the community of Fairbanks was first established. We relied heavily on the appended Streamlined Landslide Inventory Protocol (SLIP) to identify landslide extents because some landslides had well-defined deposits but unidentifiable head scarps due to age and material type. Using the SLIP method allowed us to map uncertain geomorphological features that would have been ignored using the standard protocol. We modified the SLIP to encompass all features of a landslide from the head scarp region to the toe deposits: landslide deposit polygons include displaced material, landslide scarp and flank polygons include the areal extent of the steep areas upslope of displaced ground along the perimeter of landslide deposits and the head scarp region, and landslide scarp lines include head scarps and internal scarps on the landslide body.

We developed a landslide naming convention that uses 15-minute quadrangles and the Public

Table 1. Resolution and area of lidar datasets (OCM Partners, 2020).

Lidar quality	Resolution m (ft)	Area km^2 (acres)
Quality Level 1 (QL1)	0.46 (1.5)	1,006 (248,555)
Quality Level 2 (QL2)	0.91 (3)	4,803 (1,186,822)

Land Survey System (PLSS). For example, a landslide located in the Fairbanks D-3 Quadrangle, township 2 south, range 3 west, section 10, northeast quarter is named FaiD3_T2S_R3W_10_NE1. Multiple landslides within the same quarter-section are designated NE1, NE2, etc., in the order mapped. If a landslide is within multiple quarter-sections in the same cardinal direction (e.g., north), the name would be formatted as FaiD3_T2S_R3W_10_N1. These names thus are unique and reflect the precise geographical location of each landslide.

During the summer of 2020 we field verified the existence and mapping of 51 landslides and landslide complexes. Most field-checked landslides were within the EDMAP study area (30 total), and those outside the area were along the Richardson Highway (21 total). All landslides selected for field verification are accessible from the road system and are on public land. Summaries were compiled for all field-checked landslides (app. A). We recorded field stations on handheld global positioning system (GPS) units. Our field work focused on characterizing four major feature categories: head scarp, flanks, toe/deposit, and morphology. For each landslide we rated each feature category with a confidence level from 0 to 10 (low to high) and these were summed resulting in a 40-point system for overall confidence. We also recorded any indicators of vegetation movement such as leaning or pistol butt trees, and we dug test pits with a shovel on every landslide to identify the near-surface soils. Appendix B includes locations of field stations plotted on the mapped landslides.

We spent four days conducting a detailed field survey of the Tanana 440 (T440) landslide. We cleaned the surfaces of four silt exposures in road cuts, documented the stratigraphy of the exposures, and drilled eight vertical test holes using a powerhead and a Snow, Ice, and Permafrost Research Establishment (SIPRE) coring tool. We collected 72 soil samples for a suite of soil tests (app. C) including particle-size analysis (dry sieving and hydrometer analysis), Atterberg limits, specific gravity, natural moisture content, unit weight, and direct shear. Testing followed American Society for Testing Materials (ASTM) standards (table 2). We also sent five organic samples to Beta Analytic, Inc. for radiocarbon dating.

RESULTS

Using the lidar data available within the FNSB region, we mapped 1,679 landslides; 681 of which were within the EDMAP area (fig. 2). We verified 51 landslides in the field. Figure 3 is a map detailing the T440 landslide and showing field station locations. In addition to the figures included in this report, we produced a landslide inventory map of the EDMAP region at 1:50,000 scale (mapsheets 1 and 2) and an inset Tanana 440 landslide map at 1:6,000 scale (see mapsheet 1). The landslide inventory map displays the shapefiles for the landslide deposits, scarps and flanks, scarps, and SLIP extents. It also indicates locations of the field-verified landslides and associated field stations.

Tanana 440 landslide

We are the first to document the extent and details of the Tanana 440 landslide (fig. 3), a large paleoslide in loess on a wooded south-facing slope adjacent to the Tanana River. The landslide is approximately 2 km (1.2 miles) by 1 km (0.6 miles) with a total areal extent of 1.9 km^2 (470 acres). The

Table 2. American Society for Testing Materials (ASTM) test types used in this study.

Test Name	Designation	Reference
Dry Sieve Analysis (Gradation)	D6913	ASTM (2017d)
Sedimentation Analysis (Hydrometer)	D7928	ASTM (2021b)
Water Content	D2216	ASTM (2019)
Specific Gravity	D854	ASTM (2014)
Unit Weight of Soil	D7263	ASTM (2021a)
Soil Classification	D2487	ASTM (2017a)
Atterberg Limits	D4318	ASTM (2017b)
Direct Shear	D6528	ASTM (2017c)

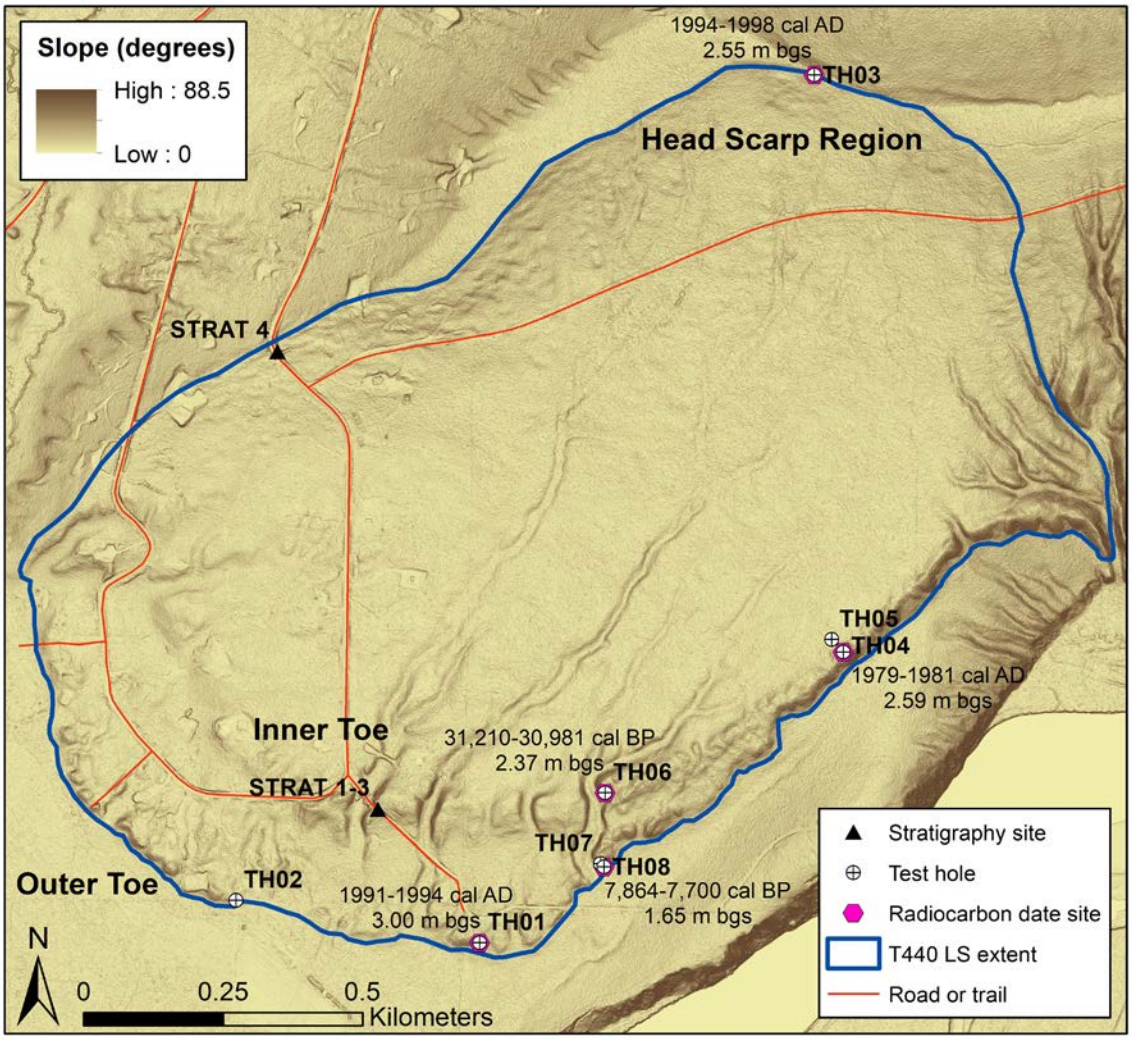

Figure 3. Tanana 440 landslide showing major landslide features and test hole and stratigraphy locations. Lidar-derived slope map background (FNSB, 2020). Radiocarbon dates and depths are shown next to the corresponding test holes.

head scarp region and right flank are along the local ridgeline and there are two distinct toe deposits; referred to here as the inner and outer toe deposits. The extent of the upper left flank is unclear as the landslide flows into the adjacent valley, but the lower left flank section is a well-defined ridge of silt. Steep-walled dry gullies incise the toe deposits in several places.

Measured stratigraphic columns and borehole logs with vane shear test results are shown in figures 4 and 5, respectively. All samples were classified using the Unified Soil Classification System (ASTM, 2017a). The particle-size analyses confirmed that soil was typically uniform silt (ML; 16 samples), with two samples consisting of sandy silt (ML) and one sample of silty sand (SM). The average specific gravity of the soils was 2.73, which is typical of a micaceous soil and similar to the published values of 2.70 for Fairbanks silt (Haynes and others, 1980; Farouki, 1981). The tested silty soil had no plastic limit but an average liquid limit of 25. Natural moisture content of the soil varied by location and depth, ranging from 4.6 to 25.8 percent. We performed direct shear tests on remolded and intact silt samples from the field, resulting in friction angles averaging 25 degrees. Schwarber and others (in review) provide a summary and in-depth discussion of these results as well as slope stability modeling.

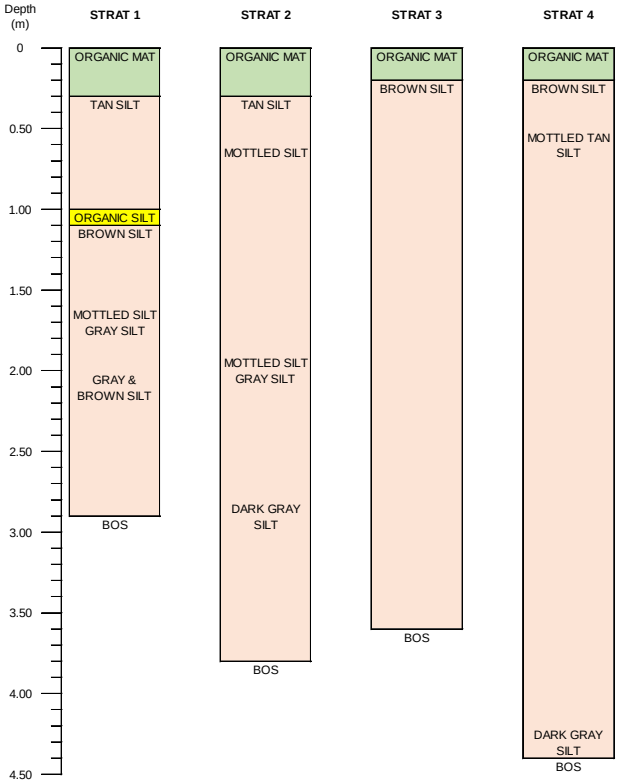

Figure 4. Stratigraphic columns from the T440 landslide; BOS = bottom of section.

DISCUSSION

Our interpretations of the landslides in this report are qualitative rather than quantitative. Quantitative spatial analyses (e.g., correlations of slope angle, slope aspect, surface roughness, material type, etc.) would be the next step. This qualitative assessment, however, meets the primary goal of this project—to document these landslide features for the first time and produce an inventory map.

We initially hypothesized that the landslides within FNSB occurred primarily in the surficial loess; however, the evidence collected during our field reconnaissance does not fully support that hypothesis. Our field assessments indicate that 30 out of the 51 field-verified landslides within the greater FNSB were within bedrock: 16 of the 30 landslides within the EDMAP region and 14 of the 20 landslides located outside of the EDMAP area. On these landslides, we observed bedrock exposures in head scarps and flanks, and features characteristic of rotational or translational movement asso-

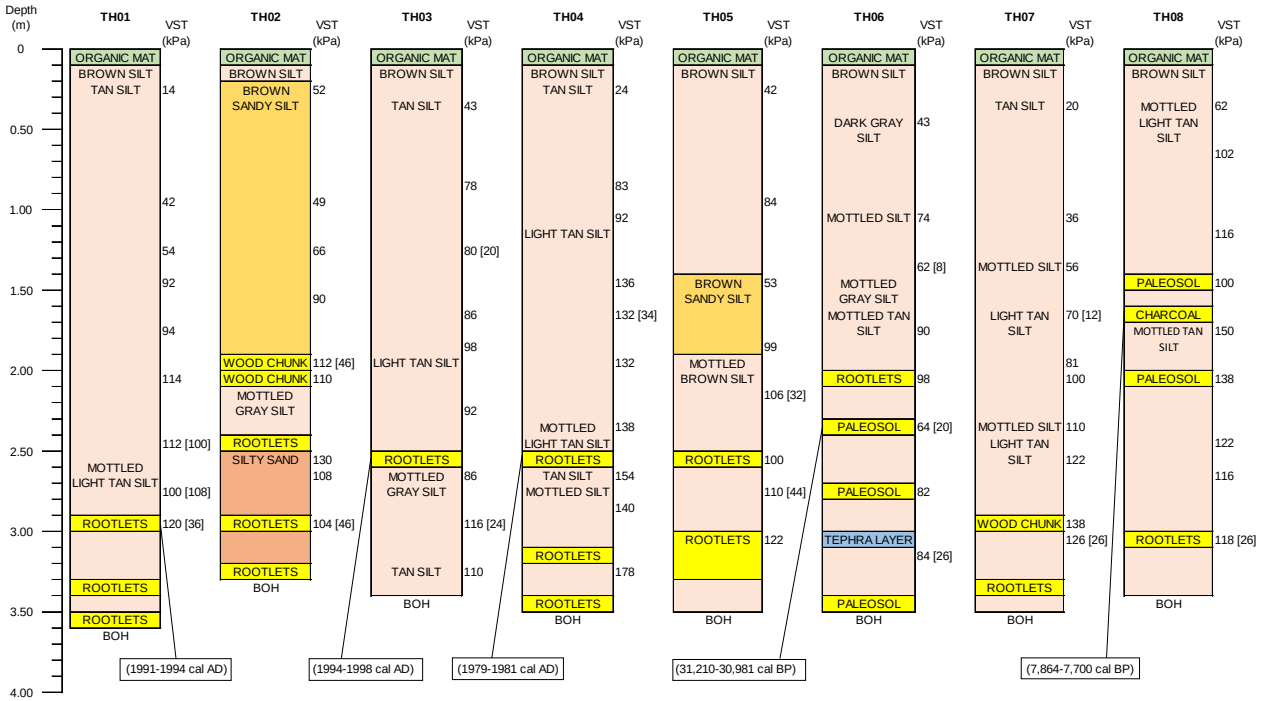

Figure 5. Simplified stratigraphic columns for test holes drilled on the T440 landslide. Vane shear test (VST) results are adjacent to the tested depth, with residual shear values in brackets. Dates in boxes are radiometric dating results for the corresponding organic layer; BOH = bottom of hole.

ciated with bedrock. These features may include cracks at the crown, a steep and bare head scarp, flanks that shift from vertical to horizontal from the head toward the foot, and a toe with a steep front that overrides the ground surface (Varnes, 1984). It was not always possible to distinguish between rotational and translational slides due to lack of geomorphological expression. In contrast to the landslides that occurred in bedrock, features of landslides that occurred in loess demonstrate flow characteristics. These may include features such as a typically concave head scarp, curved flanks, no foot, and a toe that is spreading and lobate (Varnes, 1984). We observed several complex features that combined several types of movement (e.g., flow and rotational; figs. A10, A34, A35). These features may be due to a combination of material type, or had movement of different ages or on different sections of the landslide.

In addition, the type of material in which the landslide occurs influences the geomorphic expression. For example, the toes and scarps of landslides in bedrock are generally better defined in lidar images than those that occur in surficial soils. Landslide source areas in loess are also characterized by severe gullying that further obscure potential landslide features such as scarps, grabens, and cracks. Generally, historic flows are smaller features (e.g., 0.003 km^2 [0.74 acres]) than some of the large prehistoric flow landslides (e.g., 0.56 km^2 [138 acres]). The materials in the landslide affect the rate and style of erosion, making a qualitative comparison of landslide age between those in loess and those in bedrock problematic. Figure 6 is a visual comparison of field-verified landslides by both composition and age. It is difficult to gauge the relative age of the prehistoric landslides in loess, as typically only the arcuate toe deposits remain with no clear identifiable head scarps or flanks. Based on the work by McCalpin (1984) and Keaton and DeGraff (1996), we postulate that, in general, landslides in the FNSB with rougher surface expressions are younger than those with smoother surfaces, especially those in bedrock. Most of the mapped landslides are prehistoric based on their relatively smooth geomorphic expressions.

Potential landslide triggers within the FNSB may include thawing permafrost, heavy rain events, seismic activity, and river erosion. Each of these is discussed below.

Thawing permafrost—The climate in central Alaska was cold and dry during the Last Glacial Maximum (LGM; Finkenbinder and others, 2014) and supported the formation of permafrost. The Holocene Thermal Maximum (HTM), a period of temperatures higher than in the present, occurred 9–11 kya (thousands of years ago) in Alaska (Kaufman and others, 2004), and may have resulted in favorable conditions for permafrost thaw and slope instability. Today, FNSB is within the discontinuous permafrost zone, and rising temperatures may result in additional instability of permafrost-affected slopes. Ice-rich thawing permafrost contributes water to the soil, which reduces the effective stress and may result in landslides (McRoberts and Morgenstern, 1974). Permafrost throughout Interior Alaska is warming (Osterkamp, 2005) and we observed evidence of mass movement within the EDMAP region related to currently thawing permafrost, such as retrogressive thaw slumps.

Heavy rain events—We saw some evidence of recent landslide movement during our summer 2020 fieldwork likely caused by high precipitation causing high pore water pressure (fig. A49).

Seismic activity—Earthquakes are common in Interior Alaska and may trigger landslides. Flow slides in silt may be triggered by seismic events due to silt's high liquefaction potential (Hungr and others, 2001). Rockslides were reported after the M7.3 1947 earthquake in the Interior (St. Amand, 1948). It is likely that additional landslides may be triggered within the FNSB by future earthquake events of similar magnitude.

River erosion—Along the Richardson Highway, several historic and active bedrock landslides were caused by the Tanana River eroding toe deposits of paleoslides at the slope base (figs. A34, A36,

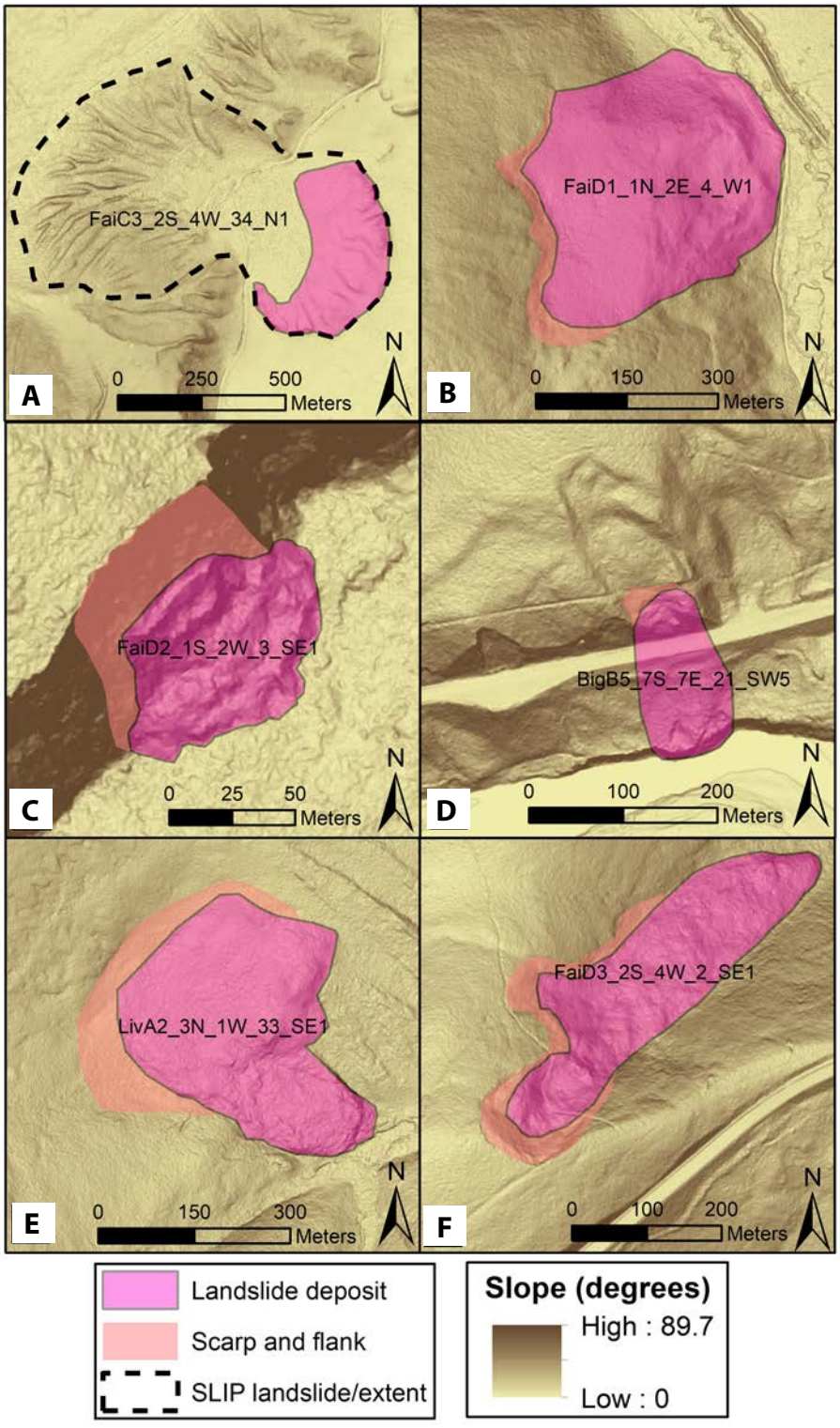

Figure 6. Representative field-checked landslides of various ages and material types: prehistoric landslides in (**A**) soil (deposits of other slides are also present in the imagery) and (**B**) bedrock; historic landslides in (**C**) soil and (**D**) bedrock (scarps of prehistoric slides are also present in the imagery); modern landslides in (**E**) soil and (**F**) bedrock. The background is lidar-derived slope map.

and A37). These areas have multiple episodes of movement, commonly resulting in nested landslide complexes (fig. B15A). During our field work, we observed active movement within several landslides that we attributed to river erosion. One historic landslide was successfully mitigated at Richardson Highway milepost 296 (fig. A31). Its displacement above the road was stopped, but smaller downslope sections are still actively moving due to the river eroding the toe deposit.

Tanana 440 landslide

Detailed field investigation and drilling of the T440 landslide provided five samples of material suitable for radiocarbon dating (fig. 7; table 3). Three samples were rootlets collected 2.55–3.00 m (8.4–9.8 ft) below ground surface (bgs) from three different test holes at the head scarp, left flank, and in front of the toe. These rootlets were less than 1 mm (0.04 in) in diameter and approximately 1 cm (0.4 in) long. We originally hypothesized that the rootlets along the left flank and toe may have been buried by the landslide event; however, the modern dates from these samples postdate activity on the landslide and indicate that the root systems of modern trees penetrate more deeply than we expected.

The other two samples were a brown paleosol (TH06, 2.37 m [7.78 ft] bgs; from a gully cut into the inner toe) and charcoal (TH08, 1.65 m [5.41 ft] bgs; downslope of the outer toe; figs. 3, 5). The dates of these samples were 31,210–30,981 and 7,864–7,700 yr cal BP, respectively, and support the hypothesis that T440 is prehistoric. They do not provide enough information to bracket the age of this landslide conclusively, but support at least two possible interpretations:

1. Single landslide model. The mass of soil carrying the ~31,000-year old paleosol failed as

Table 3. Radiocarbon dates and material type of T440 organic samples.

Test Hole No.	Depth m (ft)	Material Type	Radiocarbon Date
TH01	3.00 (9.84)	rootlets	1991-1994 cal AD
TH03	2.55 (8.37)	rootlets	1994-1998 cal AD
TH04	2.59 (8.50)	rootlets	1979-1981 cal AD
TH06	2.37 (7.78)	paleosol	31,210-30,981 cal BP
TH08	1.65 (5.41)	charcoal	7,864-7,700 cal BP

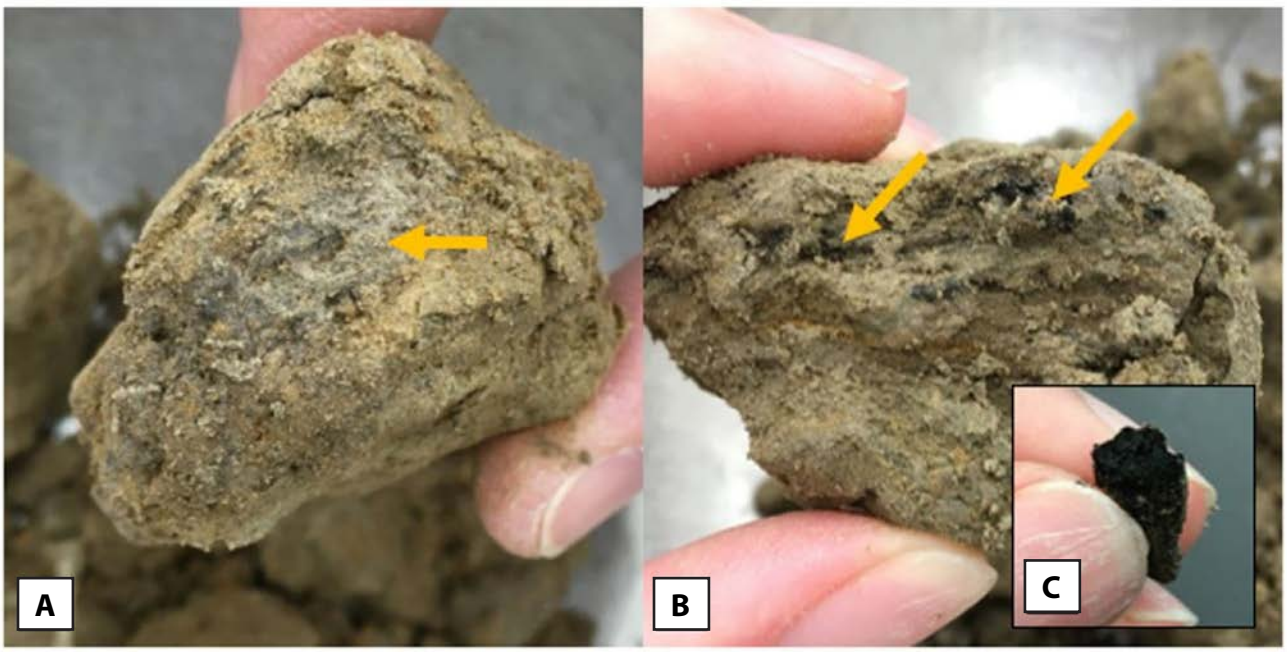

Figure 7. Photos of organic samples submitted for radiocarbon dating. **A.** TH06 paleosol layer (indicated by arrow). **B.** TH08 charcoal pieces within the soil mass (indicated by arrows). **C.** TH08 charcoal piece extracted from the soil.

a competent block, transporting the paleosol downslope to its current location as part of the inner toe; thus the landslide event occurred more recently than ~31 kya. In this interpretation, the landslide also may be younger than ~8,000 years, as erosion subsequent to the landslide may have buried the charcoal downslope of the outer toe.

2. Multiple landslide model. An initial landslide occurred prior to ~31 kya forming the inner toe. Enough time passed for the paleosol to form. The first landslide deposit was subsequently overrun by a second, younger landslide at ~8 kya that formed the outer toe and buried the charcoal downslope of the toe.

CONCLUSION

We identified 1,679 landslides within the area of the Fairbanks North Star Borough using lidar coverage; 681 of which are within the EDMAP area. Most of these landslides are prehistoric, but historic and active landslides are also present in the area. Landslides occur in both bedrock and surficial loess deposits. Observed slope failures include flows in soil, translational and rotational slides in bedrock, and complex features that combine multiple types of movement.

The landslide inventory map represents the first systematic mapping effort to identify landslides within Interior Alaska, and the first step in landslide mitigation for the FNSB area. This landslide inventory map directly benefits the borough, the state, and the general public as it can be used by public agencies to make informed land management decisions such as road alignments and land development. Local emergency managers may incorporate landslides in multiple-disaster scenarios. The availability of this landslide inventory map also may increase the public awareness of landslides as a potential geohazard.

Future work includes completing statistical analyses and developing a landslide susceptibility map for the FNSB region. Additionally, more fieldwork to verify landslides in the greater FNSB area and to determine their ages may provide valuable insight regarding types of landslide movement, material properties, susceptibility, and possible triggering mechanisms.

ACKNOWLEDGMENTS

This research was supported by the U.S. Geological Survey National Cooperative Geologic Mapping Program under USGS award number G20AC00130. The views and conclusions contained in this document are those of the authors and should not be interpreted as representing official policies, either expressed or implied, of the U.S. Government.

We extend our thanks to the staff of the Alaska Division of Geological & Geophysical Surveys for their support during fieldwork and help formatting the maps. We appreciate the thorough review and substantive feedback provided by Dr. Trent Hubbard and Katherine A. Mickelson on the report and maps. We are grateful to the homeowners who allowed us access to their private properties during the T440 fieldwork. Thanks also go to A. DuCluzeau and I. Timling for their company during the Treasure Creek landslide field reconnaissance.

REFERENCES

Alaska Climate Research Center (ACRC), [n.d.] a, Climate Normal: The Alaska State Climate Center. Accessed May 17, 2021. climate.gi.alaska.edu/Climate/Normals

———[n.d.]b, Fairbanks AP: The Alaska State Climate Center. Accessed May 17, 2021. akclimate.org/Climate/Fairbanks

Alaska Department of Transportation and Public Facilities (AKDOT&PF), 2018, Alaska DOT&PF route centerlines—September 2018. Accessed July 13, 2021. dot.alaska.gov/stwddes/gis/shapefiles.shtml

Alaska Division of Forestry (DOF), 2019, Public should be aware of potential hazards in Shovel Creek fire area: AK Fire Info. akfireinfo.com/2019/08/11/public-should-be-aware-of-potential-hazards-in-shovel-creek-fire-area/

Alaska Geospatial Council (AGC), 2020, Alaska hydrology shapefiles: Alaska Geospatial Council. Accessed July 1, 2020. agc.dnr.alaska.gov

American Society for Testing Materials (ASTM), 2014, ASTM D854-14, Standard Test Methods for Specific Gravity of Soil Solids by Water Pycnometer: ASTM International, West Conshocken, PA, 8 p.

———2017a, ASTM D2487-17e1, Standard Practice for Classification of Soils for Engineering Purposes (Unified Soil Classification System): ASTM International, West Conshocken, PA, 10 p.

———2017b, ASTM D4318-17e1, Standard Test Methods for Liquid Limit, Plastic Limit, and Plasticity Index of Soils: ASTM International, West Conshocken, PA, 20 p.

———2017c, ASTM D6528-17, Standard Test Method for Consolidated Undrained Direct Simple Shear Testing of Fine Grain Soils: ASTM International, West Conshocken, PA, 10 p.

———2017d, ASTM D6913M-17, Standard Test Methods for Particle-Size Distribution (Gradation) of Soils Using Sieve Analysis: ASTM International, West Conshocken, PA, 34 p.

———2019, ASTM D2216-19, Standard Test Methods for Laboratory Determination of Water (Moisture) Content of Soil and Rock by Mass: ASTM International, West Conshocken, PA, 7 p.

———2021a, ASTM D7263-21, Standard Test Methods for Laboratory Determination of Density and Unit Weight of Soil Specimens: ASTM International, West Conshocken, PA, 7 p.

———2021b, ASTM D7928-21, Standard Test Method for Particle-Size Distribution (Gradation) of Fine-Grained Soils Using the Sedimentation (Hydrometer) Analysis: ASTM International, West Conshocken, PA, 27 p.

Begét, J.E., Layer, P.W., Stone, D.B., Benowitz, J.A., and Addison, J.A., 2008, Evidence of permafrost formation two million years ago in Central Alaska: *in* 9th International Conference on Permafrost, Fairbanks, Alaska, 2008, Proceedings: Fairbanks, Alaska, University of Alaska Fairbanks, p. 95–100.

Bleakley, Geoffrey, 2015, History of the Valdez Trail, National Park Service. Accessed October 5, 2021. www.nps.gov/wrst/learn/historyculture/history-of-the-valdez-trail.htm

Briner, J.P., Tulenko, J.P., Kaufman, D.S., Young, N.E., Baichtal, J.F., and Lesnek, A., 2017, The last deglaciation of Alaska: Cuadernos de Investigación Geográfica, v. 43 no. 2, p. 429–448. doi.org/10.18172/cig.3229

Burns, Scott, 2007, Prevention is the best medicine: Doing site evaluations to prevent geological hazard catastrophes: Geotimes, v. 52, no. 2, p. 19–22. www.geotimes.org/feb07/feature_prevention.html

Fairbanks North Star Borough (FNSB), 2020, Get FNSB GIS data: Fairbanks North Star Borough. Accessed July 21, 2020. akfairbanksnorthstarborough.civicplus.com/438/Get-FNSB-GIS-Data

Farouki, O.T., 1981, Thermal properties of soils: CRREL Monograph 81-1, United States Army Corps of Engineers, Cold Regions Research and Engineering Laboratory (CRREL), Hanover, New Hampshire.

Finkenbinder, M.S., Abbott, M.B., Edwards, M.E., Langdon, C.T., Steinman, B.A., and Finney, B.P., 2014, A 31,000 year record of paleoenvironmental and lake-level change from Harding Lake, Alaska, USA: Quaternary Science Reviews, v. 87, p. 98–113. doi.org/10.1016/j.quascirev.2014.01.005

French, H.M., 2007, The periglacial environment, 3rd ed: John Wiley & Sons, Ltd, Chichester, England, 458 p.

Fuis, G.S., Wald, L.A., Hendley II, J.W., Stauffer, P.H., Mayfield, Susan, Boore, Sara, Omdahl, Eleanor, and Blair, J.L., 2003, Rupture in South-Central Alaska – the Denali Fault Earthquake of 2002: U.S. Department of the Interior and U.S. Geologic Survey, USGS Fact Sheet 014-13, 4 p. pubs.usgs.gov/fs/old.2003/fs014-03/fs014-03.pdf

GeoNorth, 2021, Alaska statewide high resolution imagery (50cm). Accessed July 21, 2021. soa.dnr.maps.arcgis.com/home/item.html?id=13dd1ccf165845eea5db36465e7d565c

Haynes, F.D., Carbee, D.L., and Vanpelt, D.J., 1980, Thermal diffusivity of frozen soil: Special Report 80-38: United States Army Corps of Engineers, Cold Regions Research and Engineering Laboratory (CRREL), Hanover, New Hampshire.

Heidemann, H.K., 2014, Lidar base specification (ver. 1.2, November 2014): U.S. Geological Survey Techniques and Methods, book 11, chap. B4, 67 p. with appendices. dx.doi.org/10.3133/tm11B4

Hungr, Oldrich, Evans, S.G., Bovis, M.J., and Hutchinson, J.N., 2001, A review of the classification of landslides of the flow type: Environmental and Engineering Geoscience, v. 7, no. 3, p. 221–238.

Jorgenson, Torre, Yoshikawa, Kenji, Kanevskiy, Mikhail, Shur, Yuri, Romanovsky, Vladimir, Marchenko, Sergei, Grosse, Guido, Brown, Jerry, and Jones, Ben, 2008, Permafrost Characteristics of Alaska: Institute of Northern Engineering, University of Alaska Fairbanks, 1 sheet, scale 1:7,200,000. permafrost.gi.alaska.edu/sites/default/files/AlaskaPermafrostMap_Front_Dec2008_Jorgenson_etal_2008.pdf

Josephs, R.L., 2010, Micromorphology of an Early Holocene Loess-Paleosol Sequence, Central Alaska, U.S.A: Arctic, Antarctic, and Alpine Research, v. 42, no.1, p. 67–75. doi.org/10.1657/1938-4246-42.1.67

Kaufman, D.S., Ager, T.A., Anderson, N.J., Anderson, P.M., Andrews, J.T., Bartlein, P.J., Brubaker, L.B., Coats, L.L., Cwynar, L.C., Duval, M.L., Dyke, A.S., Edwards, M.E., Eisner, W.R., Gajewski, K., Geirsdóttir, A., Hu, F.S., Jennings, A.E., Kaplan, M.R., Kerwin, M.W., Lozhkin, A.V., MacDonald, G.M., Miller, G.H., Mock, C.J., Oswald, W.W., Otto-Bliesner, B.L., Porinchu, D.F., Ruhland, K., Smol, J.P., Steig, E.J., and Wolfe, B.B., 2004, Holocene thermal maximum in the western Arctic (0–180°W): Quaternary Science Reviews, v. 23, p. 529–560.

Keaton, J.R., and DeGraff, J.V., 1996, Surface observation and geologic mapping *in* Turner, A.K., and Schuster, R.L., eds., Landslides Investigation and Mitigation Special Report 247, 673 p.

Koehler, R.D., Carver, G.A., and Alaska Seismic Hazards Safety Commission, 2018, Active faulting and seismic hazards in Alaska: Alaska Division of Geological & Geophysical Surveys Miscellaneous Publication 160, 59 p. doi.org/10.14509/29705

McCalpin, James, 1984, Preliminary age classification of landslides for inventory mapping: *in* Annual Symposium on Engineering Geology and Soils Engineering, 21st, Moscow, Idaho, 1984, Proceedings: Moscow, Idaho, University of Idaho, p. 99–111.

McRoberts, E.C., and Morgenstern, N.R., 1974, The stability of thawing slopes: Canadian Geotechnical Journal, v. 11, no. 4, p. 447–469.

Muhs, D.R., and Budahn, J.R., 2006, Geochemical evidence for the origin of late Quaternary loess in central Alaska: Canadian Journal of Earth Sciences, v. 43, no. 3, p. 323–337.

Newberry, R.J., Bundtzen, T.K., Clautice, K.H., Combellick, R.A., Douglas, Tom, Laird, G.M., Liss, S.A., Pinney, D.S., Reifenstuhl, R.R., and Solie, D.N., 1996, Preliminary geologic map of the Fairbanks mining district, Alaska: Alaska Division of Geological & Geophysical Surveys Public Data File 96-16, 17 p., 2 sheets, scale 1:63,360. doi.org/10.14509/1740

OCM Partners, 2020, 2017 USGS 3DEP Lidar: Fairbanks, AK (QL1 & QL2). www.fisheries.noaa.gov/inport/item/55358

Osterkamp, T.E., 2005, The recent warming of permafrost in Alaska: Global and Planetary Change, v. 48, no. 3–4, p. 187–202. doi.org/10.1016/j.gloplacha.2005.09.001

Péwé, T.L., 1955, Origin of the upland silt near Fairbanks, Alaska: Bulletin of the Geological Society of America, v. 66, no. 6, p. 699–724. doi.org/10.1130/0016-7606(1955)66[699:OOTUSN]2.0.CO;2

———1975, Quaternary geology of Alaska: U.S. Geological Survey Professional Paper 835, United States Government Printing Office, Washington, D.C., 145 p.

———1982, Geologic hazards of the Fairbanks area: Alaska Division of Geological & Geophysical Surveys Special Report 15, 119 p. doi.org/10.14509/2614

Porter, Claire; Morin, Paul; Howat, Ian; Noh, Myoung-Jon; Bates, Brian; Peterman, Kenneth; Keesey, Scott; Schlenk, Matthew; Gardiner, Judith; Tomko, Karen; Willis, Michael; Kelleher, Cole; Cloutier, Michael; Husby, Eric; Foga, Steven; Nakamura, Hitomi; Platson, Melisa; Wethington, Michael, Jr.; Williamson, Cathleen; Bauer, Gregory; Enos, Jeremy; Arnold, Galen; Kramer, William; Becker, Peter; Doshi, Abhijit; D'Souza, Cristelle; Cummens, Pat; Laurier, Fabien; Bojesen, Mikkel, 2018, ArcticDEM: University of Minnesota Polar Geospatial Center. Accessed May 17, 2021. doi.org/10.7910/DVN/OHHUKH

Schwarber, J.A., Darrow, M.M, Daanen, R.D., and Stevens, D.S.P., in review, Loess is more: field investigation and slope stability analysis of the Tanana 440 landslide, Interior Alaska: Environmental & Engineering Geoscience.

Slaughter, S.L., Burns, W.J., Mickelson, K.A., Jacobacci, K.E., Biel, A., and Contreras, T.A., 2017, Protocol for landslide inventory mapping from lidar data in Washington State: Washington Geological Survey Bulletin 82, 27 p. www.dnr.wa.gov/Publications/ger_b82_landslide_inventory_mapping_protocol.zip

St. Amand, Pierre, 1948, The central Alaska earthquake swarm of October 1947: Transactions, American Geophysical Union, v. 29, no. 5, p. 613–623.

Tape, Carl, Silwal, Vipul, Ji, Chen, Keyson, Laura, West, M.E., and Ruppert, Natalia, 2015, Transtensional tectonics of the Minto Flats Fault Zone and Nenana Basin, Central Alaska: Bulletin of the Seismological Society of America, v. 105, no. 4, p. 2,081–2,100. dx.doi.org/10.1785/0120150055

Varnes, D.J., 1984, Landslide hazard zonation: a review of principles and practice: Natural Hazards, UNESCO, Paris, 61 p.

Wahrhaftig, Clyde, 1965, Physiographic Divisions of Alaska: U.S. Geological Survey Professional Paper 482: United States Government Printing Office, Washington, D.C., 52 p. doi.org/10.3133/pp482

Wendler, Gerd, and Shulski, Martha, 2009, A century of climate change for Fairbanks, Alaska: Arctic, v. 2, no. 3, p. 295–300. www.jstor.org/stable/40513307

Westgate, J.A., Stemper, B.A., and Péwé, T.L., 1990, A 3 m.y. record of Pliocene-Pleistocene loess in interior Alaska: Geology, v. 18, no. 9, p. 858–861. doi.org/10.1130/0091-7613(1990)018%3C0858:AMYROP%3E2.3.CO;2

APPENDIX A: FIELD SUMMARIES

FIELD SUMMARY TEMPLATE

Each field summary contains relevant, standardized information regarding the field-verified landslides. The total confidence value is the sum of the confidence scores (from 1 to 10) of the four main feature categories (head scarp, flanks, toe/deposit, and morphology), with a maximum of 40 points. Low, moderate, and high summed confidence levels are associated with 0–10, 11–29, and 30–40 points, respectively.

Additional confidence levels for relative age, material, and movement type are included in parentheses adjacent to each of these attribute calls, with 0 as low, 5 as moderate, and 10 as high—these confidence levels are not included in the 40-point system described above but represent our level of understanding of the specific attributes. The summaries are presented in the chronological order in which the landslides were visited in the field.

The format shown below was used in documenting each landslide. The initials used for field personnel are:

JAS: Jaimy Schwarber PP: Peyton Presler

MD: Margaret Darrow RD: Ronald Daanen

LS Name:	*name in geodatabase*	**Relative Age:**	*prehistoric/historic (0/5/10)*
Date:	*date of fieldwork*	**Material:**	*earth/bedrock/debris (0/5/10)*
Personnel:	*people in the field*	**Movement Type:**	*slide, flow, etc. (0/5/10)*

Current Movement: *yes/none*

Total confidence: *sum of main feature category values/40 (Low/Moderate/High)*

Following is a short description of field observations. The narrative explains the route taken across the landslide and includes details of observed morphology such as internal scarps, sag ponds, closed depressions, compression ridges, hummocky topography, mid-slope terraces, cracks, offset drainages, affected or controlled drainages, springs, seeps, wetlands, fresh soil or rock, and internal slides. The associated confidence level for each of four main feature categories (head scarp, flanks, toe/deposit, and morphology) is included in parentheses, with a total possible qualitative confidence of 40. The summary may include vegetative indicators of movement such as leaning, jayed, or cracked/split trees; a discussion of age and confidence level; and any other relevant details.

<A figure of representative photographs of the observed landslide features follows the description.>

LS Name:	*LivA2_3N_1W_33_SE1*	**Relative Age:**	*Prehistoric (10)*
Date:	*May 15, 2020*	**Material:**	*Debris (5)*
Personnel:	*MD, RD*	**Movement Type:**	*Flow/slide complex (5)*

Current Movement: *yes*

Total confidence: *40/40 (High for currently active area)*

We accessed the landslide (fig. B1) from the west, walking down the right flank (10) to the toe area (10), and then returning uphill along the left flank until we intersected an internal scarp (10). At that point, we followed the same path away from the landslide. The morphology indicates a large, prehistoric landslide event, which occurred north of the currently active area, that forms a relatively flat area followed by a large hill mid-slope. Part of the mid-slope hill failed historically, forming the current, smaller, lower landslide. The forest covering the area contains many leaning and split trees, multiple transverse and longitudinal cracks, sag ponds, grabens, and minor scarps. Splits in most of the trees appear to be old, and the way that some of the birch trees and spruce trees have recovered suggests that the historic event occurred at least 50 years ago. One of the split spruce trees above and to the west of the main internal scarp indicates more recent splitting, suggesting that the landslide is currently active.

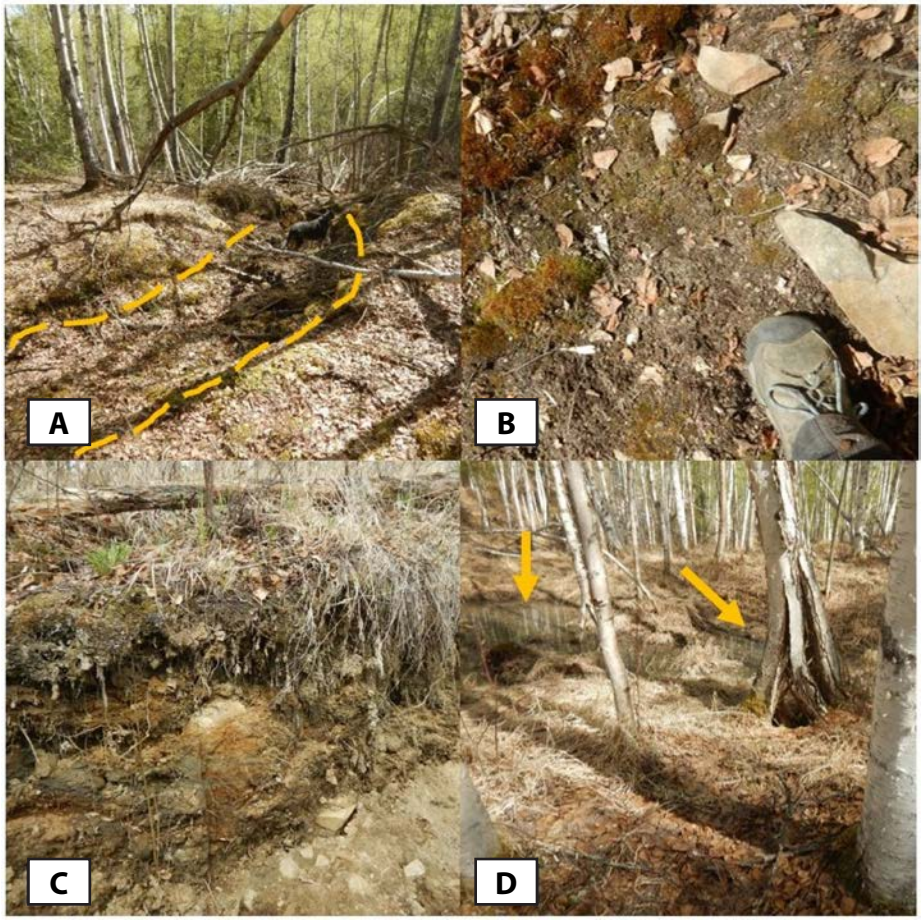

Figure A1. Images of LivA2_3N_1W_33_SE1 from May 15, 2020. **A.** Dashed lines indicate extent of crack (dog for scale), (**B**) rock and soil at the toe, (**C**) exposed soil at the main internal scarp, and (**D**) a split, leaning tree (right arrow) and sag pond in a graben (left arrow). Photographs taken by MD.

LS Name:	*FaiD3_2S_3W_12_W1*	**Relative Age:**	*Prehistoric (10)*
Date:	*May 28, 2020 (& July 6-9)*	**Material:**	*Earth (silt) (5)*
Personnel:	*JAS, MD*	**Movement Type:**	*Earth flow/complex (5)*

Current Movement: *None*

Total confidence: *35/40 (High)*

We accessed the body of Tanana 440 landslide (T440) (fig. B2) along an established trail from the east, then visited the head scarp to the north. We traveled along the right flank on the road system and investigated the toe region. We then walked north through the landslide body, returning to the trail system that follows the left flank. The key features observed were the head scarp (5), flanks (10), toe/deposit (10), and morphology (10). The left flank was more distinct than the right flank. Observed internal morphology included internal scarps, possible closed depressions, mid-slope terraces, and possible cracks. Some of these features were subtle probably due to the material (silt) and prehistoric age of the event. The movement type is an earth flow complex, exhibiting some down-dropped grabens that may be associated with rotational slide movement. We discovered a charcoal layer about 10 cm below the ground surface when digging a small (0.3 m by 0.3 m area, 0.1 m deep) test pit near the head scarp, underlain by silt. We observed silt exposures at both the toe and the upper right flank, with no obvious bedrock. Vegetation varies across the landslide with birch and poplar towards the head transitioning to mature spruce across the lower body. There was a sharp transition in the vegetation from birch trees to black spruce on the toe deposit to the area beyond the landslide extent.

We returned to the T440 slide for stratigraphic mapping, drilling, and sampling from July 6 to July 9, 2020.

Figure A2. Images of FaiD3_2S_3W_12_W1 from May 28, 2020. **A.** Vegetation transition at the toe (indicated by arrow) from birch forest to black spruce, (**B**) silt exposure along the right flank, (**C**) silt exposure along the inner toe, and (**D**) JAS standing in a depression (outlined by dashed line) near the head scarp. Photographs taken by MD.

LS Name:	*FaiD3_2S_4W_2_SE1*	**Relative Age:**	*Prehistoric (10)*
Date:	*May 29, 2020*	**Material:**	*Bedrock and debris (5)*
Personnel:	*JAS, MD, RD*	**Movement Type:**	*Translational/rotational/flow(5)*

Current Movement: *Yes (at the toe)*

Total confidence: *40/40 (High)*

This landslide (fig. B3) is adjacent to and north of the Parks Highway. We accessed the landslide from the south, walking north across the head scarp then downslope along the body to the toe. We returned to the road following a similar route. We observed strong evidence of the head scarp (10), flanks (10), toe/deposits (10), and morphology (10). Observed morphology included internal scarps, closed depressions, hummocky topography, mid-slope terraces, tension cracks, seeps, wetland areas, and fresh soil/rock at the toe. Vegetative indicators of slope movement included jayed, leaning, and cracked trees throughout the landslide body. We observed schist exposures at the head scarp, throughout the body, and along the flanks; thus the material type was predominantly schist bedrock, with silt and other granular debris present near the toe. The vegetation shifted from white spruce and birch at the head to black spruce and moss across the bottom part of the landslide body. This vegetation change may indicate the presence of frozen ground at the toe. We also observed surface wetness at the toe. Overall this landslide is prehistoric, with apparent historic movement and current, ongoing movement at the toe. It is possible that the movement at the toe is due to creep, and the landslide is similar in morphology and movement to frozen debris lobe (FDL) features observed in the Brooks Range.

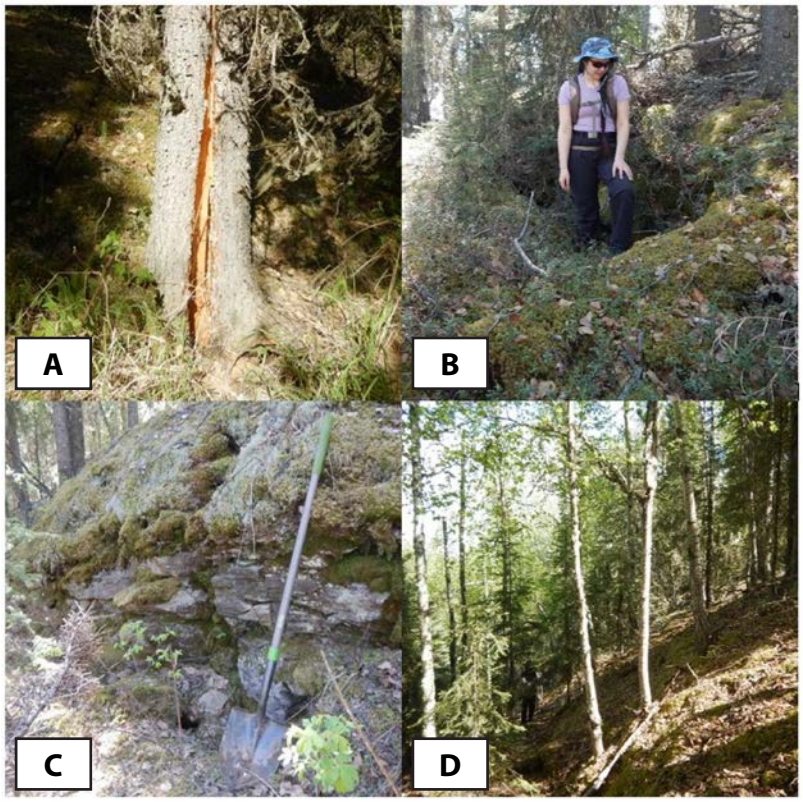

Figure A3. Images of FaiD3_2S_4W_2_SE1 from May 29, 2020. **A.** Fresh cracked spruce tree near the head scarp, (**B**) JAS standing in a crack on the slide surface, (**C**) schist bedrock exposure at the scarp (shovel for scale), and (**D**) the right flank viewed from the head scarp area (RD for scale). Photographs taken by MD.

LS Name:	*FaiD3_1N_4W_1_NE1*	**Relative Age:**	*Prehistoric (10)*
Date:	*June 2, 2020*	**Material:**	*Bedrock (10)*
Personnel:	*JAS, MD, RD*	**Movement Type:**	*Rotational (10)*

Current Movement: *None*

Total confidence: *37/40 (High)*

We hiked down to the head scarp region, then traveled along the left flank toward the toe. We visited other landslides (fig. B4) before we returned along the right flank and back up the head scarp. The key features were the head scarp (10), flanks (7), toe (10), and morphology (10). Morphology included closed depressions, mid-slope terraces, cracks, and prehistoric swales. The flanks were less obvious in the field compared to the lidar data, but we accurately located them as our GPS field station points were comparable to the mapped landslide. We saw exposed schist bedrock at the landslide head, and took one strike and dip measurement of 020/26. Ridges and internal roughness were due to the presence of bedrock. We saw a few jayed trees, but these were not due to landslide movement. The vegetation on the landslide was mature birch and spruce forest.

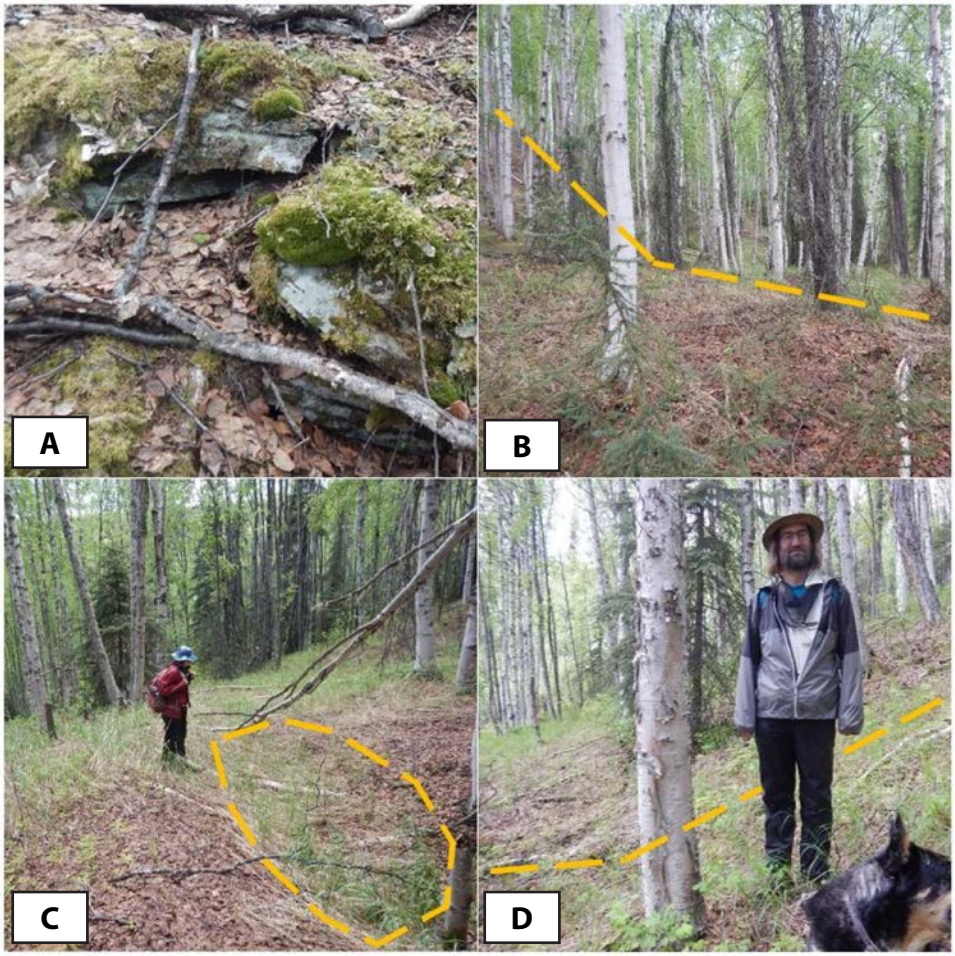

Figure A4. Images of FaiD3_1N_4W_1_NE1 from June 2, 2020. **A.** Bedrock exposure near the head scarp, (**B**) dashed line indicates slope break along the left flank, (**C**) JAS standing at the edge of a closed depression (dashed line indicates extent), and (**D**) RD and dog along the slope break at the toe (indicated by dashed line; view to the southwest). Photographs taken by MD.

LS Name:	*FaiD3_1N_4W_1_NE3*	**Relative Age:**	*Prehistoric (10)*
Date:	*June 2, 2020*	**Material:**	*Bedrock (10)*
Personnel:	*JAS, MD, RD*	**Movement Type:**	*Translational (5)*

Current Movement: *None*

Total confidence: *20/40 (Moderate)*

We hiked down the bottom portion of the left flank of the landslide (fig. B4) and along the toe (5) and then returned across the right flank and up past the head scarp (10). The flanks (5) were subtle as only a faint break in slope indicated their location. Vegetation obscured morphological features (0). We observed schist bedrock exposures, with occasional quartz veins, at the head scarp, flanks, and body of the landslide.

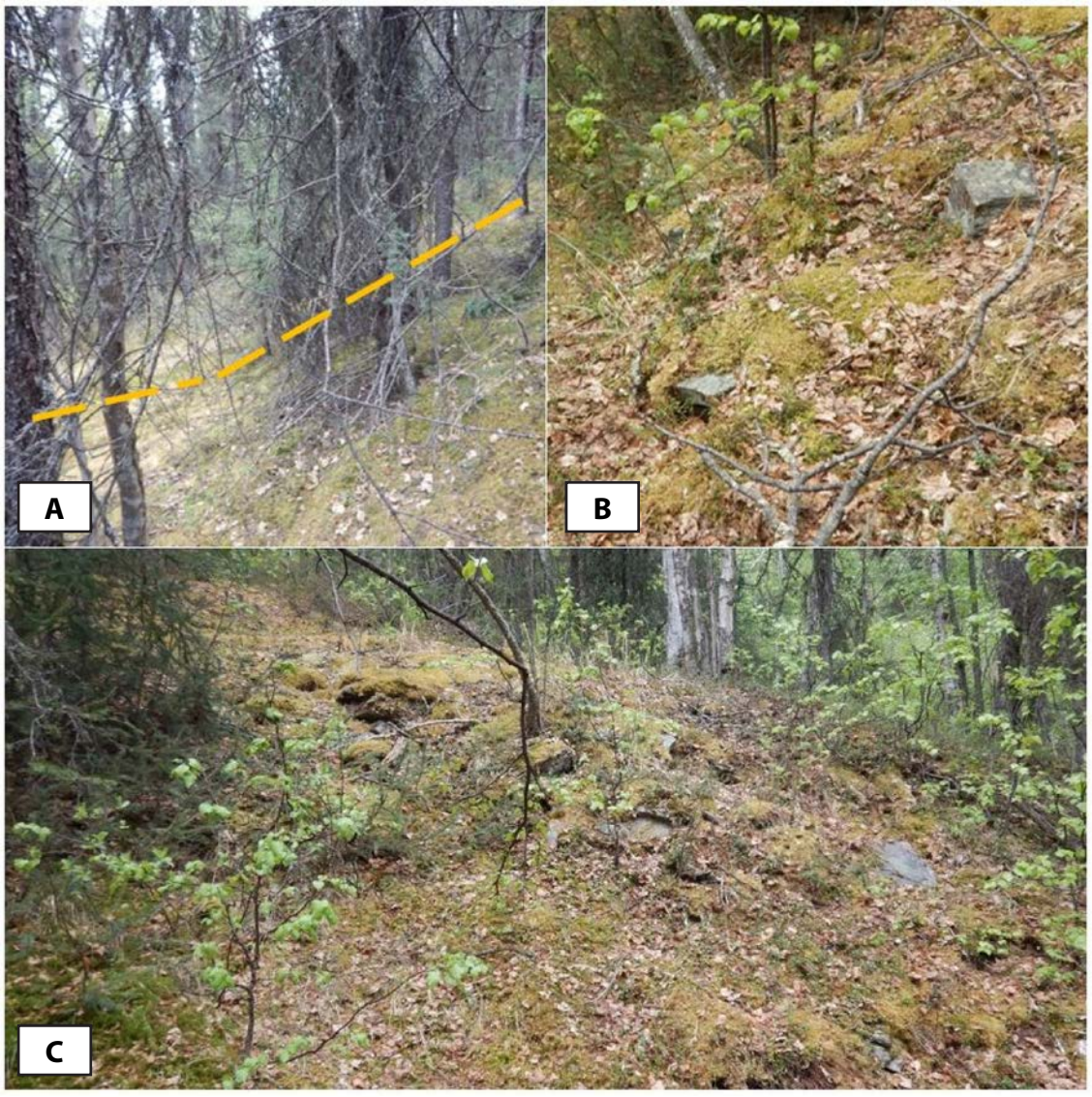

Figure A5. Images of FaiD3_1N_4W_1_NE3 from June 2, 2020. **A.** Slope break near the head scarp region (indicated by dashed line), (**B**) small bedrock exposure near the toe, and (**C**) weathered bedrock exposure near the toe. Photographs taken by MD.

LS Name:	*FaiD3_1N_4W_1_NE2*	**Relative Age:**	*Prehistoric (10)*
Date:	*June 2, 2020*	**Material:**	*Bedrock (10)*
Personnel:	*JAS, MD, RD*	**Movement Type:**	*Translational (5)*

Current Movement: *None*

Total confidence: *25/40 (Moderate)*

We hiked along the lower body and toe (5) and returned across the right flank (7) and along the head scarp (10). We did not visit the left flank. Internal scarps were the main observed morphology (3). We also observed solifluction lobes as evidence for creep movement. This likely translational slide occurred in bedrock with bedrock exposures at the head scarp. We estimate that vegetation on the landslide was at least 100-years old and consisted of black spruce, moss, and old lichen. A break in the moss revealed bedrock. The presence of this type of vegetation supports the conclusion that the soil is frozen and thus may experience creep. We observed bare mineral soil at a scarp adjacent to the right flank extent. It is possible that this landslide and FaiD3_1N_3W_6_NW1 may actually be one large landslide along this slope (fig. B4).

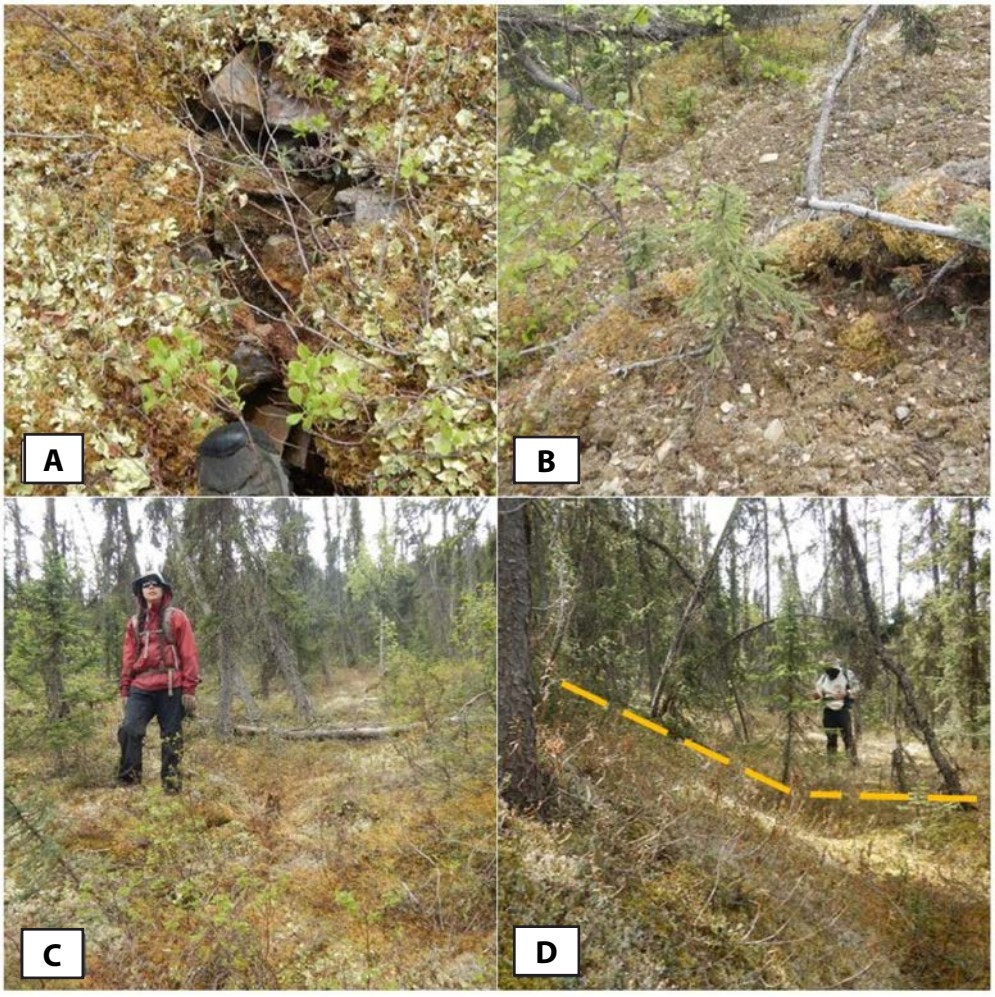

Figure A6. Images of FaiD3_1N_4W_1_NE2 from June 2, 2020. **A.** Bedrock exposure in a moss crack, (**B**) bare mineral soil on the slope adjacent to the right flank, (**C**) JAS standing among the typical vegetation of moss, lichen, and black spruce on the landslide body, and (**D**) slope break at the head scarp (RD as scale). Photographs taken by MD.

LS Name:	*FaiD3_1N_3W_6_NW1*	**Relative Age:**	*Prehistoric (10)*
Date:	*June 2, 2020*	**Material:**	*Bedrock (10)*
Personnel:	*JAS, MD, RD*	**Movement Type:**	*Rotational/translational (0)*

Current Movement: *None*

Total confidence: *15/40 (Moderate)*

We hiked across the left flank and up toward the head scarp of the landslide (fig. B4). We did not visit the right flank or the toe/deposit (0). The left flank (5) and head scarp (5) both were subtle with a faint break in slope. Although more visible in the lidar, these features may be subtle due to their age. This landslide is prehistoric, and vegetation development indicates that it occurred over 200 years ago. We observed roughness on the landslide body and lichen on bedrock at the surface. We also saw potential solifluction lobes on the landslide surface. Other visible morphology (5) included internal scarps and fresh soil/rock at the surface. We observed flowing water on the feature as well as some leaning trees, but they did not appear to be caused by landslide movement. The initial landslide movement mechanism may have been rotational or translational within the bedrock. It is possible that this landslide and FaiD3_1N_4W_1_NE2 may actually be one large landslide along this slope.

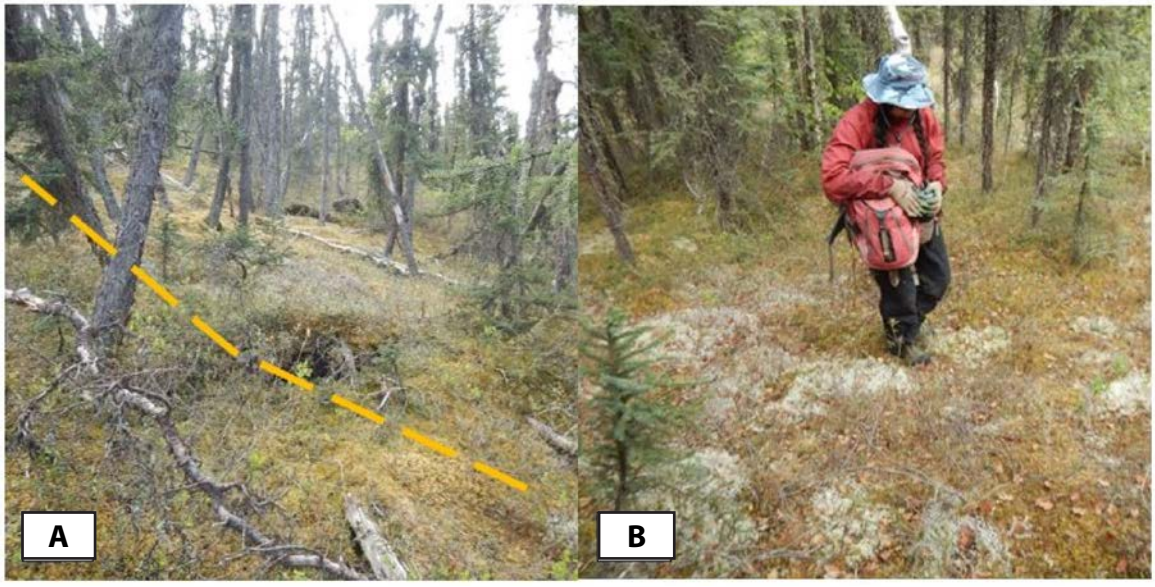

Figure A7. Images of FaiD3_1N_3W_6_NW1 from June 2, 2020. **A.** Subtle upslope slope break at the head scarp region (indicated by dashed line), and (**B**) JAS standing on a bedrock ridge covered with lichen slightly upslope of the head scarp region. Photographs taken by MD.

LS Name:	*FaiD2_1N_1W_30_SE1*	**Relative Age:**	*Prehistoric (10)*
Date:	*June 5, 2020*	**Material:**	*Earth, silt (10)*
Personnel:	*JAS, MD*	**Movement Type:**	*Flow (5)*

Current Movement: *None*

Total confidence: *9/40 (Low)*

We walked along the high points of the landslide's bump-like toe deposits. Only the toe deposits (8) remain from this landslide (fig. B5A), with no discernible flanks (0) or head scarp (0). It also lacks internal morphology (1) although there may have been offset drainages. Mature forest grows on the toe deposits, and the vegetation changes to birch and aspen due to drainage off of the toe. We observed only silt within the toe deposits with two different colors that changed from tan to gray with depth in soil pits.

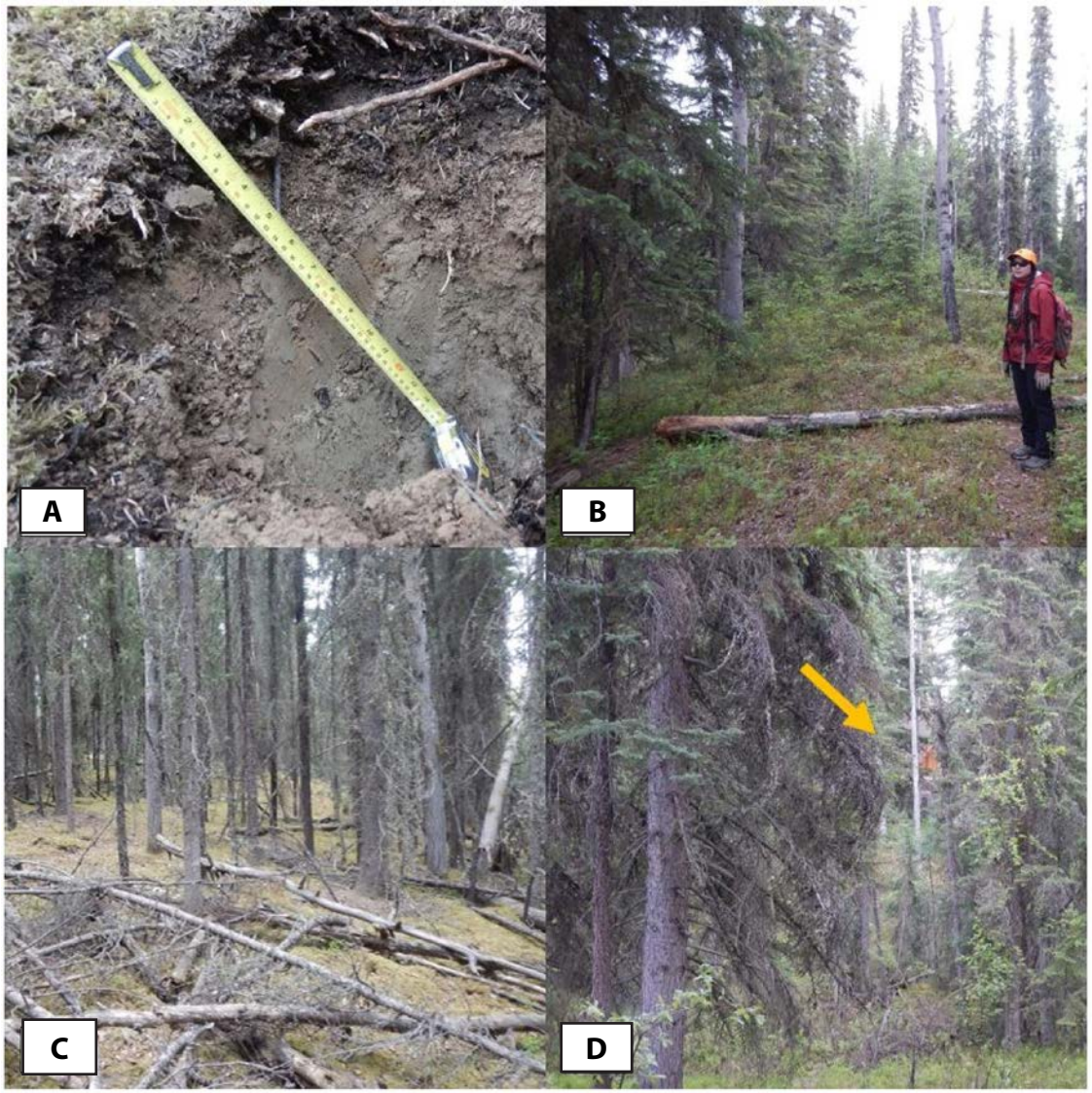

Figure A8. Images of FaiD2_1N_1W_30_SE1 from June 5, 2020. **A.** Silt in a small test pit (tape measure for scale; silt was cold to the touch), (**B**) JAS standing on the middle toe bump, (**C**) the view along a toe bump ridge, and (**D**) a house built on a toe bump (indicated by arrow). Photographs taken by MD and JAS.

LS Name:	*FaiD2_1S_2W_3_SE1*	**Relative Age:**	*Historic (10)*
Date:	*June 5, 2020*	**Material:**	*Earth, silt (10)*
Personnel:	*JAS, MD*	**Movement Type:**	*Translational/rotational (5)*

Current Movement: *Maybe*

Total confidence: *35/40 (High)*

We walked to the middle of the toe then up the body of the landslide (fig. B5B) to the head scarp. From there we hiked down the left flank and returned along the toe. The right flank was inaccessible as it was on private land. The head scarp (10) and toe deposit (10) were prominent, with the left flank less prominent (5). There were many geomorphic features (10) including mid-slope terraces, a tension crack above the head scarp, and exposed silt at the scarp. This is an historic slide that occurred after mining in the Gold Hill area. The vegetation on the landslide is approximately 50-years old. We saw some pistol butt trees and cracked trees. There was one jayed spruce tree about 100-years old at the head scarp that predates movement as it was leaning and has since corrected. We observed rocks at the toe that may be mine tailings, as we saw only silt everywhere else on the slide. The movement type is possibly rotational, since the shape of the toe deposit is circular.

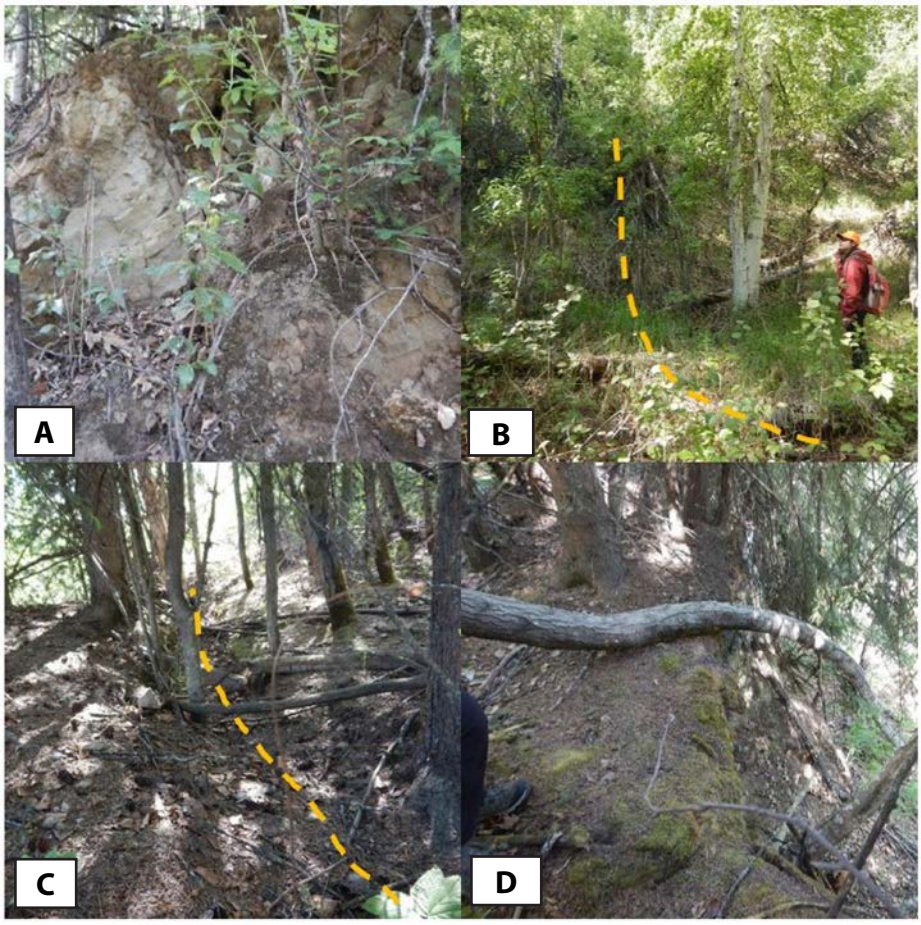

Figure A9. Images of FaiD2_1S_2W_3_SE1 from June 5, 2020. **A.** Silt exposure at a minor scarp, (**B**) JAS standing in a graben (indicated by dashed line), (**C**) tension crack above the scarp (indicated by dashed line), and (**D**) looking along the steep head scarp. Photographs taken by MD.

LS Name:	*FaiD2_2N_1W_17_SW2*	**Relative Age:**	*Prehistoric (10)*
Date:	*June 8, 2020*	**Material:**	*Earth, colluvium (10)*
Personnel:	*JAS, MD*	**Movement Type:**	*Rotational or flow (5)*

Current Movement: *Yes, at the toe*

Total confidence: *25/40 (Moderate)*

We hiked down to the head scarp region then followed the right flank and crossed onto the body (fig. B6) to reach the toe deposit. We returned adjacent to the left flank walking through FaiD2_2N_1W_17_SW1 back toward the head scarp region. The extent of the head scarp (3) was uncertain— it was subtle in the field but more visible in the lidar imagery. We observed a few slope breaks but no strong slope changes. The left flank (0) was not visible, but the right flank (5) was defined. The toe (10) was clearly defined, presented as a small dome, and consisted of colluvium. Internal morphology (7) included sag ponds, subtle internal scarps, and hummocky topography on the toe. The material type consisted of silty colluvium, with gravel and sand. The toe deposit appears to have moved a great distance (approximately 0.5 km), suggesting flow movement based on material type and geomorphologic expression. We observed solifluction lobes on the main body of the landslide and surficial movement at the toe. There was one jayed tree on the toe. A stream runs in the valley along the right flank of the landslide. Across the stream from the landslide, we observed exposed bedrock in the slope.

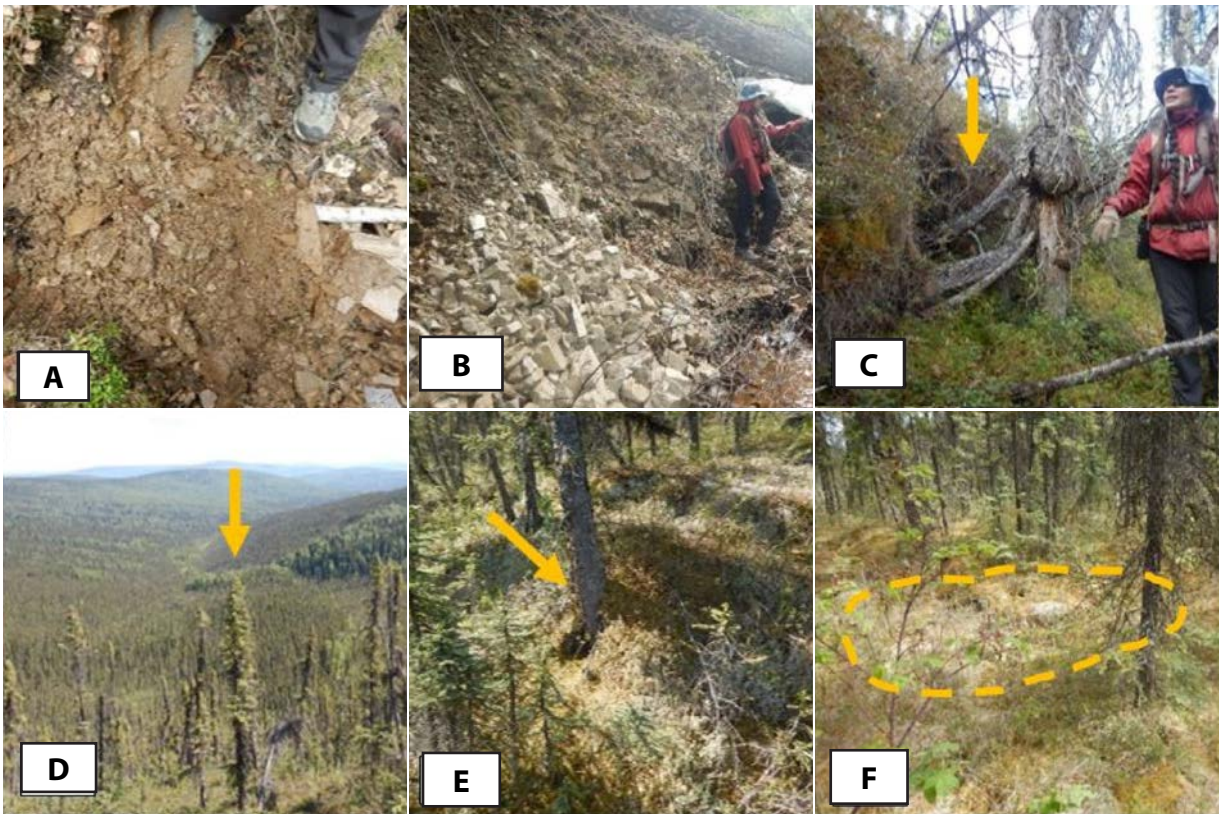

Figure A10. Images of FaiD2_2N_1W_17_SW2 from June 8, 2020. **A.** Colluvium at the toe, (**B**) JAS next to exposed bedrock across the creek from the landslide toe, (**C**) JAS standing next to a tree being overrun by the landslide toe (indicated by arrow), (**D**) view down the landslide body toward the toe (location indicated with an arrow), (**E**) solifluction lobe flowing around a tree (indicated by arrow), and (**F**) dashed line delineating a closed depression on the toe. Photographs taken by MD.

LS Name:	*FaiD2_2N_1W_17_SW1*	**Relative Age:**	*Prehistoric (5)*
Date:	*June 8, 2020*	**Material:**	*Earth, silt (10)*
Personnel:	*JAS, MD*	**Movement Type:**	*Uncertain*

Current Movement: *None*

Total confidence: *7/40 (Low)*

We walked along the toe and then up the left flank to the head scarp region. All observed features of the left flank, body, and toe deposit occurred in silt and were subtle. The head scarp (0) was indiscernible in the field, and the flank (3), morphology (1), and toe (3) were subtle. The surface roughness may be due to the vegetational features such as tree throws. We observed a few solifluction lobes on the surface. We are uncertain that this feature is a landslide based on the field survey, but landslide features are visible in the lidar-derived hillshade (fig. B6).

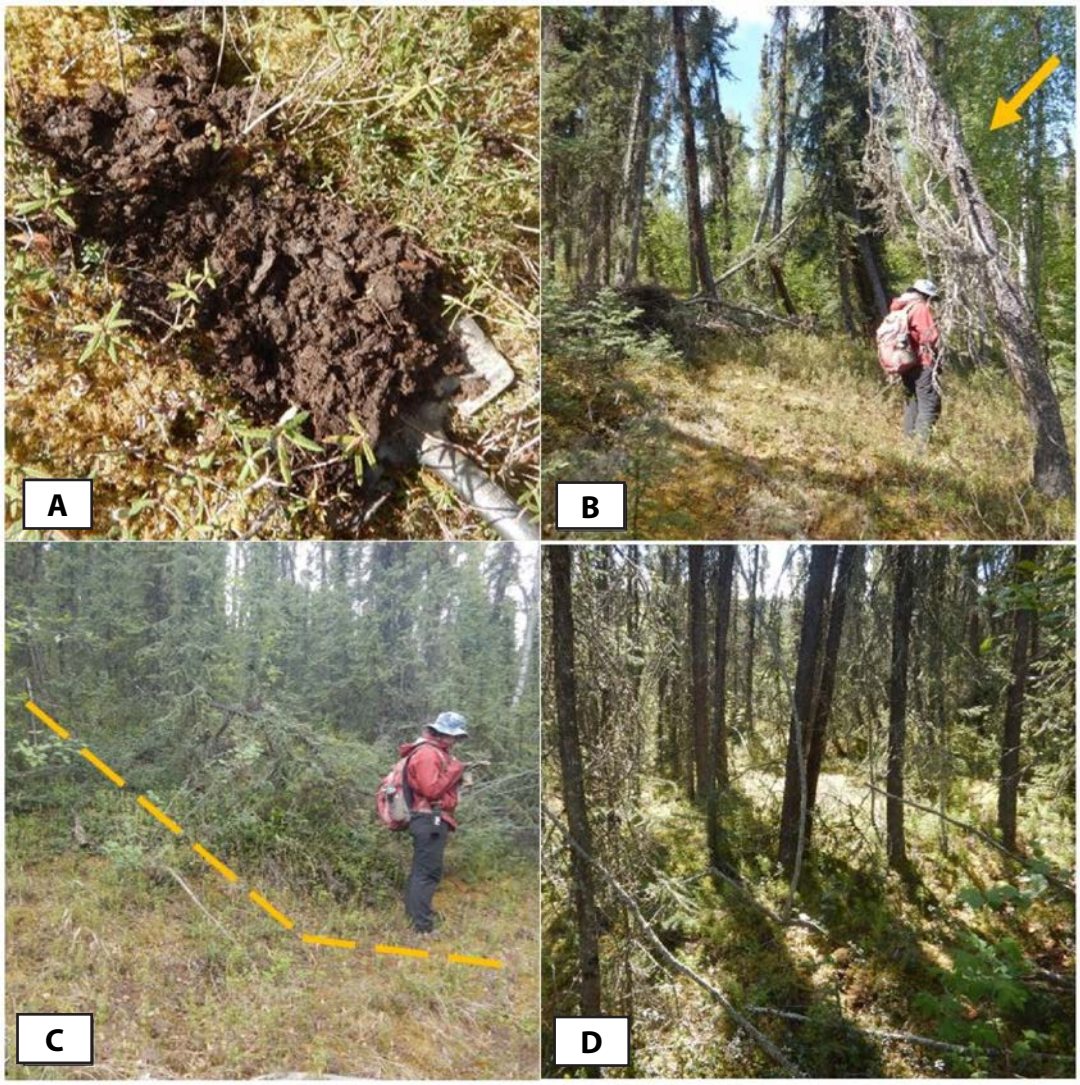

Figure A11. Images of FaiD2_2N_1W_17_SW1 from June 8, 2020. **A.** Organic silt with wood pieces observed in a test pit along the left flank, (**B**) JAS standing amongst leaning trees, (**C**) JAS standing on a faint slope break along the left flank, and (**D**) typical vegetation and surface roughness on the body. Photographs taken by MD and JAS.

LS Name:	*FaiD3_2S_3W_10_NE2*	**Relative Age:**	*Prehistoric (10)*
Date:	*June 11, 2020*	**Material:**	*Earth, silt (10)*
Personnel:	*JAS, MD, RD*	**Movement Type:**	*Flow (10)*

Current Movement: *None*

Total confidence: *10/40 (Low)*

The FaiD3_2S_3W_10_NE2 and FaiD3_2S_3W_10_NE1 landslides are informally referred to as the Quist landslides, due to their proximity to Quist Farm.

We followed established trails, which wove through the gullied toe deposit (10), on four-wheelers. We stopped at the top of what we suspected was the head scarp region (0), traveling along severe gullying. We did not see evidence of flanks (0) or internal morphology (0). We saw no vegetative movement indicators; this landslide (fig. B7) is prehistoric based on its geomorphology. We dug a test pit in front of a toe deposit bump, which revealed dry to moist silt (field-estimated to be about 5 percent moisture content). Test pits in the inferred head scarp region revealed silt, with no bedrock or debris. There was considerable gullying and rills in the inferred head scarp region, which may explain why there was no identifiable head scarp feature. The ground appeared deflated behind the toe deposits, on the landslide body. The toe deposit bumps were steeper on their distal slopes, with shallower slopes toward the landslide body (proximal). We also cleaned off a section of exposed silt at the summit of one of the toe bumps along the trail, revealing it to be micaceous.

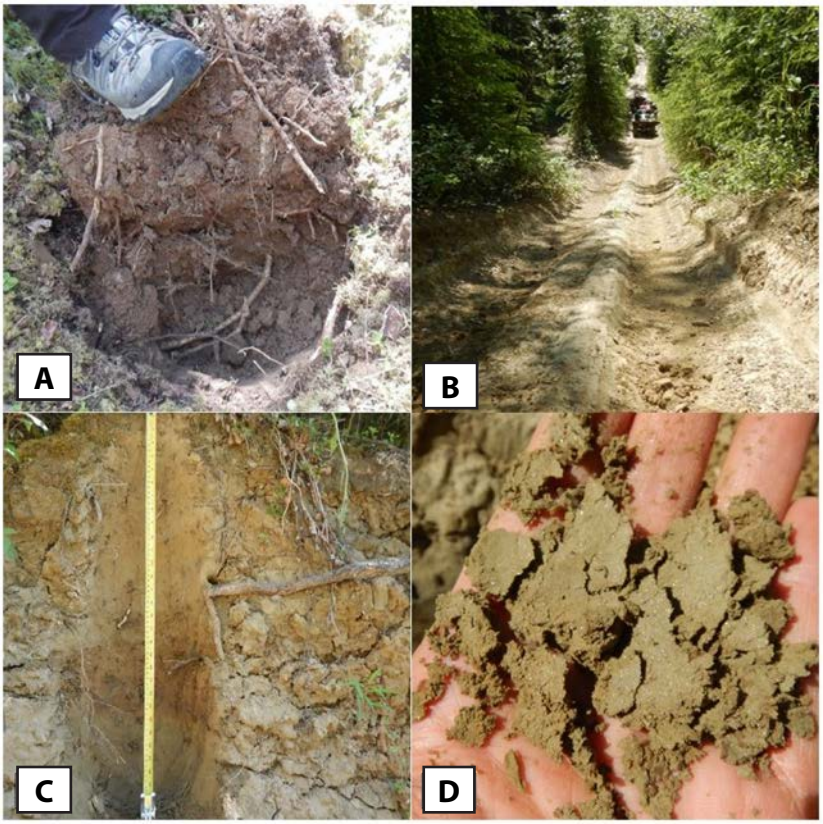

Figure A12. Images of FaiD3_2S_3W_10_NE2 from June 11, 2020. **A.** Test Pit 6 in silt, (**B**) view down the trail that steeply descends a toe bump, (**C**) cleaned silt exposure at the top of the toe bump, and (**D**) close view of the micaceous silt from the silt exposure. Photographs taken by MD and JAS.

LS Name:	*FaiD3_2S_3W_10_NE1*	**Relative Age:**	*Prehistoric (10)*
Date:	*June 11, 2020*	**Material:**	*Earth, silt (10)*
Personnel:	*JAS, MD, RD*	**Movement Type:**	*Flow (10)*

Current Movement: *None*

Total confidence: *10/40 (Low)*

The FaiD3_2S_3W_10_NE2 and FaiD3_2S_3W_10_NE1 landslides are informally referred to as the Quist landslides, due to their proximity to Quist Farm.

We visited the south-east part of the gullied toe deposit (10) after returning from the head scarp region (0). There was no evidence of flanks (0) or internal morphology (0). There were no vegetative movement indicators on this prehistoric feature. We dug a test pit (TP3) between the toe deposits in a gully, which revealed dry to moist silt (field-estimated to have about 5 percent moisture content) above frozen silt. We dug two more test pits, both of which contained silt. We dug TP5 in the gully adjacent to TP3, and encountered frozen silt at depth. Similar to FaiD3_2S_3W_10_NE2, there was significant gullying and rills in the inferred head scarp region (fig. B7). The ground also appeared deflated behind the toe deposit bumps, which were steeper on their distal slopes.

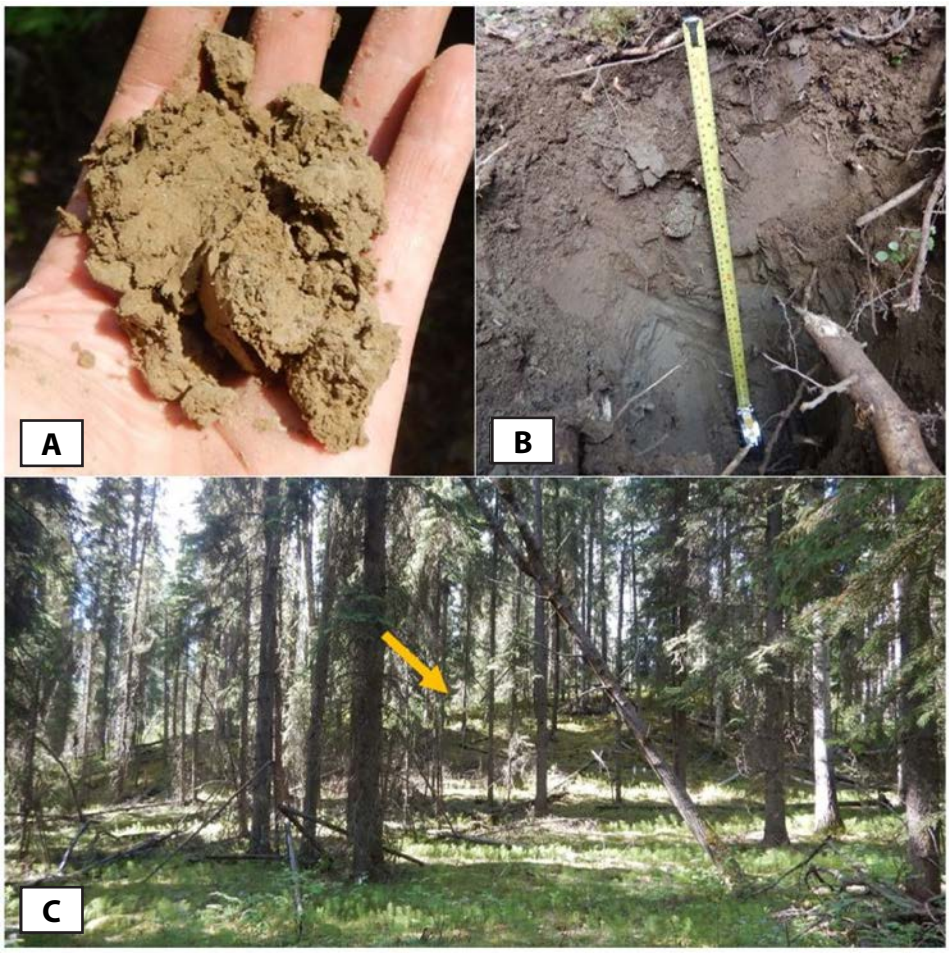

Figure A13. Images of FaiD3_2S_3W_10_NE1 from June 11, 2020. **A.** Silt from TP3, (**B**) TP5 dug in silt to frost depth, and (**C**) view of one of the numerous toe bumps (arrow indicates the upper surface). Photographs taken by MD and JAS.

LS Name:	*FaiC3_2S_4W_32_SW1*	**Relative Age:**	*Prehistoric (10)*
Date:	*June 12, 2020*	**Material:**	*Earth, silt (10)*
Personnel:	*JAS, MD, RD*	**Movement Type:**	*Flow (10)*

Current Movement: *None*

Total confidence: *15/40 (Moderate)*

We began our field investigation at the western-most toe deposit, then hiked along the toe deposits and up the left flank. We later returned to this landslide (fig. B8) via a road along the top of the ridge and hiked down to the head scarp region. The toe deposits (10) were clearly identifiable, but the right flank (0) and head scarp (0) were not. There was evidence of a left flank (5) due to a slope break, along which we identified a dropped block. There were rills and gullying in the inferred head scarp region and along the left flank. There were no internal features of inner morphology (0). We dug test pits at the toe and left flank of the landslide, which revealed only silt; however, there was a bedrock exposure forming a ridge to the east of the landslide.

The morphology of all landslides surveyed on June 12, informally referred to as the Bonanza Creek landslides, varied from the Quist landslides surveyed on June 11. Their toe deposits had more material behind them than the "deflated" Quist toes. We hypothesize that the Bonanza Creek landslides moved due to a flow mechanism, with drier material moving as a competent block (now forming the toe), perhaps rafted on the flowing water-saturated body.

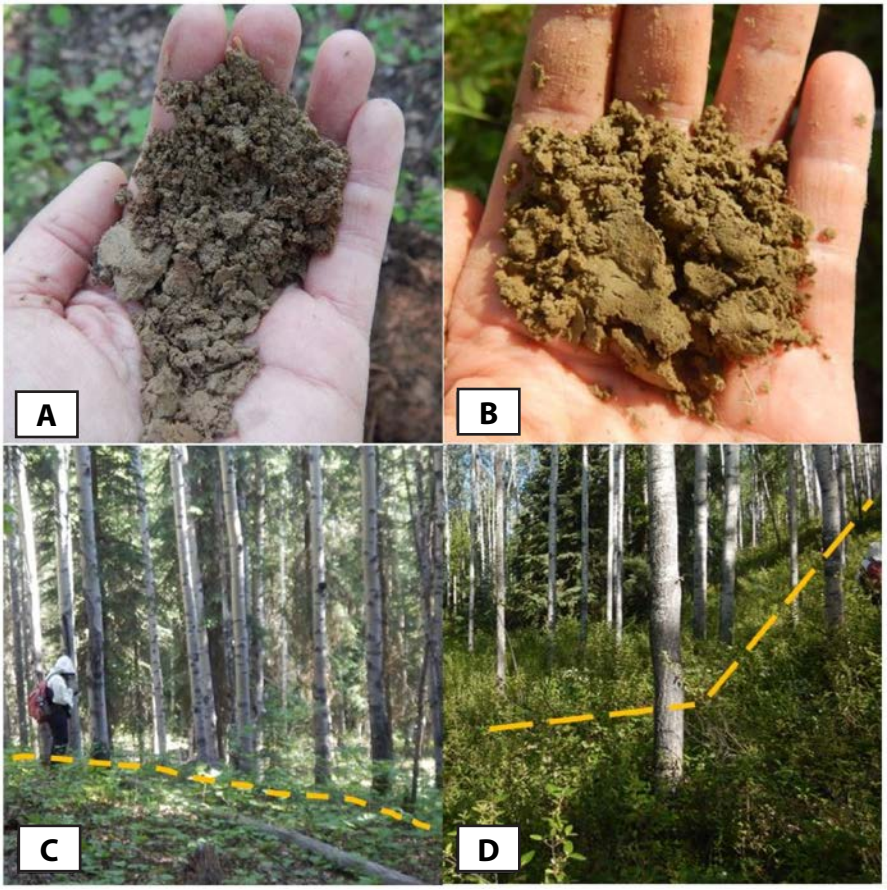

Figure A14. Images of FaiC3_2S_4W_32_SW1 from June 12, 2020. **A.** Silt from a test pit dug on a toe deposit, (**B**) silt from a test pit dug near the left flank, (**C**) JAS standing along the slope break boundary at the end of the toe deposit (dashed line), and (**D**) slope break (dashed line) on a dropped block along the left flank. Photographs taken by MD.

LS Name:	*FaiC3_2S_4W_34_N1*	**Relative Age:**	*Prehistoric (10)*
Date:	*June 12, 2020*	**Material:**	*Earth, silt (10)*
Personnel:	*JAS, MD, RD*	**Movement Type:**	*Flow (10)*

Current Movement: *None*

Total confidence: *10/40 (Low)*

We hiked out from the road to the body of the landslide (fig. B8) toward the toe deposit bumps (10), and walked along them from the center towards the left flank. This was the largest landslide of those at Bonanza Creek, with an arcuate toe that retains material behind it. The inferred headscarp (0) region was characterized by rills and gullying, and no identifiable flanks (0). The vegetation on the toe deposits was typically spruce and moss, and there were no morphological indicators (0) of landslide movement. RD attempted to collect very low frequency (VLF) electromagnetic geophysical data on the landslide body, but the results were inconclusive due to the moisture content of the soil.

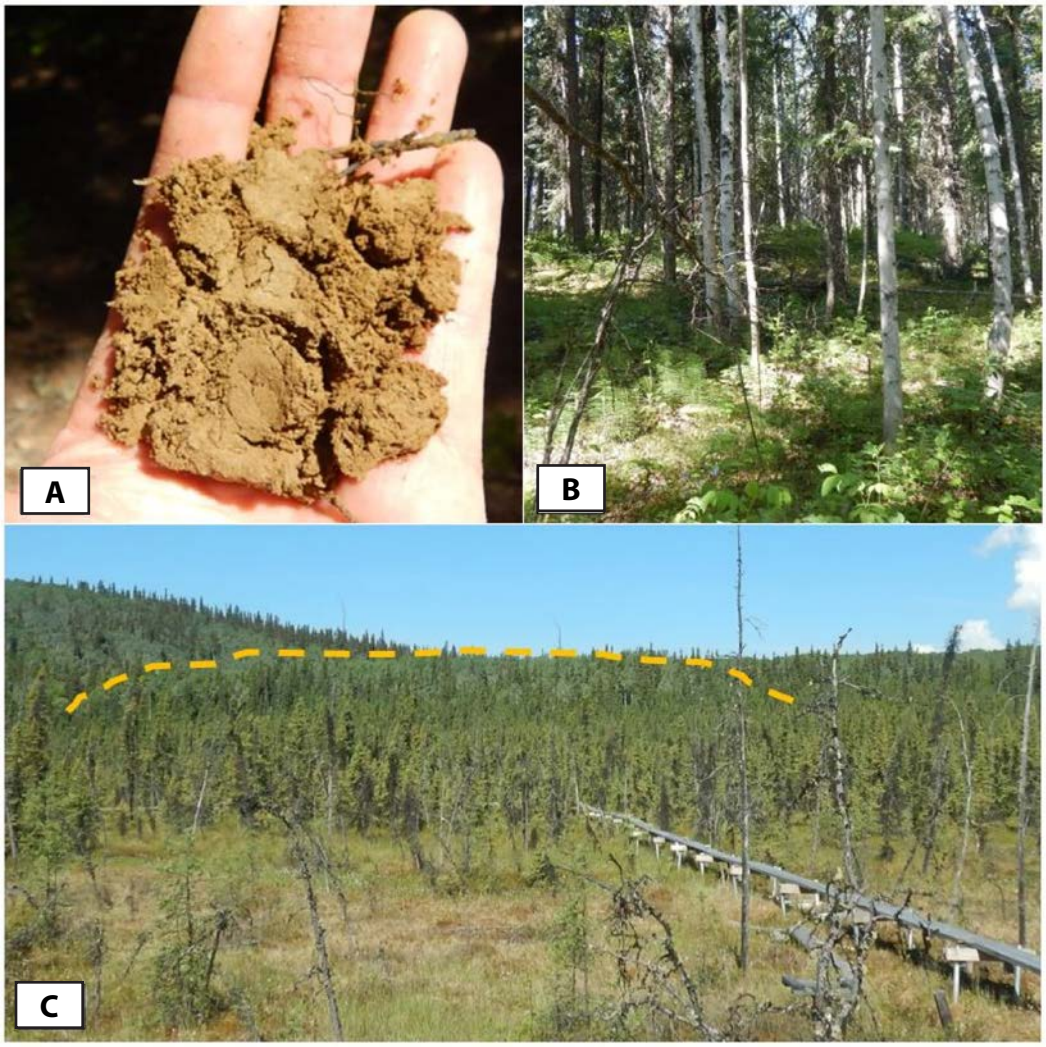

Figure A15. Images of FaiC3_2S_4W_34_N1 from June 12, 2020. **A.** Silt from a test pit dug on a toe deposit, (**B**) view of a toe deposit, and (**C**) view of the toe deposits (location indicated by dashed line) from the fen downslope of the landslide. Photographs taken by MD.

LS Name:	*FaiC3_2S_4W_34_NE1*	**Relative Age:**	*Prehistoric (10)*
Date:	*June 12, 2020*	**Material:**	*Earth, silt (10)*
Personnel:	*JAS, MD, RD*	**Movement Type:**	*Flow (10)*

Current Movement: *None*

Total confidence: *10/40 (Low)*

We hiked toward the toe (10) from the toe deposit bumps of FaiC3_2S_4W_34_N1 and then returned to the road. As with the other Bonanza Creek landslides (fig. B8), there were no discernible flanks (0) or head scarp (0). The inferred head scarp region was characterized by gullying and rills. There was no inner morphology (0) indicative of landslides. This landslide had the smallest toe deposit of the Bonanza Creek slides, and little landslide material was present behind the toe deposit. We dug a test pit on the toe deposit that contained silt. The typical vegetation on the landslide was spruce forest with moss.

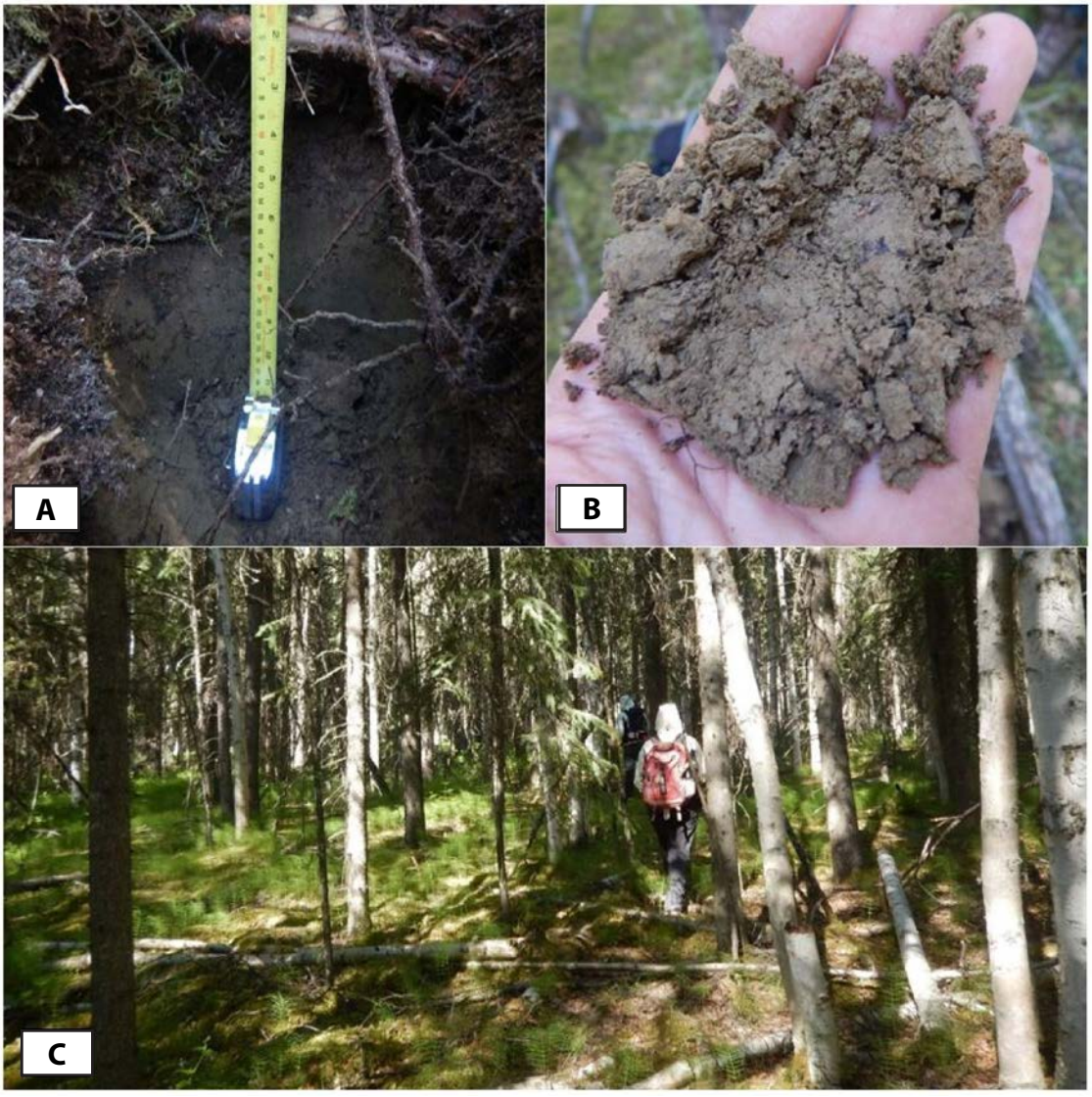

Figure A16. Images of FaiC3_2S_4W_34_NE1 from June 12, 2020. **A.** Test pit dug into silt on a toe deposit, (**B**) silt taken from the test pit in (**A**), and (**C**) JAS and RD amongst the typical vegetation on the toe deposits. Photographs taken by MD and JAS.

LS Name:	*FaiC3_2S_4W_27_SE2*	**Relative Age:**	*Prehistoric (10)*
Date:	*June 12, 2020*	**Material:**	*Earth, silt (10)*
Personnel:	*JAS, MD, RD*	**Movement Type:**	*Flow (10)*

Current Movement: *None*

Total confidence: *11/40 (Moderate)*

We traveled across the front of the toe deposit bumps (10) to the left flank region (1). There was no head scarp (0)—only an inferred head scarp region—and no discernible right flank (fig. B8). The inferred head scarp region was dominated by gullying. The only observable inner morphology (1) indicative of a landslide was small depressions on the toe deposits. Road cuts provided 3-m high silt exposures, which were massive with no structure, within the toe deposits. We cleaned off two silt exposures and collected one soil sample. We dug a test pit that revealed silty soil in front of the toe deposit near the left flank. We hypothesize that these toe deposits are prehistoric; perhaps thousands of years old.

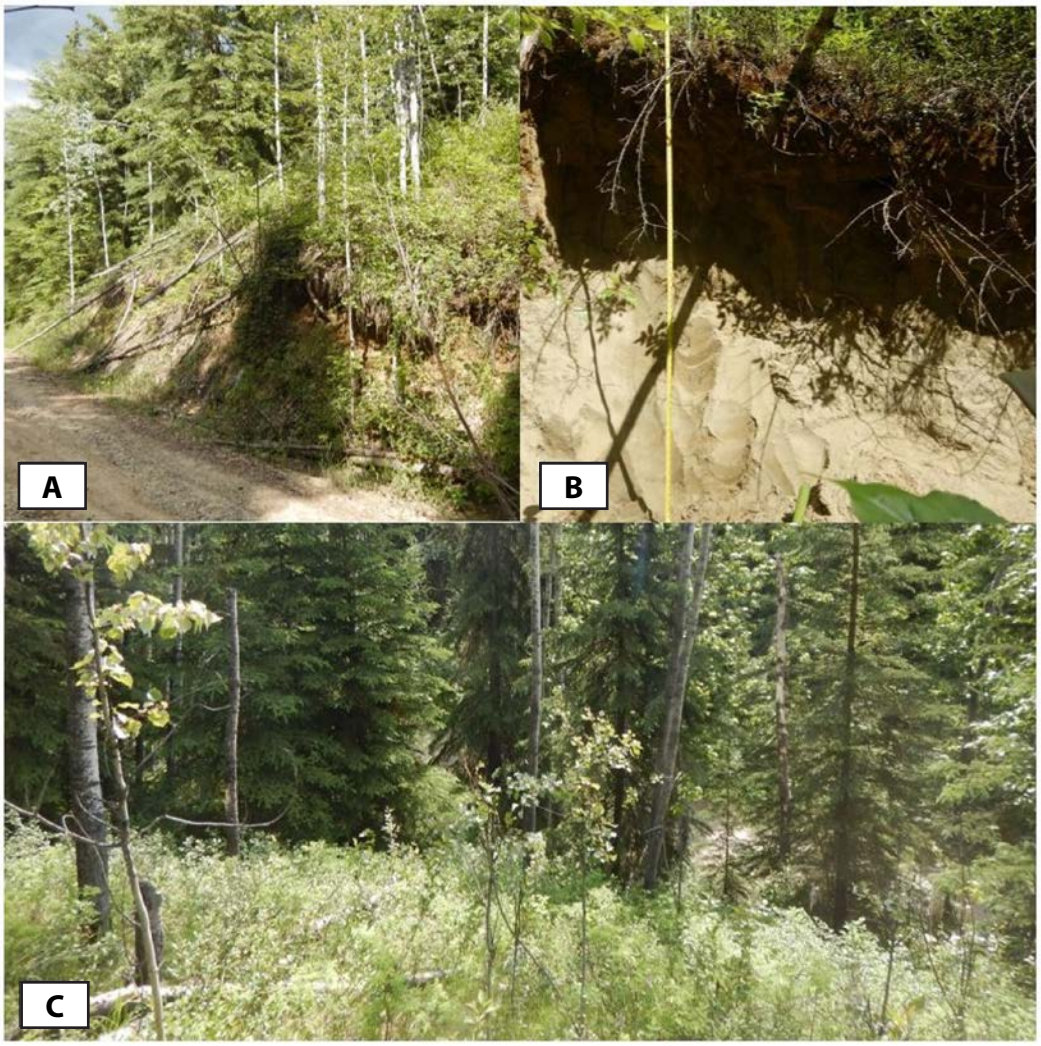

Figure A17. Images of FaiC3_2S_4W_27_SE2 from June 12, 2020. **A.** Silt exposure along the road cutting into the toe deposits, (**B**) cleaned off silt exposure at Site 2, and (**C**) view down the steep distal slope of the toe deposit toward the road. Photographs taken by MD and JAS.

LS Name:	*FaiC3_2S_4W_27_SE1*	**Relative Age:**	*Prehistoric (10)*
Date:	*June 12, 2020*	**Material:**	*Earth, silt (10)*
Personnel:	*JAS, MD, RD*	**Movement Type:**	*Flow (10)*

Current Movement: *None*

Total confidence: *10/40 (Low)*

We traveled along the roads that cross the body of the landslide (fig. B8) and into the head scarp region (0) and hiked to the inferred head scarp region just below the ridge. The toe deposits (10) were clearly identifiable in the lidar imagery, but there were no obvious flanks (0) or inner morphology (0). The head scarp region had severe gullying and rills. We dug a test pit that revealed silty soil.

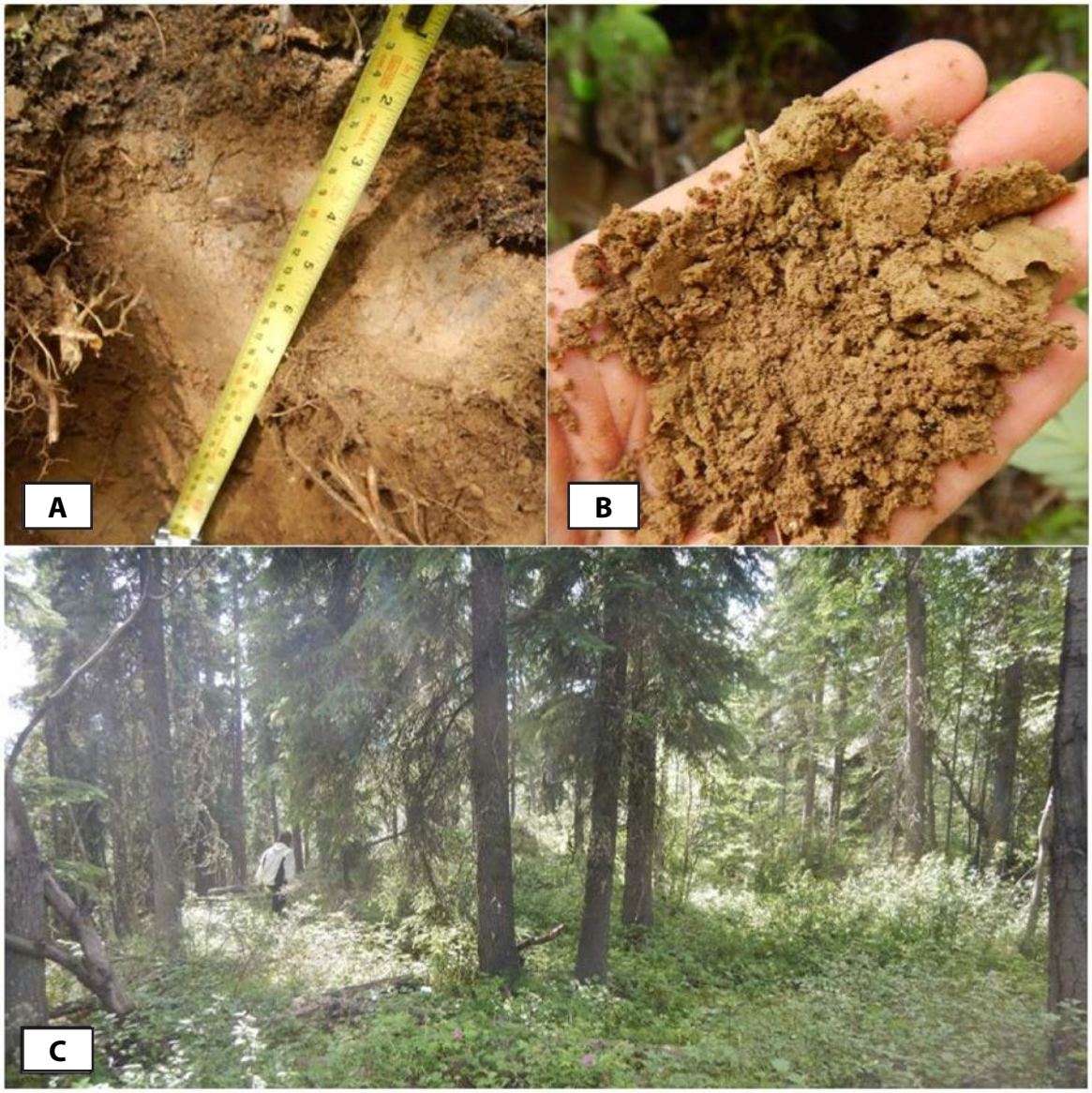

Figure A18. Images of FaiC3_2S_4W_27_SE1 from June 12, 2020. **A.** Test pit in silt dug in the head scarp region, (**B**) silt sample from the test pit, and (**C**) RD and typical vegetation on the upper landslide body near the left flank. Photographs taken by MD and JAS.

LS Name:	*FaiD3_2N_4W_34_SE1*	**Relative Age:**	*Prehistoric (10)*
Date:	*June 15, 2020*	**Material:**	*Bedrock (10)*
Personnel:	*JAS, MD, PP*	**Movement Type:**	*Translational/rotational (5)*

Current Movement: *None*

Total confidence: *28/40 (Moderate)*

We walked along the head scarp (10) and down the body to the left flank (2). We then crossed through the landslide body (fig. B9) toward the right flank (2), then returned to the body and hiked to the toe deposit (7). The flank extents were difficult to delineate due to the landslide's inner roughness. Observed morphology (7) included internal scarps and mid-slope terraces. We observed several displaced rock blocks throughout the landslide body and flanks. The Shovel Creek wildfire of 2019 (DOF, 2019) had burned across the landslide surface, so vegetative indicators were hard or impossible to evaluate. Stretching or cracks in the organic mat may be due to the burn and not indicative of landslide movement. There were multiple bedrock exposures and rock debris across the landslide body and toe. A thin silt layer covered the surface, and the underlying weathered phyllitic bedrock was blocky with its foliation oriented downslope (where in place). We observed a large quartz boulder near the head scarp region (fig. A19A). The roughness of the landslide made it difficult to distinguish between translational and rotational movement.

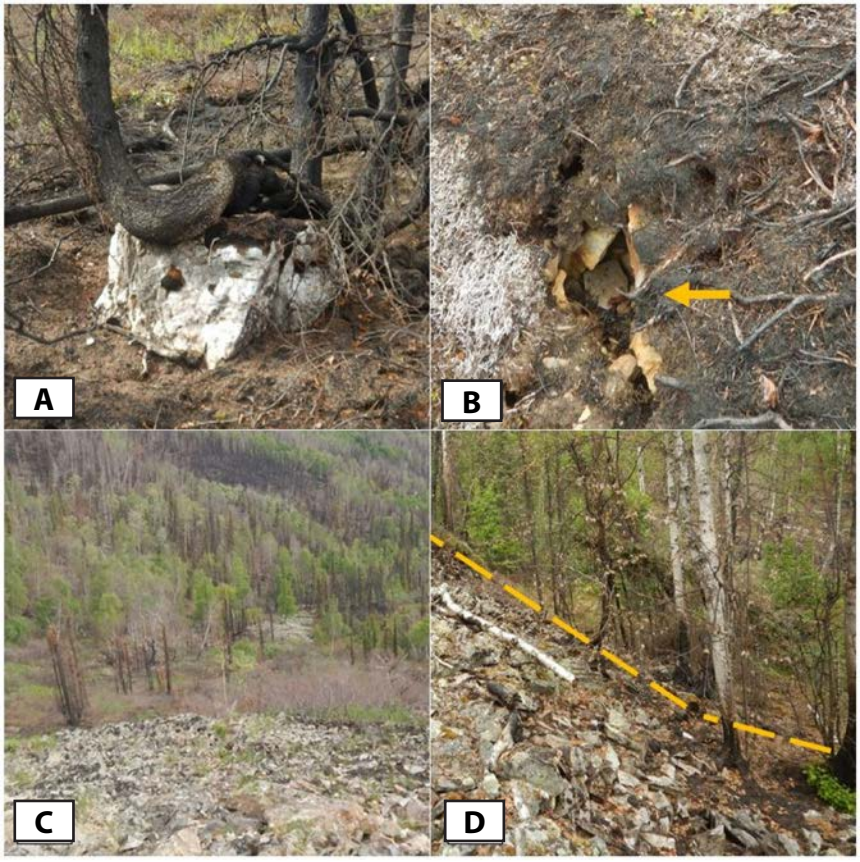

Figure A19. Images of FaiD3_2N_4W_34_SE1 from June 15, 2020. **A.** An exposed quartz boulder near the head scarp region, (**B**) cracks in the vegetation (indicated with arrow) due to the burn or to landslide movement, (**C**) view down the landslide body toward the toe with lichen-covered rock debris, and (**D**) lichen-covered rock debris forming the toe deposit, with slope break indicated by dashed line. Photographs taken by MD and JAS.

LS Name:	*FaiD3_2N_4W_35_SW1*	**Relative Age:**	*Prehistoric (10)*
Date:	*June 15, 2020*	**Material:**	*Bedrock (10)*
Personnel:	*JAS, MD, PP*	**Movement Type:**	*Rotational (5)*

Current Movement: *None*

Total confidence: *11/40 (Moderate)*

We visited the lower left flank (1) and toe (10). We observed a stream along the left flank and a wet, grassy area at the toe. We saw one feature at the toe that may have been a solifluction lobe. The landslide's rough appearance in the lidar is similar to the other two landslides in the vicinity (FaiD3_2N_4W_34_SE1 and FaiD3_2N_4W_35_SE1) (fig. B9).

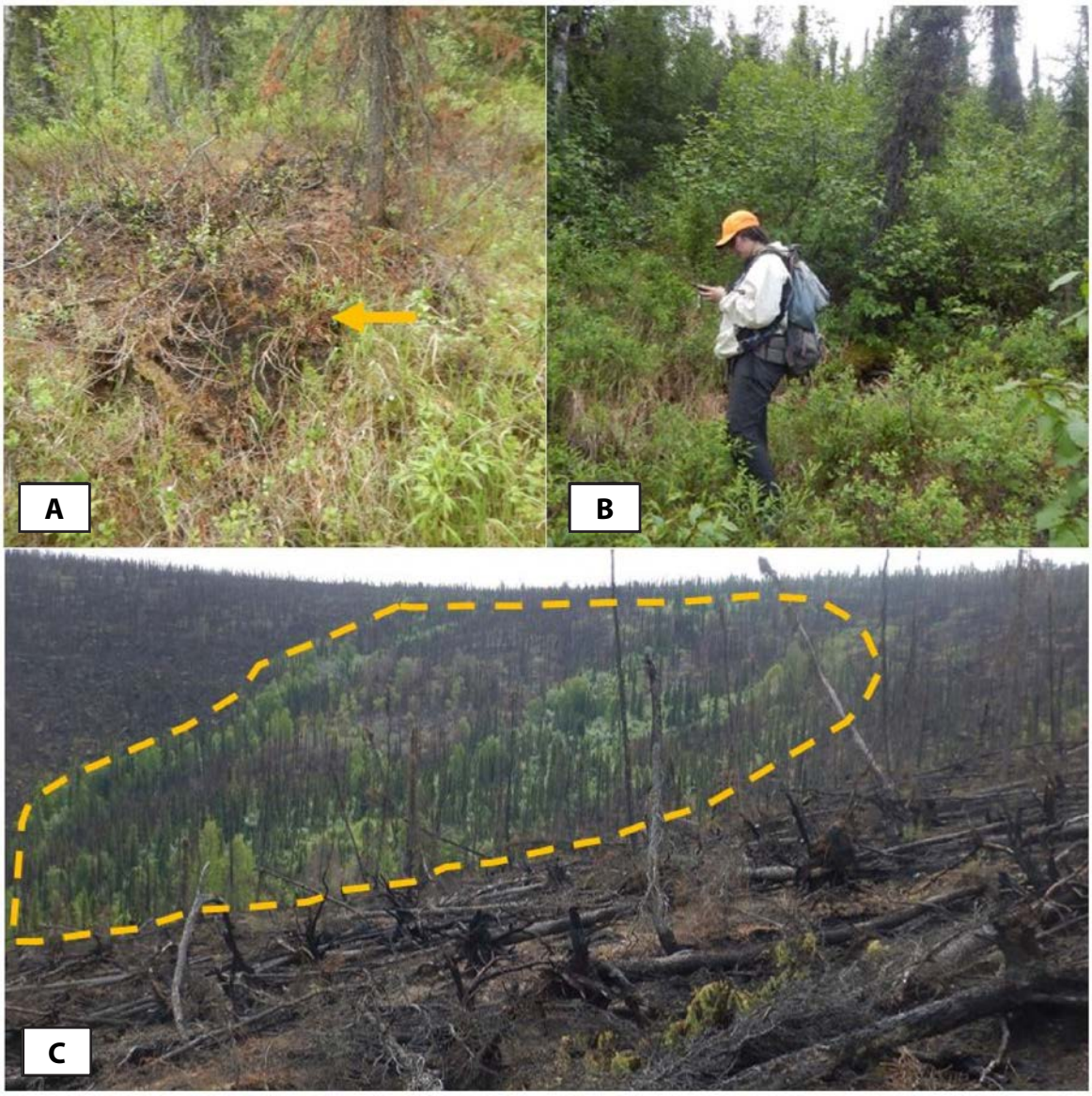

Figure A20. Images of FaiD3_2N_4W_35_SW1 from June 15, 2020. **A.** Possible solifluction lobe along the left flank (indicated by arrow, and burned from recent fire), (**B**) JAS standing in a wet area at the toe, and (**C**) view of the landslide (delineated by dashed line) looking south. Photographs taken by MD.

LS Name:	*FaiD3_2N_4W_35_SE1*	**Relative Age:**	*Prehistoric (10)*
Date:	*June 15, 2020*	**Material:**	*Bedrock (10)*
Personnel:	*JAS, MD, PP*	**Movement Type:**	*Rotational (10)*

Current Movement: *None*

Total confidence: *32/40 (High)*

We hiked upslope from the toe deposits (10) through the landslide body (fig. B9), angling toward the left flank (2) and head scarp region (10). We did not visit the right flank. Internal morphology (10) included internal scarps, a closed depression, mid-slope terraces, and wetlands. We hypothesize that this landslide had rotational movement due to its morphology. The 2019 Shovel Creek Fire (DOF, 2019) burned across this landslide's surface so there were no useful vegetative indicators. There was exposed rock debris at the toe. In the middle of the landslide body, we saw a closed depression and a graben adjacent to a bedrock ridge. On the upper half of the body, we observed that approximately 6 inches of silt overlaid the bedrock. The head scarp was easily identifiable and similar in shape to the landslide we visited along Old Murphy Dome Road (FaiD3_1N_4W_1_NE1). This head scarp was easier to observe in the field due to the lack of moss because of the wildfire.

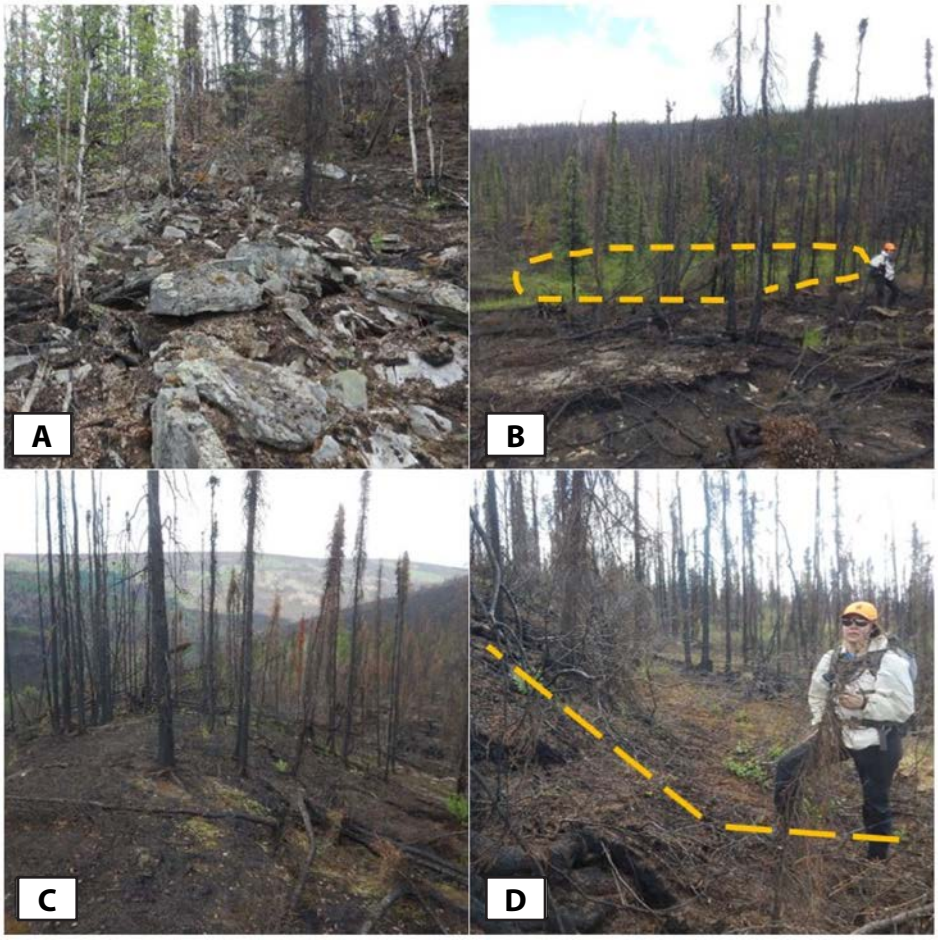

Figure A21. Images of FaiD3_2N_4W_35_SE1 from June 15, 2020. **A.** Looking upslope of the toe deposit covered with weathered rock debris, (**B**) JAS standing in front of a graben (delineated by dashed line) on the landslide body, (**C**) ridge on the landslide body, and (**D**) JAS standing on of the slope break at the head scarp (delineated by dashed line), looking towards the left flank. Photographs taken by MD.

LS Name:	*FaiD2_1N_1W_18_SE1*	**Relative Age:**	*Prehistoric (10)*
Date:	*June 18, 2020*	**Material:**	*Earth, silt (10)*
Personnel:	*JAS, MD*	**Movement Type:**	*Flow (5)*

Current Movement: *None*

Total confidence: *15/40 (Moderate)*

We walked along a trail through the middle of the landslide body (fig. B10) towards the east to visit an inner toe bump, then towards the west and the most distal toe deposits (10), before returning the same way. There were no discernible flanks (0) or head scarp (0) in the lidar, although there were some internal morphological features (5). We saw mid-slope terraces; however, closed depressions and leaning trees also may be due to permafrost degradation in the area. Only the toe deposits were clearly visible, and had interesting shapes. It is possible that pulses of movement resulted in subsequent circular deposits. We dug a test pit at the top of an inner toe deposit, which revealed moist to wet silt frozen at 0.3 m below the ground surface. We dug another test pit in a wet gully in the toe deposit, and intercepted wet silt.

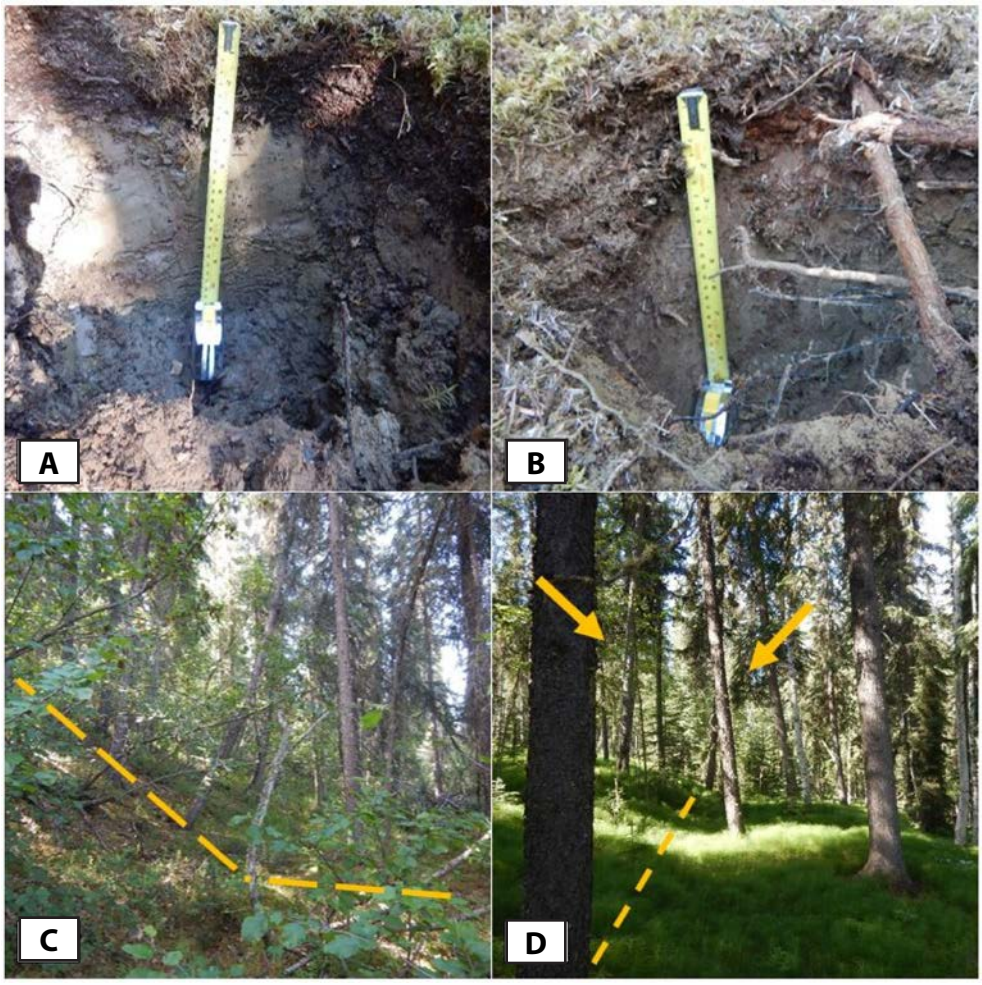

Figure A22. Images of FaiD2_1N_1W_18_SE1 from June 18, 2020. **A.** Silt profile with frozen soil at depth at first inner toe bump to the east, (**B**) silt profile with dry to moist soil on the large, inner toe bump, (**C**) slope break (indicated by dashed line) and leaning trees along the distal slope of a toe bump, and (**D**) leaning trees (indicated by arrows) along a linear feature (indicated by dashed line) on an inner toe bump. Photographs taken by MD and JAS.

LS Name:	*FaiD1_1N_2E_4_W1*	**Relative Age:**	*Prehistoric (10)*
Date:	*June 19, 2020*	**Material:**	*Bedrock (10)*
Personnel:	*JAS, MD, RD*	**Movement Type:**	*Rotational (10)*

Current Movement: *None*

Total confidence: *40/40 (High)*

We hiked down to the head scarp and then followed the landslide extent (fig. B11) from the left flank to the toe, and returned along the right flank. This feature was a rotational slide in schist bedrock, with a well-defined, steep head scarp (10), flanks (10), and toe deposit (10). The toe's distal slope was steep. We observed morphology (10) of hummocky topography and mid-slope terraces. We also observed possible solifluction lobes on the main body. We saw exposed, weathered schist bedrock and rock debris at the surface of the landslide with a thin cover of silt. The vegetation on the landslide was mainly moss and spruce.

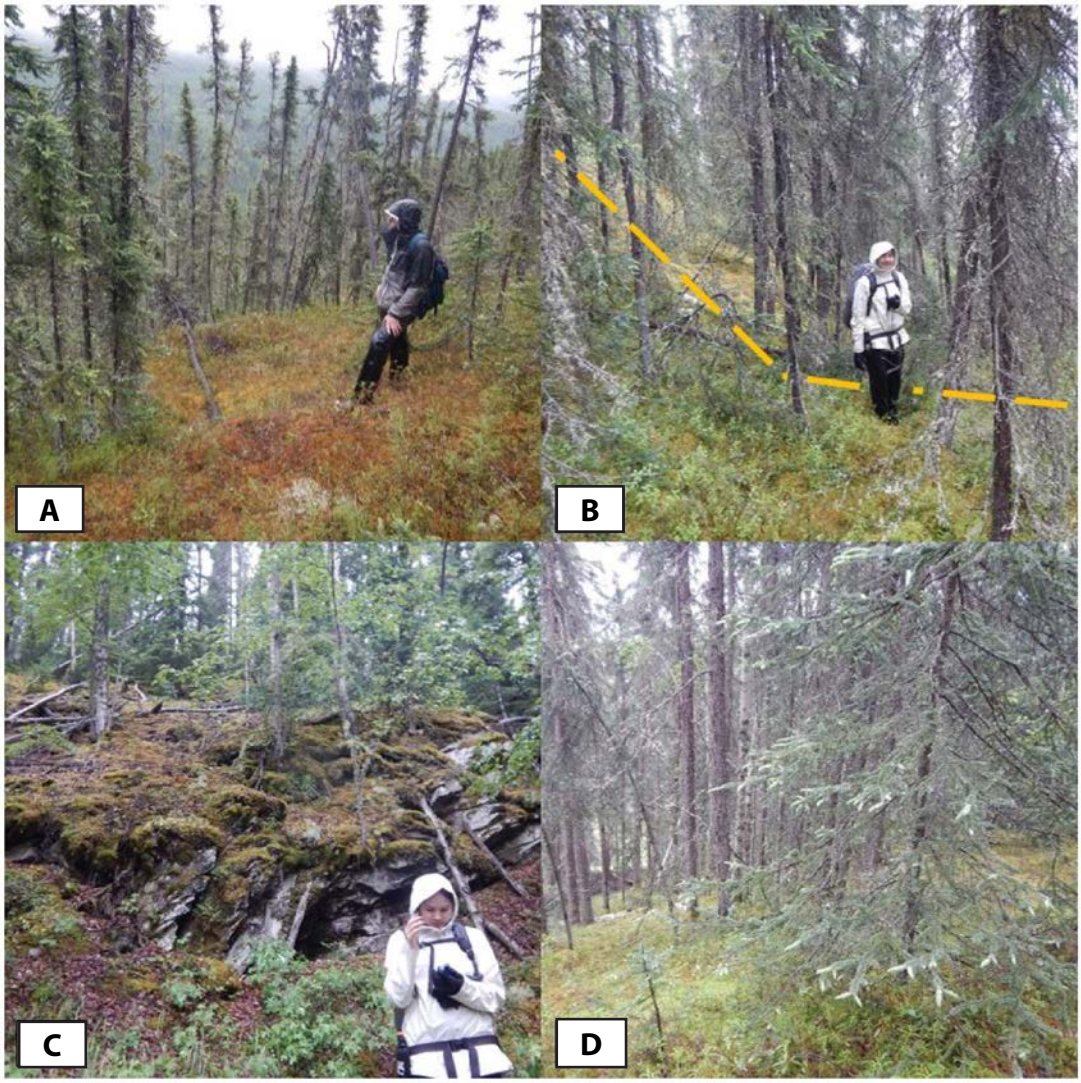

Figure A23. Images of FaiD1_1N_2E_4_W1 from June 19, 2020. **A.** RD standing on hummocky topography on the landslide body, (**B**) JAS standing along the slope break (indicated by dashed line) of the left flank and body, (**C**) JAS standing in front of the steep head scarp with exposed schist bedrock, and (**D**) view down the steep distal slope of the toe. Photographs taken by MD.

LS Name:	*FaiD3_1N_3W_36_NW1*	**Relative Age:**	*Prehistoric (10)*
Date:	*June 24, 2020*	**Material:**	*Bedrock (10)*
Personnel:	*JAS, MD*	**Movement Type:**	*Rotational (10)*

Current Movement: *None*

Total confidence: *31/40 (High)*

We hiked down the head scarp region onto the upper half of the landslide body (fig. B12) and exited the left flank to an adjacent landslide (FaiD3_1N_3W_35_NE1). We returned from the toe deposits along the right flank and crossed through the middle body back upslope. The toe deposits were easily identifiable (10) as was the right flank (5). The left flank (1) was difficult to distinguish from the extent of FaiD3_1N_3W_35_NE1, and although the head scarp (7) was subtle in the lidar, it was discernible by small slope breaks in the field. The internal roughness (8) indicated rocky debris. We saw several rock debris exposures near the toe and right flank. The vegetation changed from an open forest of mature poplar, grasses, and alder on the central body to black spruce with mossy cover at the head scarp and toe deposits. There was a relatively flat region below the head scarp that supported a forest with little understory, possibly due to better drainage. We also observed some benching on the landslide body.

Figure A24. Images of FaiD3_1N_3W_36_NW1 from June 24, 2020. **A.** JAS standing in a rocky area along the right flank, (**B**) JAS hiking upslope toward a bench on the landslide body (slope break indicated by dashed line), and (**C**) typical vegetation of poplar, grasses, and low brush in the center of the landslide. Photographs taken by MD.

LS Name:	*FaiD3_1N_3W_35_NE1*	**Relative Age:**	*Prehistoric (10)*
Date:	*June 24, 2020*	**Material:**	*Bedrock (10)*
Personnel:	*JAS, MD*	**Movement Type:**	*Rotational (5)*

Current Movement: *None*

Total confidence: *34/40 (High)*

We hiked to the head scarp and traveled along it toward the left flank, then went down across the landslide body (fig. B12) toward the toe. The head scarp (10) and toe deposits (10) were distinct, as was the left flank (5) but the right flank (1) was harder to identify. There was internal roughness on the landslide body (8). We observed weathered rock debris on the landslide surface, as well as a bedrock ridge along the left side; this may delineate the landslide extent along the left flank. All of the bedrock we observed was schist. The vegetative indicators of movement were areas with a stretched vegetation mat and some leaning trees; however, the leaning trees also may be due to permafrost degradation. The forest transitioned from white to black spruce with mossy cover from the head scarp to the toe. The rocky areas of the landslide body were vegetated with poplar. Due to the presence of schist bedrock, we hypothesize that the movement type is rotational.

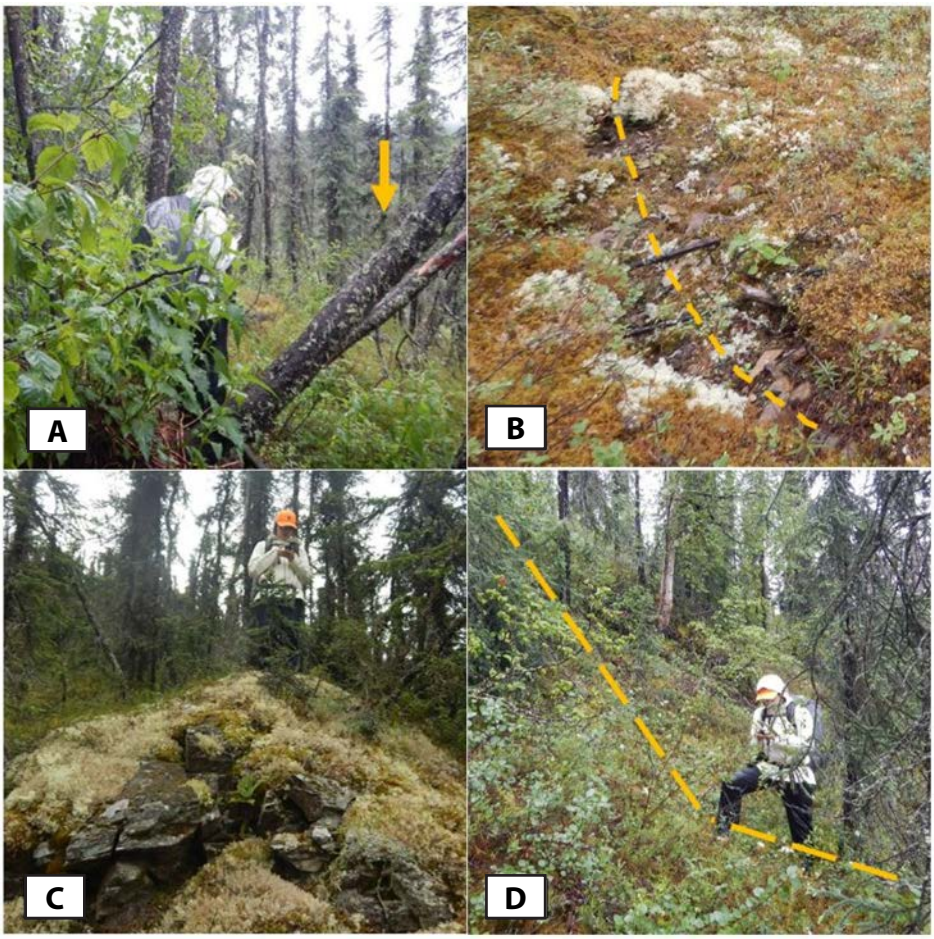

Figure A25. Images of FaiD3_1N_3W_35_NE1 from June 24, 2020. **A.** JAS standing in front of some leaning trees (indicated by arrow) at the head scarp, which may be related to permafrost degradation, (**B**) stretched organic mat (delineated by dashed line) near the head scarp revealing rocky debris underneath, (**C**) JAS standing on an exposed bedrock ridge near the left flank, and (**D**) JAS standing along a steep slope break (indicated by dashed line) near the left flank. Photographs taken by MD.

LS Name:	*FaiD3_1N_4W_3_NW1*	**Relative Age:**	*Prehistoric (10)*
Date:	*June 25, 2020*	**Material:**	*Bedrock (10)*
Personnel:	*JAS, MD*	**Movement Type:**	*Rotational (5)*

Current Movement: *None*

Total confidence: *30/40 (High)*

We hiked down to the head scarp (10) then walked along the upper right flank (5). We did not go to the left flank or cross most of the landslide body (fig. B13). We visited FaiD3_1N_4W_3_SW1 and then returned to the toe deposit (10). Regarding morphology (5), we observed down-dropped blocks and corresponding depressions on the upper half of the landslide body. We saw some jayed trees, but these were likely due to growing on a steep slope of the right flank and not indicative of landslide movement. We saw exposed schist bedrock on the landslide surface along the right flank. We also dug a small test pit that revealed rock debris. The landslide surface was wet, and we observed active creeks in the valley bottoms. The wetness may not be typical, as we did this survey after a record rainfall. We observed exposed bedrock in the active creeks and toe. Vegetation varied from grass, ferns, and dwarf birch to spruce and moss.

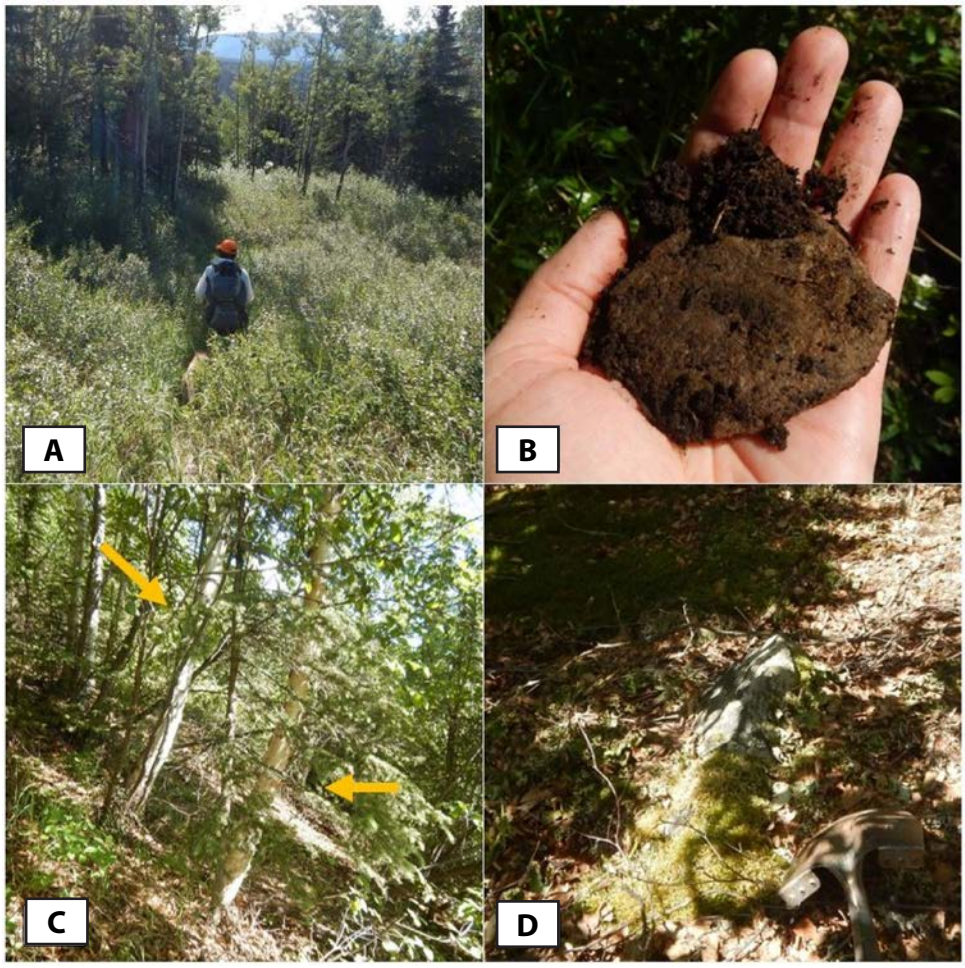

Figure A26. Images of FaiD3_1N_4W_3_NW1 from June 25, 2020. **A.** JAS standing on a down-dropped block, (**B**) rock piece found in a soil pit dug along the right flank, (**C**) steep slope with jayed trees (indicated by arrows) along the right flank, and (**D**) exposed weathered bedrock along the right flank. Photographs taken by MD.

LS Name:	*FaiD3_1N_4W_3_SW1*	**Relative Age:**	*Prehistoric (10)*
Date:	*June 25, 2020*	**Material:**	*Bedrock (5)*
Personnel:	*JAS, MD*	**Movement Type:**	*Rotational (5)*

Current Movement: *None*

Total confidence: *25/40 (Moderate)*

We hiked to the head scarp (10) and upper left flank (5), then went to the middle body and down to the toe (5). The toe deposit was difficult to identify in the field. We did not visit the right flank. Inner morphology (5) included internal roughness and a wet and grassy depression. There were some leaning trees near the toe. We saw mostly paper birch and aspen on the landslide body. We dug a test pit that revealed silt and rock debris. This landslide (fig. B13) appeared to contain more silt than FaiD3_1N_4W_3_NW1.

Figure A27. Images of FaiD3_1N_4W_3_SW1 from June 25, 2020. **A.** A soil pit with silt and rock debris dug near the left flank, (**B**) rock debris and silt found in a tree throw on the landslide body, and (**C**) leaning trees (indicated by arrows) near the toe region. Photographs taken by MD and JAS.

LS Name:	*FaiD3_1N_4W_3_NE1*	**Relative Age:**	*Prehistoric (10)*
Date:	*June 25, 2020*	**Material:**	*Bedrock (5)*
Personnel:	*JAS, MD*	**Movement Type:**	*Rotational (5)*

Current Movement: *None*

Total confidence: *26/40 (Moderate)*

We started at the toe (7), hiked upslope to the lower body and then went to the left flank (4) and head scarp region (7). We did not survey the right flank. Inner morphology (8) included several slope breaks in the landslide body and down-dropped blocks, that produced surface roughness. We saw exposed weathered bedrock at the surface and observed silt and rock debris in a tree throw. The landslide body (fig. B13) was wet, especially near the left flank.

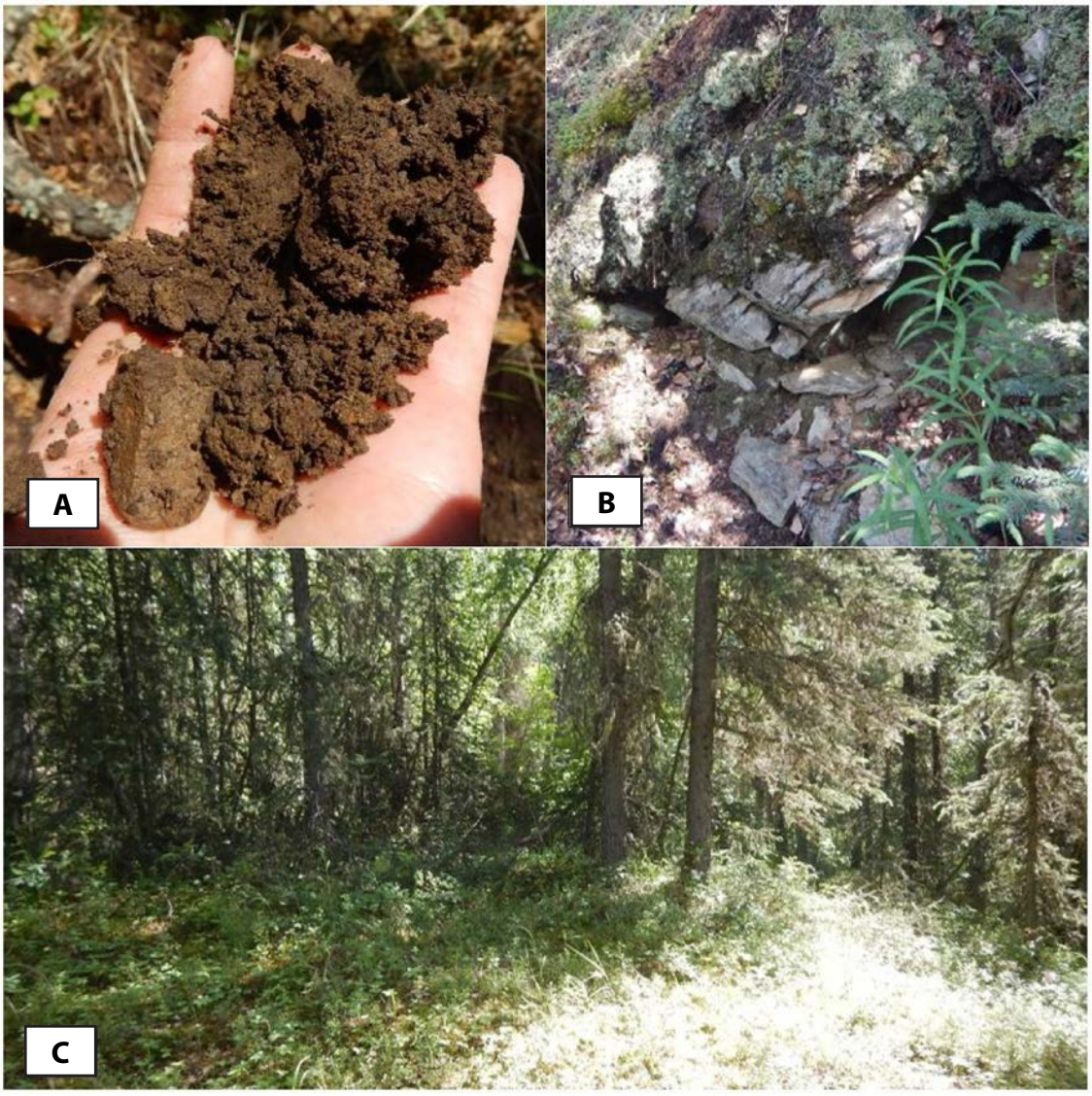

Figure A28. Images of FaiD3_1N_4W_3_NE1 from June 25, 2020. **A.** Rocks and silt in a tree throw at the head scarp, (**B**) exposed weathered bedrock on the landslide body, and (**C**) a relatively flat area near a slope break on the landslide body. Photographs taken by MD.

LS Name:	*LivA1_5N_3E_36_NE1*	**Relative Age:**	*Prehistoric (10)*
Date:	*June 26, 2020*	**Material:**	*Bedrock (10)*
Personnel:	*JAS, MD*	**Movement Type:**	*Rotational (5)*

Current Movement: *None*

Total confidence: *30/40 (High)*

We walked along a road that cuts through the upper half of the landslide body (fig. B14A), and then went upslope toward the head scarp. We hiked along the head scarp, had a brief encounter with two bears that shortened our duration there, and then returned to the road. We then went along the lower half of the body toward the toe and lower left flank. The head scarp (10), toe deposits (10), and left flank (5) were easily identifiable. We did not visit the right flank in the field. The landslide body is well-defined in the lidar, but less so in the field (5). The surface is indicative of bedrock, and we saw a large weathered boulder, and rock debris at several sites on the landslide body and in the head scarp area. There was evidence of several down-dropped blocks on the landslide body. We hypothesize that the movement type is rotational. We estimate that the landslide is prehistoric in age and predates the infrastructure crossing it. Landslide features were less obvious on the lower half of the body.

Figure A29. Images of LivA1_5N_3E_36_NE1 from June 26, 2020. **A.** A large boulder at the head scarp area, (**B**) rock debris in a tree throw near the head scarp, (**C**) JAS standing at the head scarp, and (**D**) JAS standing on a slope break (indicated by dashed line) along the left flank. Photographs taken by MD.

LS Name:	*CirA6_5N_4E_32_NW1*	**Relative Age:**	*Prehistoric (10)*
Date:	*June 26, 2020*	**Material:**	*Bedrock (10)*
Personnel:	*JAS, MD*	**Movement Type:**	*Rotational (5)*

Current Movement: *Yes, at the toe*

Total confidence: *19/40 (Moderate)*

From the road, we hiked down the left flank (5), followed the body and toe deposits (10) along the Chatanika River, and returned upslope along the right flank (1). We did not visit the head scarp (0) because it was on private property. We observed tension cracks and stretched vegetation due to river erosion undercutting the toe (3). The age is prehistoric overall, but there is historic evidence of movement at the toe. The vegetation changed as we moved downslope, from birch boreal forest to black spruce and moss cover. The landslide body (fig. B14B) was mostly dry. We saw several rock debris exposures and schist bedrock outcrops, which may be large displaced rock slabs. There was a silt exposure near a down-dropped block on the left flank. We took two samples from the silt exposure, one of a gray ash layer and another of a brown organic layer. This material may have moved as a cohesive block within the landslide.

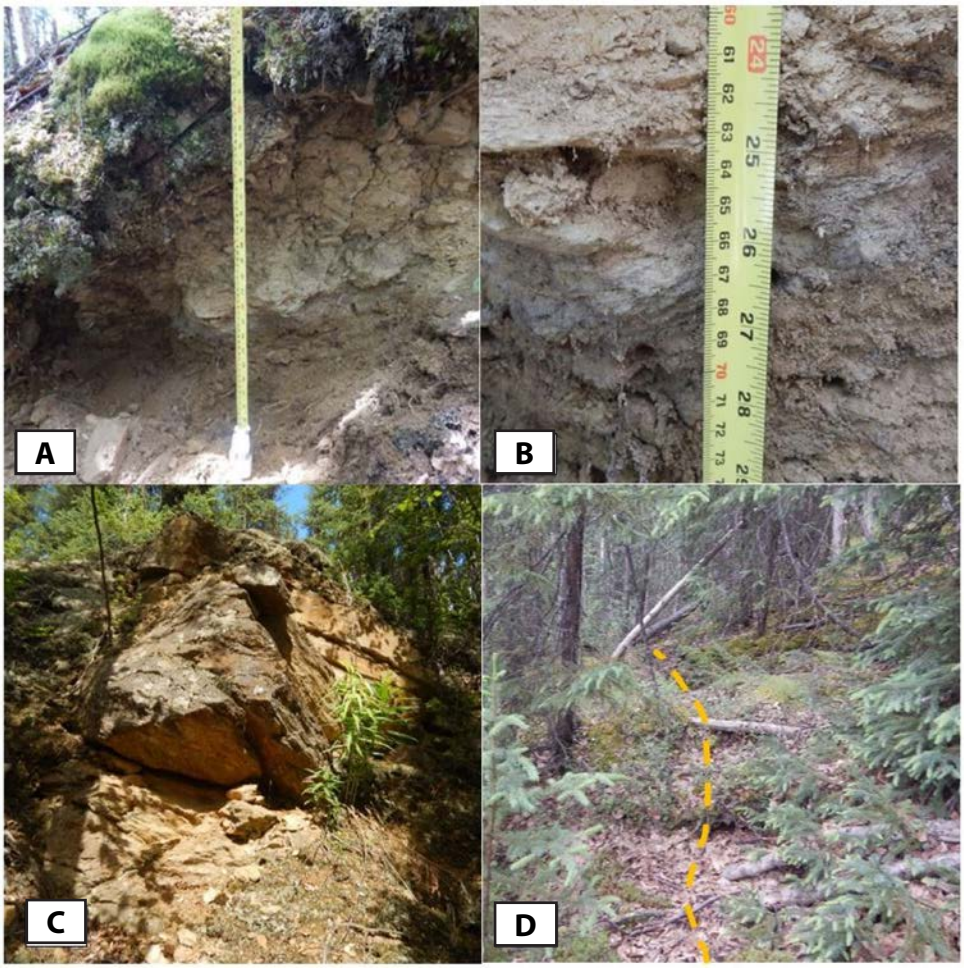

Figure A30. Images of CirA6_5N_4E_32_NW1 from June 26, 2020. **A.** Silt exposure with gray-white ash layer along the left flank, (**B**) closer image of the gray-white ash layer in place, (**C**) possible schist bedrock outcrop along the toe, and (**D**) view down a tension crack (indicated by dashed line) with vegetation stretching near the toe. Photographs taken by MD and JAS.

LS Name:	*BigB5_7S_7E_21_SW5*	**Relative Age:**	*Historic (10)*
Date:	*July 1, 2020*	**Material:**	*Bedrock (10)*
Personnel:	*JAS, MD, PP*	**Movement Type:**	*Translational (10)*

Current Movement: *None*

Total confidence: *40/40 (High)*

This landslide (fig. B15A) is part of a landslide complex that includes BigB5_7S_7E_21_SW4, BigB5_7S_7E_21_SW6, and BigB5_7S_7E_21_SW7.

We hiked upslope along the left flank (5) and visited the head scarp region (10). We later visited the toe deposit region (10), which is part of the landslide complex. The right flank (5) was visible from the road. Internal morphology (10) included internal scarps, cracks, and exposed rock debris. The landslide was well-drained with no standing water. This landslide was documented as a historic, translational slide that required mitigation to protect the Richardson Highway at Milepost 296. We did not observe any indicators of deep-seated movement since mitigation. We saw some indicators of surficial movement near the head scarp in alluvium.

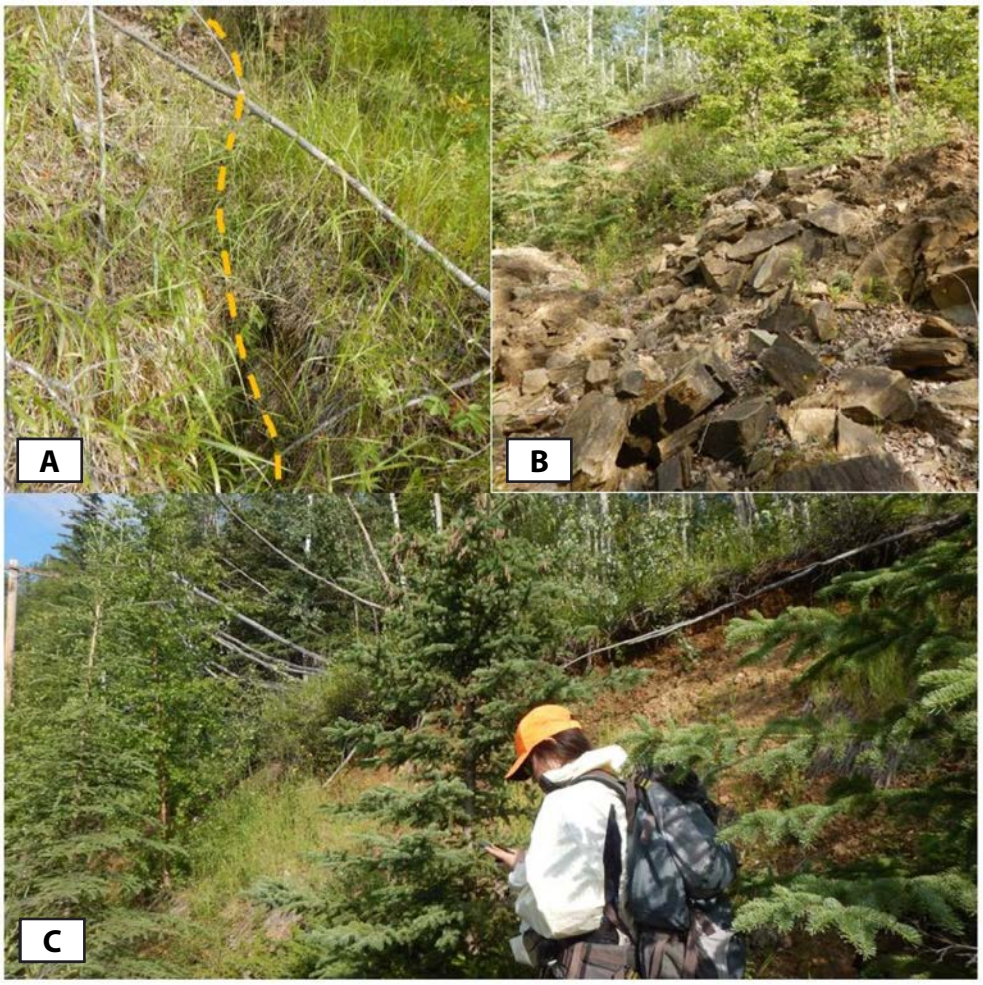

Figure A31. Images of BigB5_7S_7E_21_SW5 from July 1, 2020. **A.** Crack (indicated by dashed line) in the vegetation near the head scarp, (**B**) rock debris near the head scarp, and (**C**) JAS standing at the head scarp. Photographs taken by MD.

LS Name:	*BigB5_7S_7E_21_SW4*	**Relative Age:**	*Prehistoric (10)*
Date:	*July 1, 2020*	**Material:**	*Bedrock (10)*
Personnel:	*JAS, MD, PP*	**Movement Type:**	*Translational (5)*

Current Movement: *None*

Total confidence: *38/40 (High)*

This landslide (fig. B15A) is part of a landslide complex that includes BigB5_7S_7E_21_SW5, BigB5_7S_7E_21_SW6, and BigB5_7S_7E_21_SW7.

We hiked upslope through the landslide body and left flank (5) toward the head scarp region (10), and then later visited the toe deposit region (10) of the landslide complex. The right flank (5) is also shared within the landslide complex. Internal morphology (8) included internal roughness due to down-dropped blocks on the upper landslide body just below the head scarp. Above the head scarp, the slope evened out to a uniform, flatter grade than the landslide body.

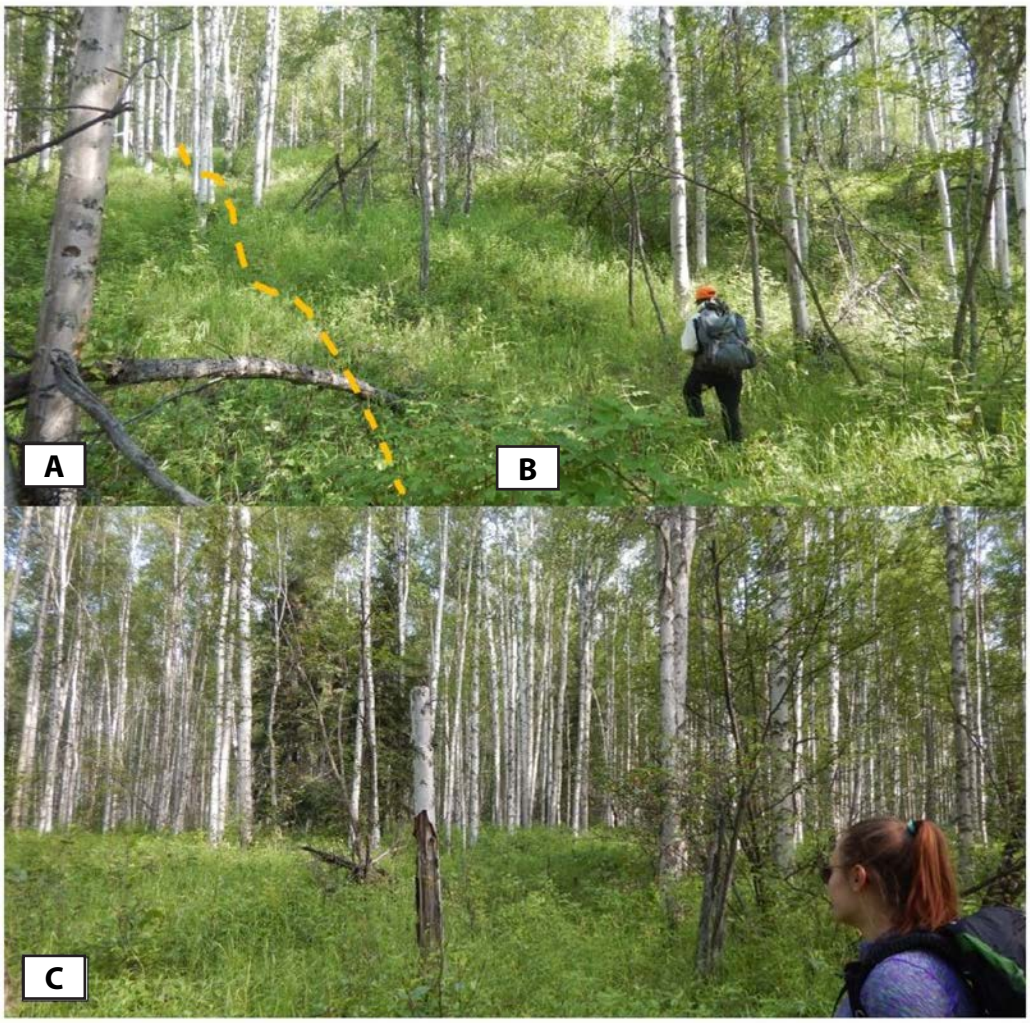

Figure A32. Images of BigB5_7S_7E_21_SW4 from July 1, 2020. **A.** JAS hiking upslope toward down-dropped blocks near the head scarp (slope breaks indicated by dashed line), and (**B**) PP looking toward the uniform, flatter slope above the head scarp. Photographs taken by MD.

LS Name:	*BigB5_7S_7E_21_SW8*	**Relative Age:**	*Prehistoric (10)*
Date:	*July 1, 2020*	**Material:**	*Bedrock (10)*
Personnel:	*JAS, MD, PP*	**Movement Type:**	*Rotational/translational (5)*

Current Movement: *Yes*

Total confidence: *30/40 (High)*

We walked along the head scarp region (9) from east to west, then hiked across the lower landslide body and toe deposit region (7) from the west to the east. The extent of the left flank (5) was easier to identify than the right flank (2), as there was a boundary break with another landslide complex. Inner morphological features (7) included internal scarps and slides with fresh soil exposed. We observed from the road some historic and current scarps in the upper landslide body, but we estimate that the main landslide (fig. B15A) is prehistoric in age. The head scarp was vegetated with straight, mature spruce trees.

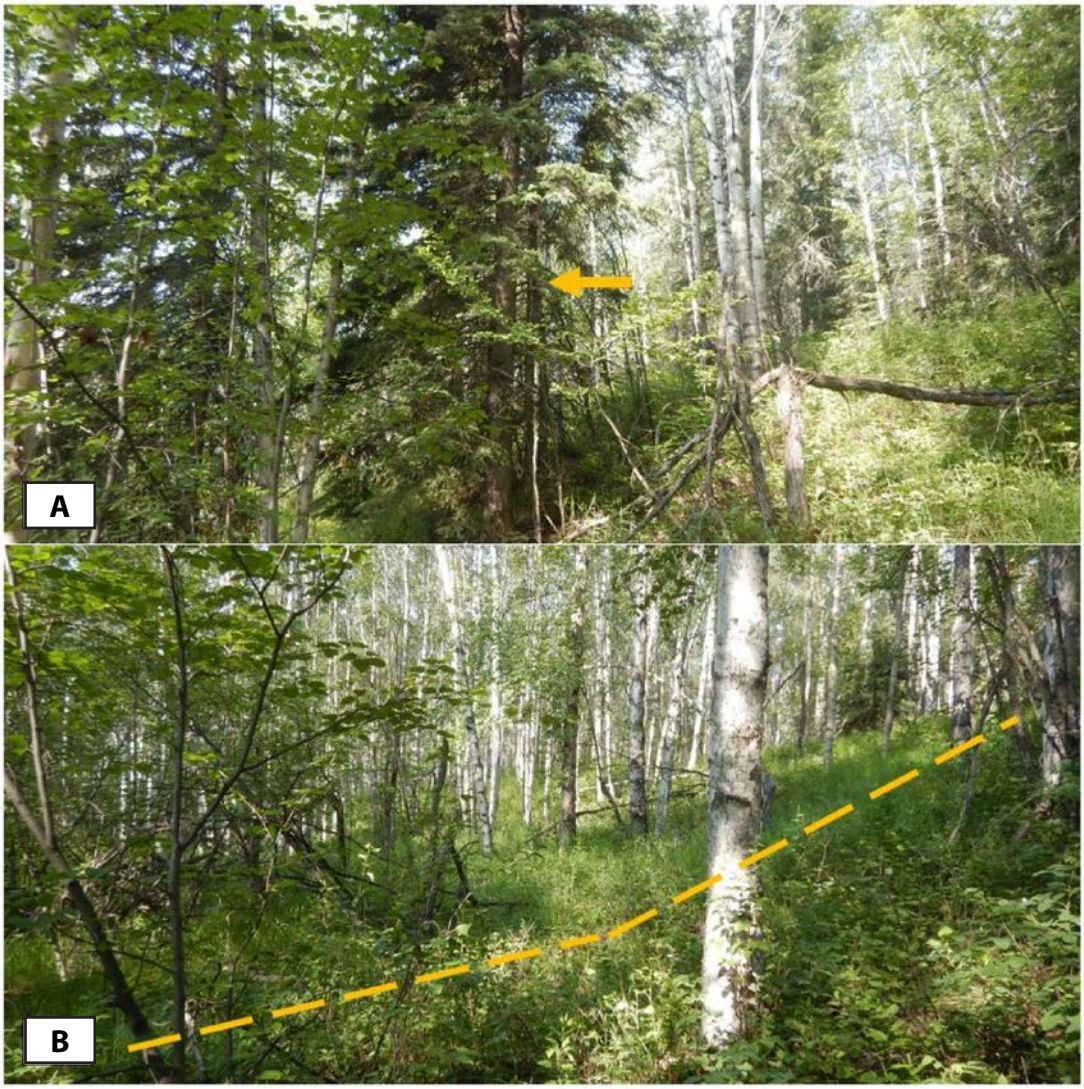

Figure A33. Images of BigB5_7S_7E_21_SW8 from July 1, 2020. **A.** A straight, mature spruce (arrow indicates location) growing at the head scarp, and (**B**) view to the west walking along the head scarp (slope break indicated by dashed line). Photographs taken by MD.

LS Name:	*BigB5_7S_7E_20_SE2*	**Relative Age:**	*Historic (10)*
Date:	*July 1, 2020*	**Material:**	*Earth, alluvium (10)*
Personnel:	*JAS, MD, PP*	**Movement Type:**	*Flow/Rotational (5)*

Current Movement: *Yes*

Total confidence: *28/40 (Moderate)*

We hiked down to the head scarp (10) and continued downslope along the left flank (5) toward the toe deposit region (10) of the landslide (fig. B15A). We did not visit the right flank. There was minor evidence (e.g., rock debris) of inner morphological features (3). We observed bare soil (alluvium) at the head scarp region, and found rock debris on the landslide body.

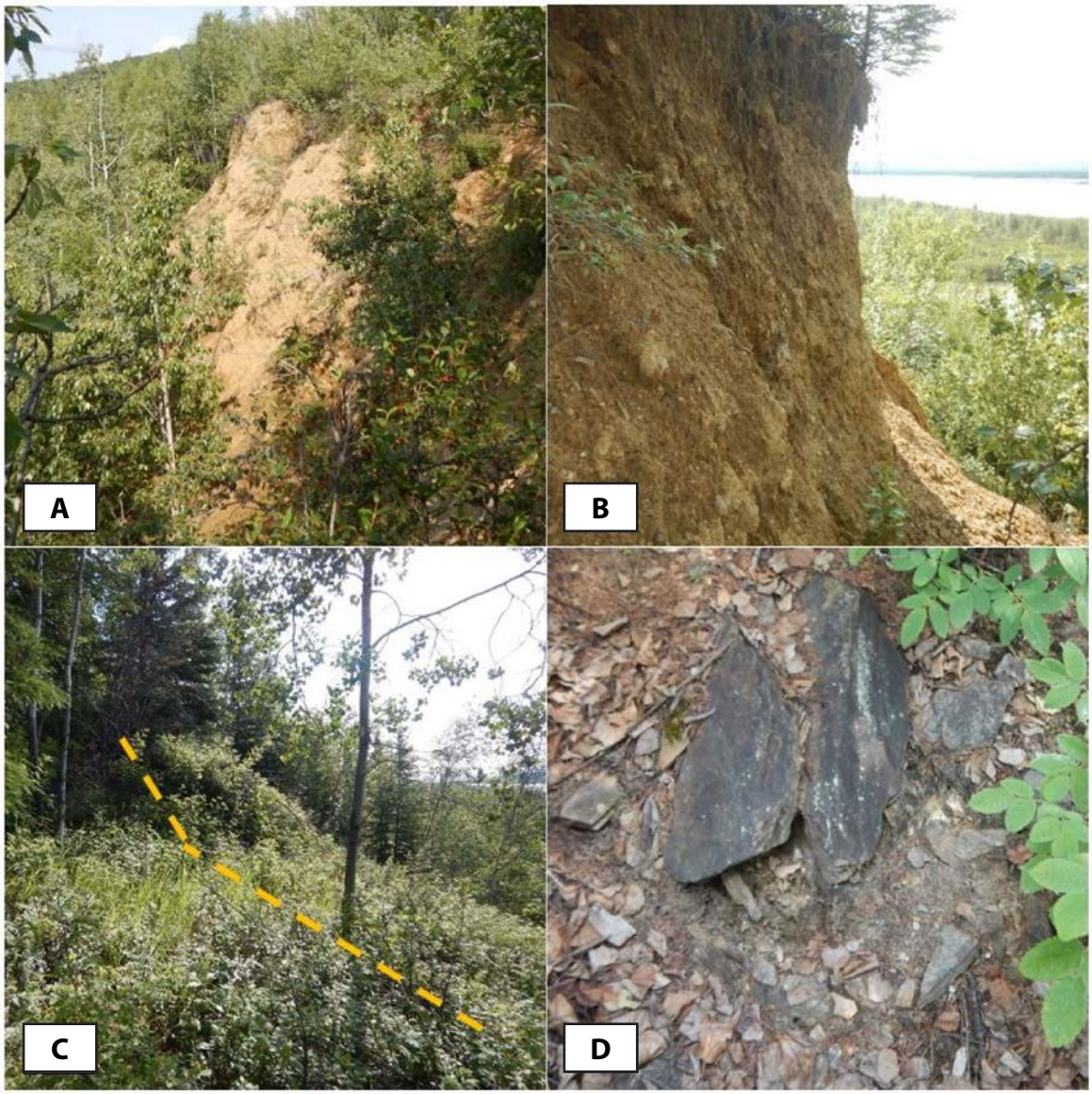

Figure A34. Images of BigB5_7S_7E_20_SE2 from July 1, 2020. **A.** Head scarp with exposed soil, (**B**) closer image of the head scarp in alluvium, (**C**) the left flank of the landslide (slope break indicated by dashed line), and (**D**) exposed rock debris on the landslide body surface. Photographs taken by MD.

LS Name:	*BigB5_7S_7E_20_SE1*	**Relative Age:**	*Historic (10)*
Date:	*July 1, 2020*	**Material:**	*Earth, alluvium (10)*
Personnel:	*JAS, MD, PP*	**Movement Type:**	*Flow/Rotational (5)*

Current Movement: *None*

Total confidence: *35/40 (High)*

We began at the head scarp region (10), hiked downslope along the right flank (5), then crossed through the lower landslide body (fig. B15A) and toe deposit (10) and returned to the left flank (5). Inner morphological features (5) included cracks in the alluvium and some surface roughness. Vegetative indicators of movement included jayed and leaning trees on the lower landslide body and toe. We saw fresh soil exposures at the head scarp, which may indicate surficial movement on the landslide.

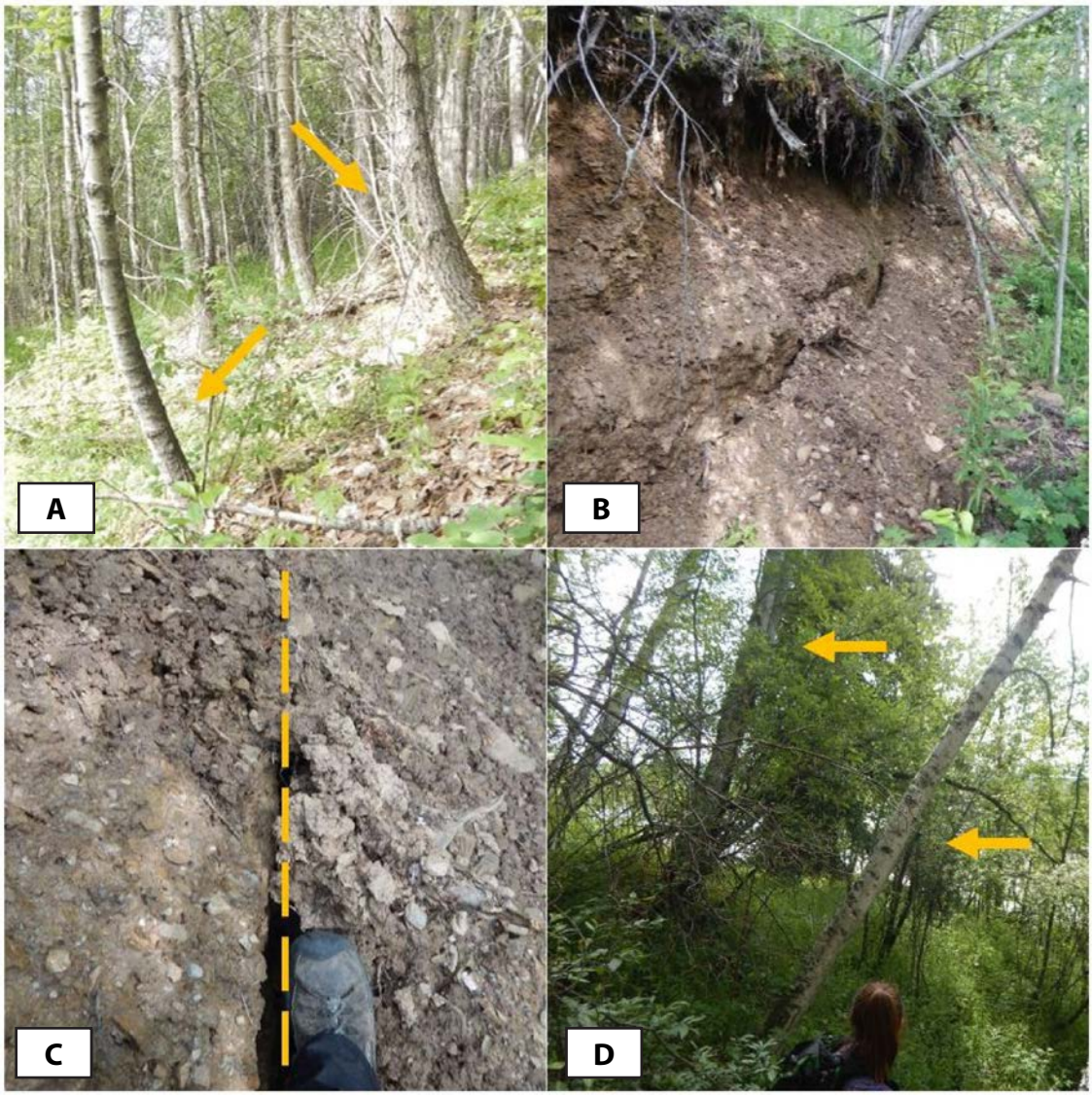

Figure A35. Images of BigB5_7S_7E_20_SE1 from July 1, 2020. **A.** Jayed trees (indicated by arrows) on the lower landslide body, (**B**) an exposure indicating recent movement along the right flank, (**C**) a fresh crack (indicated by dashed line) in the alluvium along the left flank, and (**D**) leaning trees at the toe (indicated by arrows). Photographs taken by MD.

LS Name:	*BigB5_7S_7E_21_SW6*	**Relative Age:**	*Historic (10)*
Date:	*July 1, 2020*	**Material:**	*Earth, alluvium (10)*
Personnel:	*JAS, MD, PP*	**Movement Type:**	*Rotational/Translational (5)*

Current Movement: *Yes*

Total confidence: *37/40 (High)*

This landslide (fig. B15A) is part of a landslide complex that includes BigB5_7S_7E_21_SW4, BigB5_7S_7E_21_SW5, and BigB5_7S_7E_21_SW7.

We hiked from the right flank (4) to the head scarp region (10), and then traveled along the left flank (5) toward the toe deposit (10). Inner morphological features (8) included cracks in trees and fresh soil exposed in scarps caused by recent movement. The Tanana River is actively eroding the toe, causing current landslide movement. We observed fresh soil exposures along the head scarp and the left flank. The head scarp was fresh, as a tree had been cracked and split, but not yet died, across the scarp distance. We also saw gray ash layers exposed in the alluvium at the head scarp.

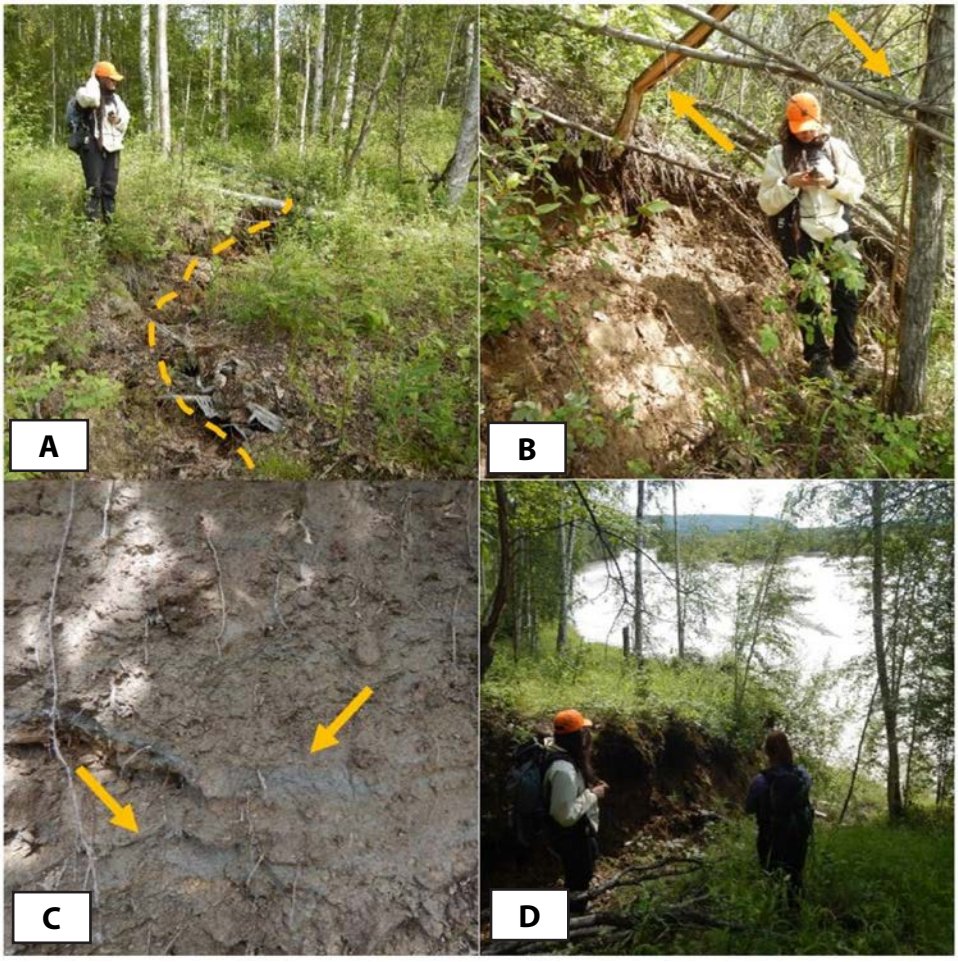

Figure A36. Images of BigB5_7S_7E_21_SW6 from July 1, 2020. **A.** JAS standing near a large crack (indicated by dashed line) above the head scarp, (**B**) JAS standing under a stretched, cracked tree (each slide of split tree indicated by an arrow) at the head scarp, (**C**) gray ash layers exposed in the head scarp (noted by arrows), and (**D**) JAS and PP standing along the left flank exposure. Photographs taken by MD and JAS.

LS Name:	*BigB5_7S_7E_21_SW7*	**Relative Age:**	*Historic (10)*
Date:	*July 1, 2020*	**Material:**	*Earth, alluvium (10)*
Personnel:	*JAS, MD, PP*	**Movement Type:**	*Rotational (5)*
Current Movement: *Yes*			
Total confidence: *37/40 (High)*			

This landslide (fig. B15A) is part of a landslide complex that includes BigB5_7S_7E_21_SW4, BigB5_7S_7E_21_SW5, and BigB5_7S_7E_21_SW6.

We hiked upslope from the toe deposit region (10) across the landslide body and toward the left flank (5) and head scarp region (10). The right flank (2) was not as easily identifiable as the left flank. Inner morphological features (10) included historic inner scarps, tension cracks, and a dropped block. Vegetative indicators of movement included small trees that were rotated so that they were growing at an angle pointing upslope. We saw evidence in the head scarp of recent movement, which may have been due to a high volume of precipitation in the days preceding the survey, and measured separation at the head scarp.

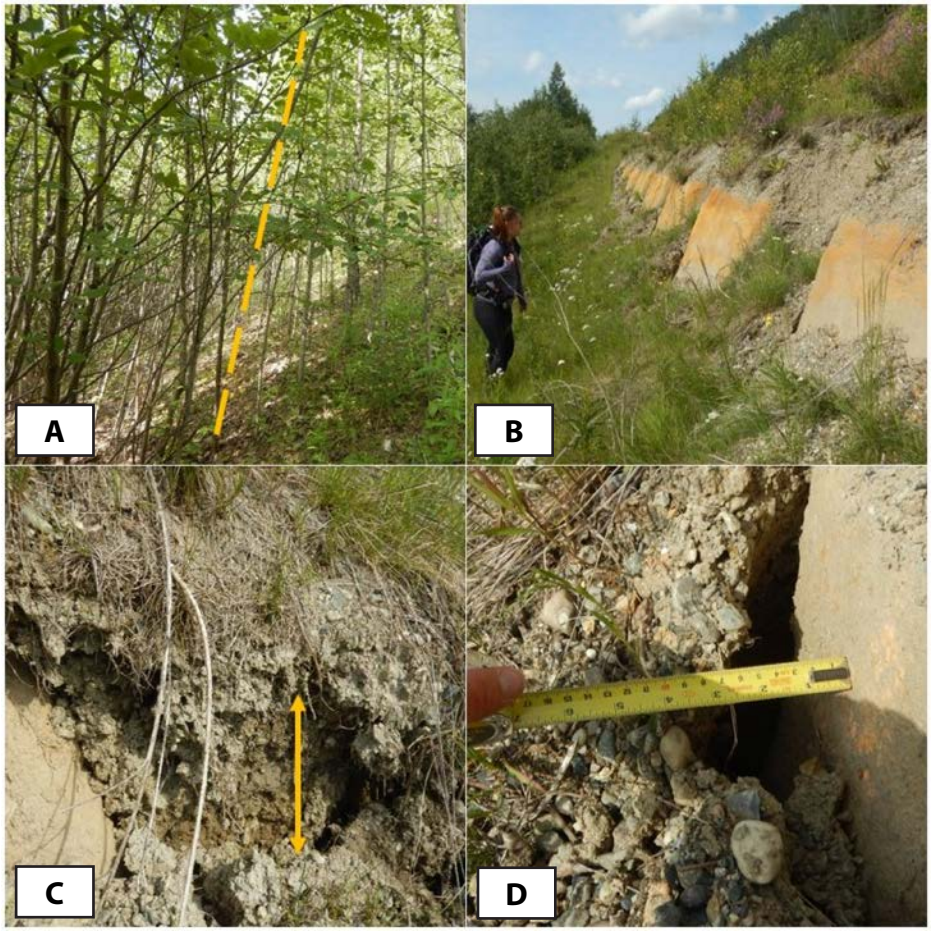

Figure A37. Images of BigB5_7S_7E_21_SW7 from July 1, 2020. **A.** Trees rotating upslope (dashed line indicates direction of lean) on the upper landslide body just below the head scarp region, (**B**) dropped soil below the road at the head scarp region, exposing buried tie-back blocks used to mitigate BigB5_7S_7E_21_SW5, (**C**) recent movement possibly due to preceding rainfall event, and (**D**) the measured separation of approximately 8 cm between soil and concrete block below the road. Photographs taken by MD.

LS Name:	*BigB5_7S_6E_24_SW4*	**Relative Age:**	*Historic (5)*
Date:	*July 1, 2020*	**Material:**	*Earth (10)*
Personnel:	*JAS, MD*	**Movement Type:**	*Rotational (5)*

Current Movement: *None*

Total confidence: *38/40 (High)*

We observed this small (380 m^2) landslide (fig. B15B) in its entirety from the road at the base of the slope. All features of flanks (10), toe deposit (10), and head scarp (10) were easily identifiable. The inner morphology (8) included vegetation cracks and exposed soil at the scarp and throughout the body. The movement was surficial and historic.

Figure A38. Image of BigB5_7S_6E_24_SW4 from July 1, 2020; image taken from the Richardson Highway. Photograph taken by MD.

LS Name:	*BigB5_7S_6E_24_SW3*	**Relative Age:**	*Historic (5)*
Date:	*July 1, 2020*	**Material:**	*Earth (10)*
Personnel:	*JAS, MD*	**Movement Type:**	*Rotational (5)*

Current Movement: *None*

Total confidence: *33/40 (High)*

We observed this small (345 m^2) landslide (fig. B15B) from the base of the slope at the toe (10) and hiked to the head scarp region (10). The toe deposits were pushing on downslope trees and causing them to jay. We observed defined flanks (8), and inner morphology included bare mineral soil at the head scarp (5). The landslide movement was primarily surficial and historic, but we did observe some exposed rock on the landslide body.

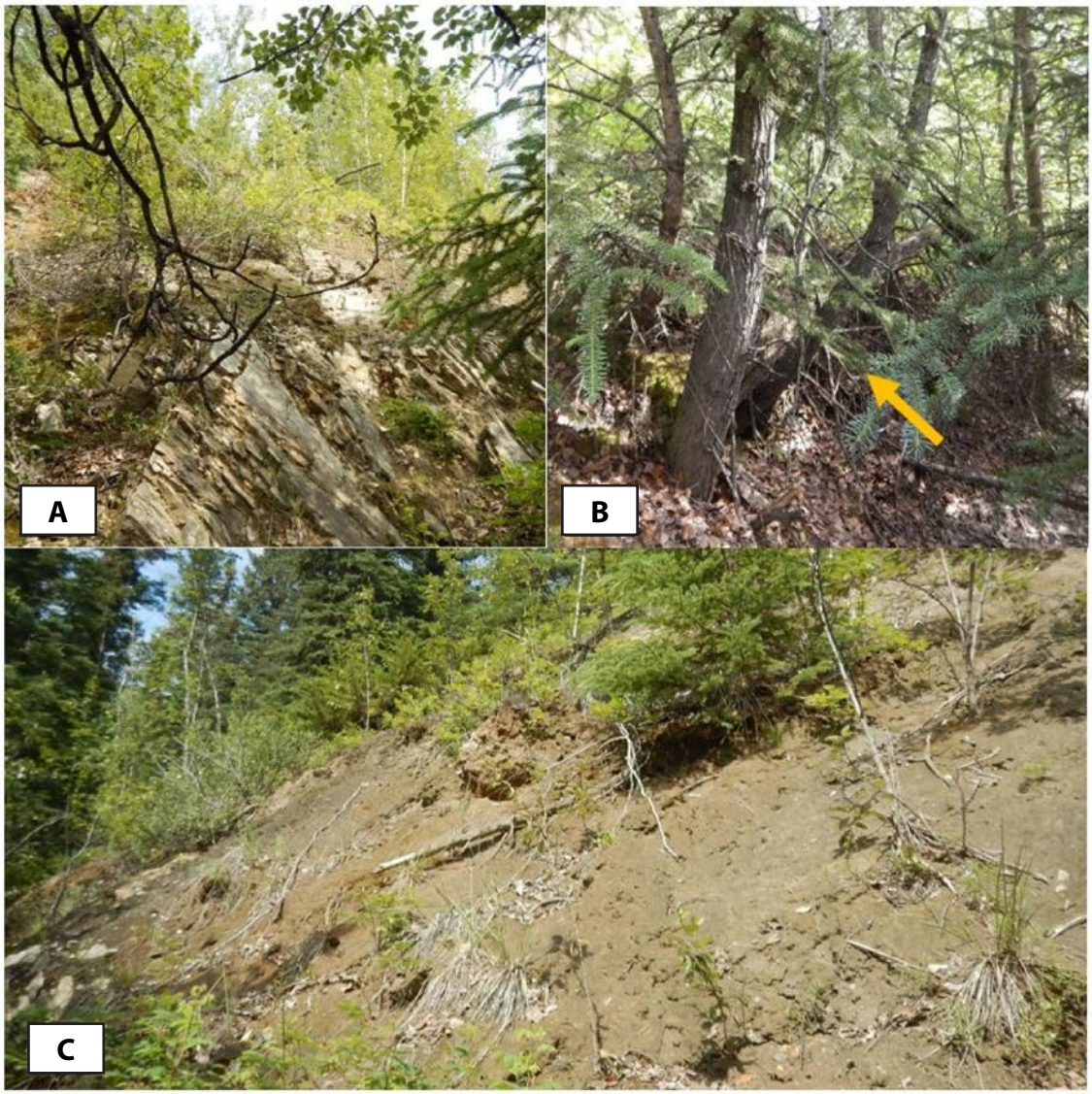

Figure A39. Images of BigB5_7S_6E_24_SW3 from July 1, 2020. **A.** View from the toe looking upslope at exposed bedrock, (**B**) toe deposit material pushing and causing the trees to jay (indicated by arrow), and (**C**) view of exposed mineral soil at the head scarp. Photographs taken by MD.

LS Name:	*BigB5_7S_6E_24_SW2*	**Relative Age:**	*Prehistoric (5)*
Date:	*July 1, 2020*	**Material:**	*Earth or bedrock (5)*
Personnel:	*JAS, MD*	**Movement Type:**	*Rotational (5)*

Current Movement: *None*

Total confidence: *25/40 (Moderate)*

We started our survey along the toe deposits (10), headed up to the head scarp region (10) through the landslide body (fig. B15B), and returned down the left flank (5). We did not visit the right flank (0) and there were no notable inner morphological features (0). We hypothesize that this landslide is prehistoric, based on the lack of roughness in the lidar and the presence of straight mature trees growing on the landslide body. It is possible that this landslide may be more deep-seated than many of the other small landslides along this slope, as the head scarp was better defined. It may have occurred in the bedrock and not just in the surficial soil.

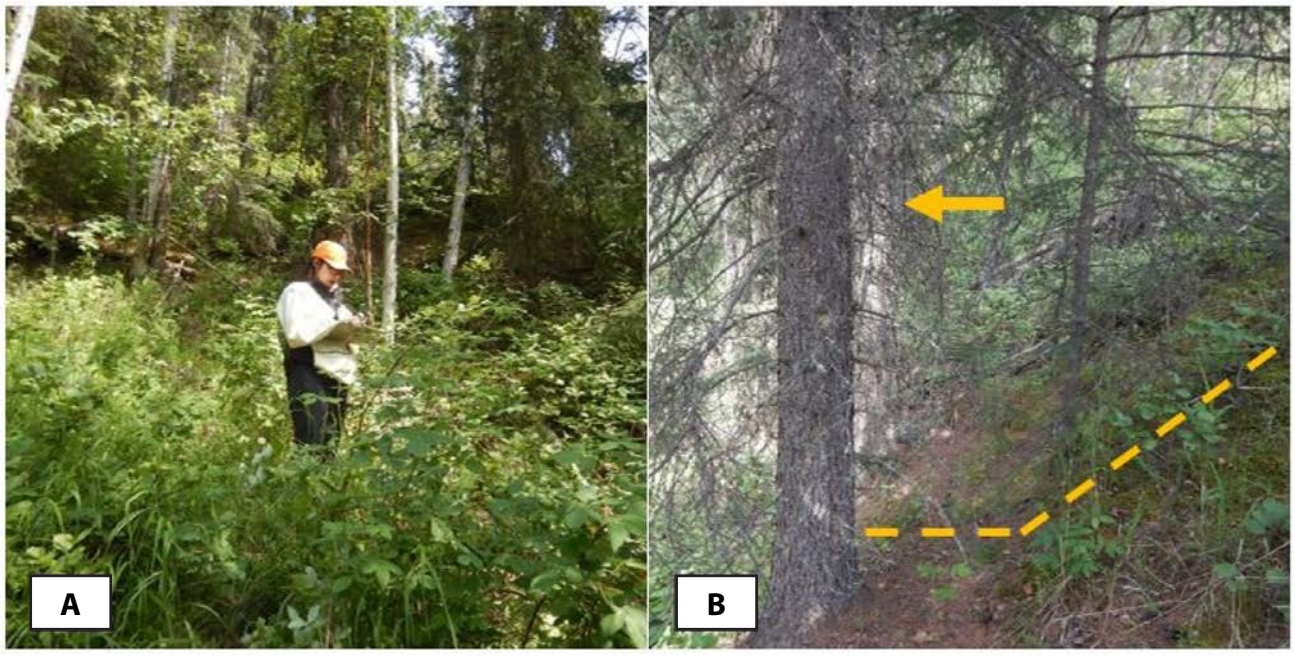

Figure A40. Images of BigB5_7S_6E_24_SW2 from July 1, 2020. **A.** JAS standing at the head scarp, and (**B**) an example of a straight mature spruce tree (indicated by arrow) growing on a narrow bench (indicated by dashed line) on the landslide body. Photographs taken by MD.

LS Name:	*BigB5_7S_6E_24_SW1*	**Relative Age:**	*Prehistoric (5)*
Date:	*July 1, 2020*	**Material:**	*Bedrock (5)*
Personnel:	*JAS, MD*	**Movement Type:**	*Rotational (5)*

Current Movement: *None*

Total confidence: *33/40 (High)*

We hiked from the right flank (5) to the head scarp region (10). The left flank (5) and toe deposit (10) were easily identifiable. There were no significant inner morphological features (3) except for surface roughness. We observed significant bedrock exposures at the head scarp region and upper landslide body. This landslide (fig. B15B) was small (about 350 m^2) and likely prehistoric in age.

Figure A41. Image of BigB5_7S_6E_24_SW1 from July 1, 2020. This view is looking upslope at the head scarp region and exposed bedrock outcrop. Photograph taken by MD.

LS Name:	*BigB5_7S_6E_24_SE3*	**Relative Age:**	*Prehistoric (5)*
Date:	*July 1, 2020*	**Material:**	*Bedrock (5)*
Personnel:	*JAS, MD*	**Movement Type:**	*Rotational (5)*

Current Movement: *None*

Total confidence: *32/40 (High)*

We hiked across the upper landslide body (fig. B15B) toward the head scarp region (10). The flanks (10) and toe deposit (10) were easily identifiable, with subtle inner morphology (2). We observed exposed rock in the landslide body. We hypothesize that this is a small (970 m^2) prehistoric landslide.

Figure A42. Image of BigB5_7S_6E_24_SE3 from July 1, 2020. Large rocky debris is exposed in the lower landslide body. Photograph taken by MD.

LS Name:	*BigB5_7S_6E_24_SE2*	**Relative Age:**	*Prehistoric (5)*
Date:	*July 1, 2020*	**Material:**	*Bedrock (5)*
Personnel:	*JAS, MD*	**Movement Type:**	*Rotational (5)*

Current Movement: *None*

Total confidence: *28/40 (Moderate)*

We began at the toe (10) and hiked upslope along the left flank (5) toward the head scarp region (10). We saw concrete at the toe, probably a remnant from the Old Valdez Trail—the original route of the Richardson Highway. The trail was originally constructed from 1898 to 1906, and in 1919 it became the Richardson Highway (Bleakley, 2015). Inner morphology (3) included only some small slope breaks on the landslide body. Similar to BigB5_7S_6E_24_SW2, this small (695 m^2) landslide (fig. B15B) may be deep-seated in the bedrock due to its clearly defined head scarp.

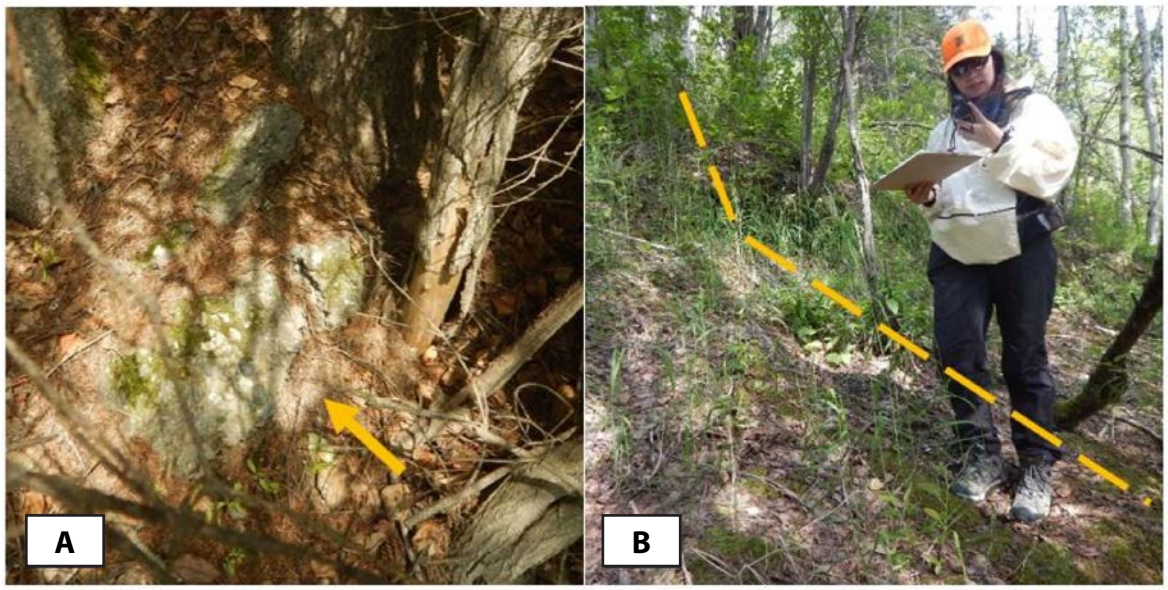

Figure A43. Images of BigB5_7S_6E_24_SE2 from July 1, 2020. **A.** Concrete near the toe, and (**B**) JAS standing along a slope break (indicated by dashed line) on the left flank. Photographs taken by MD.

LS Name:	*BigB5_7S_7E_19_SE3*	**Relative Age:**	*Historic (10)*
Date:	*July 2, 2020*	**Material:**	*Bedrock (10)*
Personnel:	*JAS, MD*	**Movement Type:**	*Rotational (5)*

Current Movement: *Yes*

Total confidence: *28/40 (Moderate)*

We hiked down to the head scarp region (10) and continued along the left flank (5). The right flank was not surveyed, and we only observed the toe deposit (5) from upslope. We found tension cracks along the access road just above the head scarp region. We also saw inner morphological features (8) of cracks and down-dropped blocks within the landslide body (fig. B16A). This small landslide is historic, but the straight mature vegetation on the steep slopes indicates that there has been no recent movement in the main landslide body. The cracks in the access road may indicate the onset of activity.

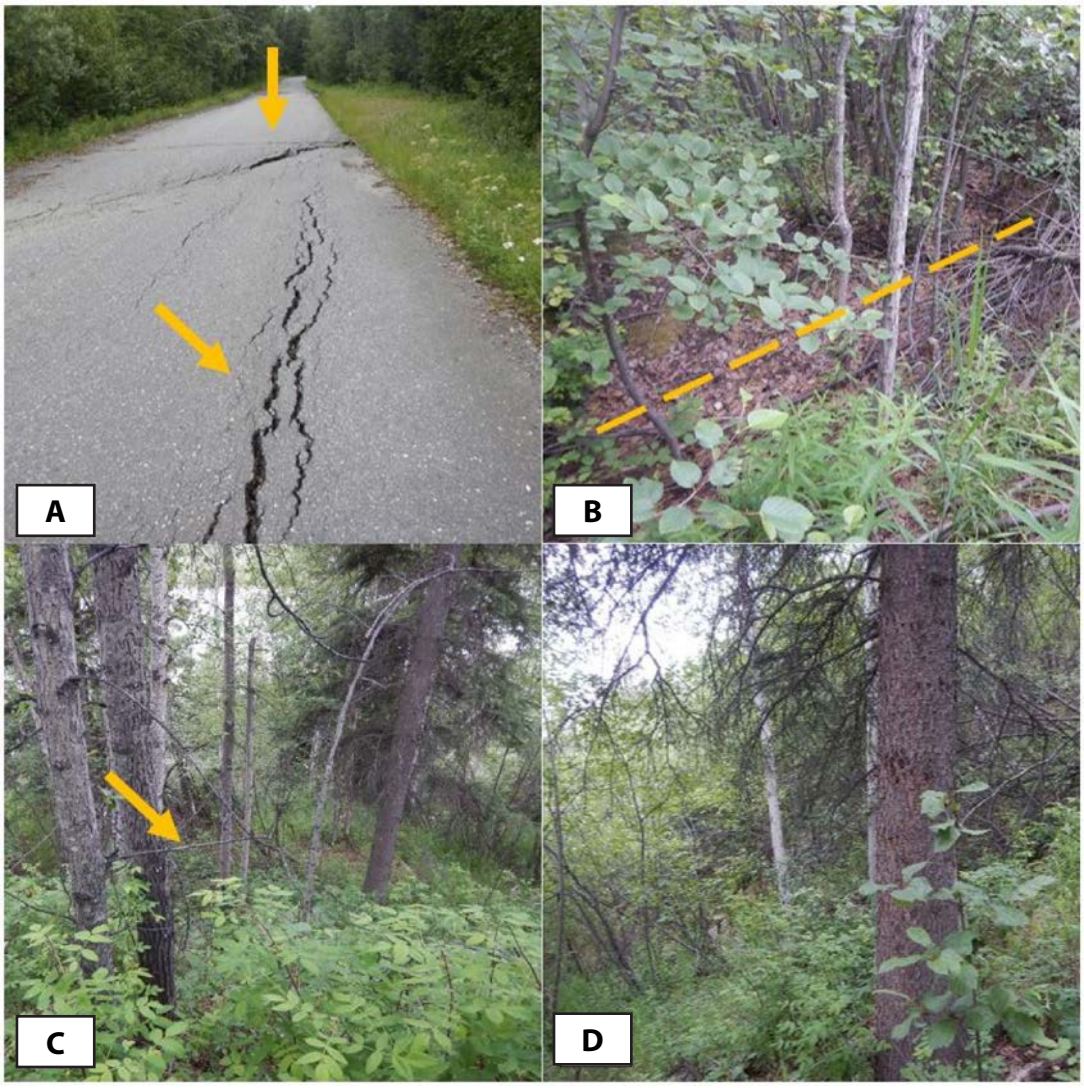

Figure A44. Images of BigB5_7S_7E_19_SE3 from July 2, 2020. **A.** Cracks on the access road above the head scarp region, (**B**) crack (indicated by dashed line) below the road, (**C**) view downslope toward a slope break (indicated by arrow) and down-dropped block, and (**D**) straight mature spruce tree on a steep slope below the head scarp area. Photographs taken by MD.

LS Name:	*BigB5_7S_7E_20_SW8*	**Relative Age:**	*Prehistoric (10)*
Date:	*July 2, 2020*	**Material:**	*Bedrock (10)*
Personnel:	*JAS, MD*	**Movement Type:**	*Rotational (5)*

Current Movement: *None*

Total confidence: *40/40 (High)*

This landslide (fig. B16A) is part of a landslide complex that includes BigB5_7S_7E_20_SW4, BigB5_7S_7E_20_SW5, BigB5_7S_7E_20_SW6, and BigB5_7S_7E_20_SW7.

We hiked along the lower landslide body and toe deposits (10) from west to east, and then traveled upslope along the left flank (5) and across the middle landslide body toward the head scarp region (10). We moved along the head scarp region to the right flank (5) and returned downslope to the highway. Inner morphological features (10) included cracks, grabens, closed depressions, down-dropped blocks, and mid-slope terraces. We saw leaning trees along the lower landslide body. We hypothesize that this large, deep-seated landslide in bedrock is prehistoric, with some historic movement on the lower body and at the toe. We saw rock exposures on the lower landslide body and within historic scarp exposures. The head scarp region was interesting, as the slope break along the left extent was much steeper than the right. This may be due to bedrock control and the orientation of planes of weakness. It is unlikely that permafrost is present in this landslide, as the vegetation was typically birch and aspen forest with grassy ground cover. The landslide was likely triggered in the past due to the toe being eroded by the river.

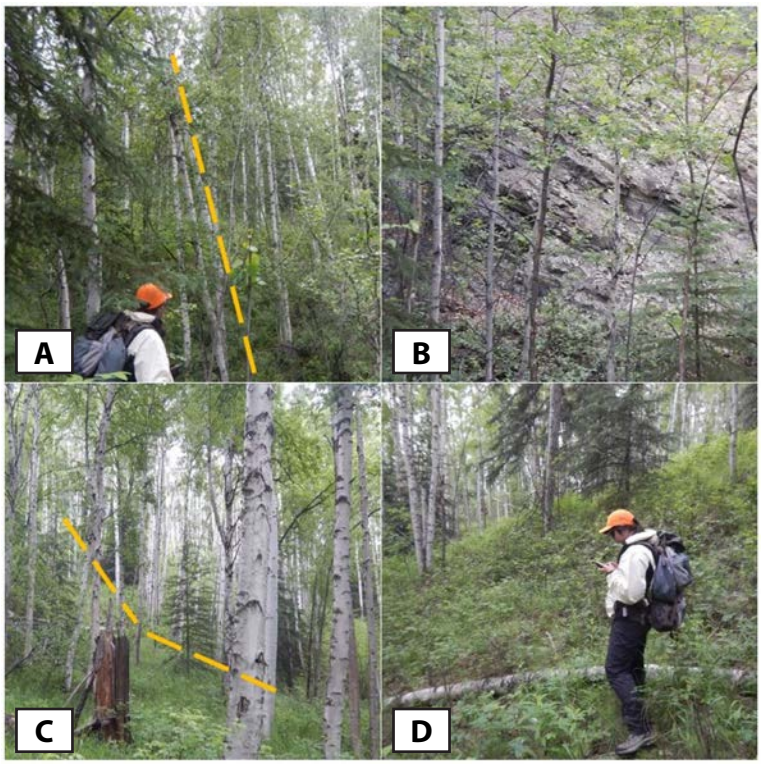

Figure A45. Images of BigB5_7S_7E_20_SW8 from July 2, 2020. **A.** JAS and leaning trees (dashed line indicates direction of lean) below the Old Valdez Trail on the lower landslide body, (**B**) bedrock exposure below the Richardson Highway on the lower landslide body, (**C**) steep slope of the head scarp (dashed line indicates slope break), and (**D**) JAS standing along the right flank near the head scarp region. Photographs taken by MD.

LS Name:	*BigB5_7S_7E_20_SW7*	**Relative Age:**	*Historic (10)*
Date:	*July 2, 2020*	**Material:**	*Bedrock (5)*
Personnel:	*JAS, MD*	**Movement Type:**	*Rotational (5)*

Current Movement: *Yes*

Total confidence: *40/40 (High)*

This landslide (fig. B16A) is part of a landslide complex that includes BigB5_7S_7E_20_SW4, BigB5_7S_7E_20_SW5, BigB5_7S_7E_20_SW6, and BigB5_7S_7E_20_SW8.

We hiked to the head scarp region (10) of this small landslide and were able to observe it in its entirety from there. It had easily identifiable flank extents (10) and the toe deposit (10) was currently being eroded by the Tanana River. This landslide exhibited inner morphological features (10) of fresh soil and alluvium exposed along the upper body.

Figure A46. Images of BigB5_7S_7E_20_SW7 from July 2, 2020. **A.** View of the fresh soil exposed at the head scarp to the east, and (**B**) view of the head scarp with exposed soil to the west. Photographs taken by MD.

LS Name:	*BigB5_7S_7E_20_SW5*	**Relative Age:**	*Historic (10)*
Date:	*July 2, 2020*	**Material:**	*Bedrock (5)*
Personnel:	*JAS, MD*	**Movement Type:**	*Rotational (5)*

Current Movement: *Yes*

Total confidence: *38/40 (High)*

This landslide (fig. B16A) is part of a landslide complex that includes BigB5_7S_7E_20_SW4, BigB5_7S_7E_20_SW6, BigB5_7S_7E_20_SW7, and BigB5_7S_7E_20_SW8.

We hiked along the right flank (5) and head scarp region (10), then down the landslide body toward the left flank (5) and toe deposit (10). Inner morphological features (8) and vegetative movement indicators included large cracks and leaning trees, respectively. The cracks we observed were all fresh, and this small landslide is likely currently moving because the toe is being eroded by the Tanana River.

Figure A47. Images of BigB5_7S_7E_20_SW5 from July 2, 2020. **A.** Crack with exposed soil along the right flank (arrows indicate separation), and (**B**) crack with exposed soil (indicated by arrow) at the head scarp. Photographs taken by MD.

LS Name:	*BigB5_7S_7E_20_SW6*	**Relative Age:**	*Historic (10)*
Date:	*July 2, 2020*	**Material:**	*Bedrock (5)*
Personnel:	*JAS, MD*	**Movement Type:**	*Rotational (5)*

Current Movement: *Yes*

Total confidence: *40/40 (High)*

This landslide (fig. B16A) is part of a landslide complex that includes BigB5_7S_7E_20_SW4, BigB5_7S_7E_20_SW5, BigB5_7S_7E_20_SW7, and BigB5_7S_7E_20_SW8.

We hiked along the head scarp region (10) and then down the landslide body toward the toe deposit (10). The flanks (10) were easy to identify. Inner morphological features (10) included large cracks, small gullies and grabens, and down-dropped blocks. Vegetative movement indicators included leaning trees on the landslide body. Cracks occurred throughout the landslide, from the head scarp region to the toe deposit. These cracks were all fresh and indicate recent landslide movement, likely due to the toe being eroded by the Tanana River.

Figure A48. Images of BigB5_7S_7E_20_SW6 from July 2, 2020. **A.** JAS standing on a dropped block with a relatively fresh crack (arrows indicate separation), (**B**) cracks with leaning trees (dashed line indicates direction of lean), (**C**) head scarp with exposed soil near the river, and (**D**) JAS and a relatively fresh crack (dashed line positioned mid-crack). Photographs taken by MD.

LS Name:	*BigB5_7S_7E_20_SW4*	**Relative Age:**	*Historic (10)*
Date:	*July 2, 2020*	**Material:**	*Bedrock (10)*
Personnel:	*JAS, MD*	**Movement Type:**	*Rotational (5)*

Current Movement: *Yes*

Total confidence: *34/40 (High)*

This landslide (fig. B16A) is part of a landslide complex that includes BigB5_7S_7E_20_SW5, BigB5_7S_7E_20_SW6, BigB5_7S_7E_20_SW7, and BigB5_7S_7E_20_SW8.

We observed surface roughness of the lower landslide body and toe deposit region (8) from the Richardson Highway. Then we hiked upslope through the body toward the left flank (4) and head scarp region (10), eventually angling toward the right flank (2). Inner morphological features (10) included surface roughness on the landslide body and down-dropped blocks. We observed blocky bedrock in all of the head scarp exposures. This small landslide is historic, and we observed evidence of recent movement, including about 10 cm of displacement in the soil at the head scarp.

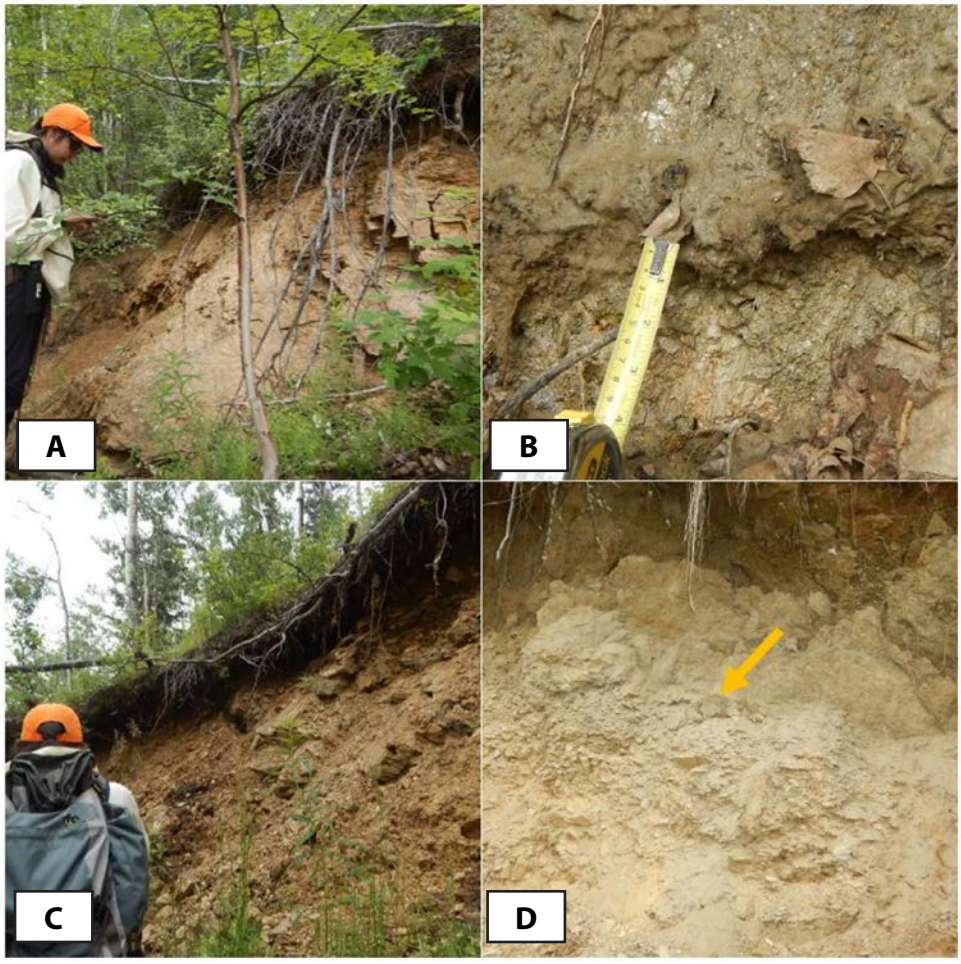

Figure A49. Images of BigB5_7S_7E_20_SW4 from July 2, 2020. **A.** JAS standing in front of exposed bedrock at the head scarp, (**B**) approximately 10 cm of recent movement at the head scarp likely caused by high precipitation, (**C**) JAS standing in front of the right flank and scarp with exposed soil and bedrock, and (**D**) a light gray ash layer (indicated by arrow) in the exposed head scarp. Photographs taken by MD.

LS Name:	*BigB5_7S_7E_19_SE1*	**Relative Age:**	*Historic (10)*
Date:	*July 2, 2020*	**Material:**	*Bedrock (5)*
Personnel:	*JAS, MD*	**Movement Type:**	*Rotational (5)*

Current Movement: *Yes*

Total confidence: *35/40 (High)*

We hiked down to the head scarp region (10) and continued downslope along the left flank (5) toward the toe (10) of the landslide (fig. B16A). We did not observe the right flank in the field. Inner morphology (10) included cracks in the upper landslide body and fresh soil exposures in the scarps.

Figure A50. Images of BigB5_7S_7E_19_SE1 from July 2, 2020. **A.** Lower head scarp (top of scarp indicated by dashed line), (**B**) fresh soil exposure (indicated by arrow) at the upper head scarp, and (**C**) crack (indicated by dashed line) just below the head scarp region. Photographs taken by MD.

LS Name:	*BigB5_7S_6E_24_SE1*	**Relative Age:**	*Historic (5)*
Date:	*July 2, 2020*	**Material:**	*Earth (10)*
Personnel:	*JAS, MD*	**Movement Type:**	*Rotational (5)*

Current Movement: *None*

Total confidence: *33/40 (High)*

We began at the toe deposit (10) and then hiked upslope along the left flank (5) toward the head scarp region (10) of the landslide (fig. B16B). The right flank was apparent (5), and we observed inner morphological features (3). The head scarp was covered in vegetation and there were no fresh soil exposures. It appears that the toe has bulged out toward the road, which leads us to think that it may be a historic surficial landslide.

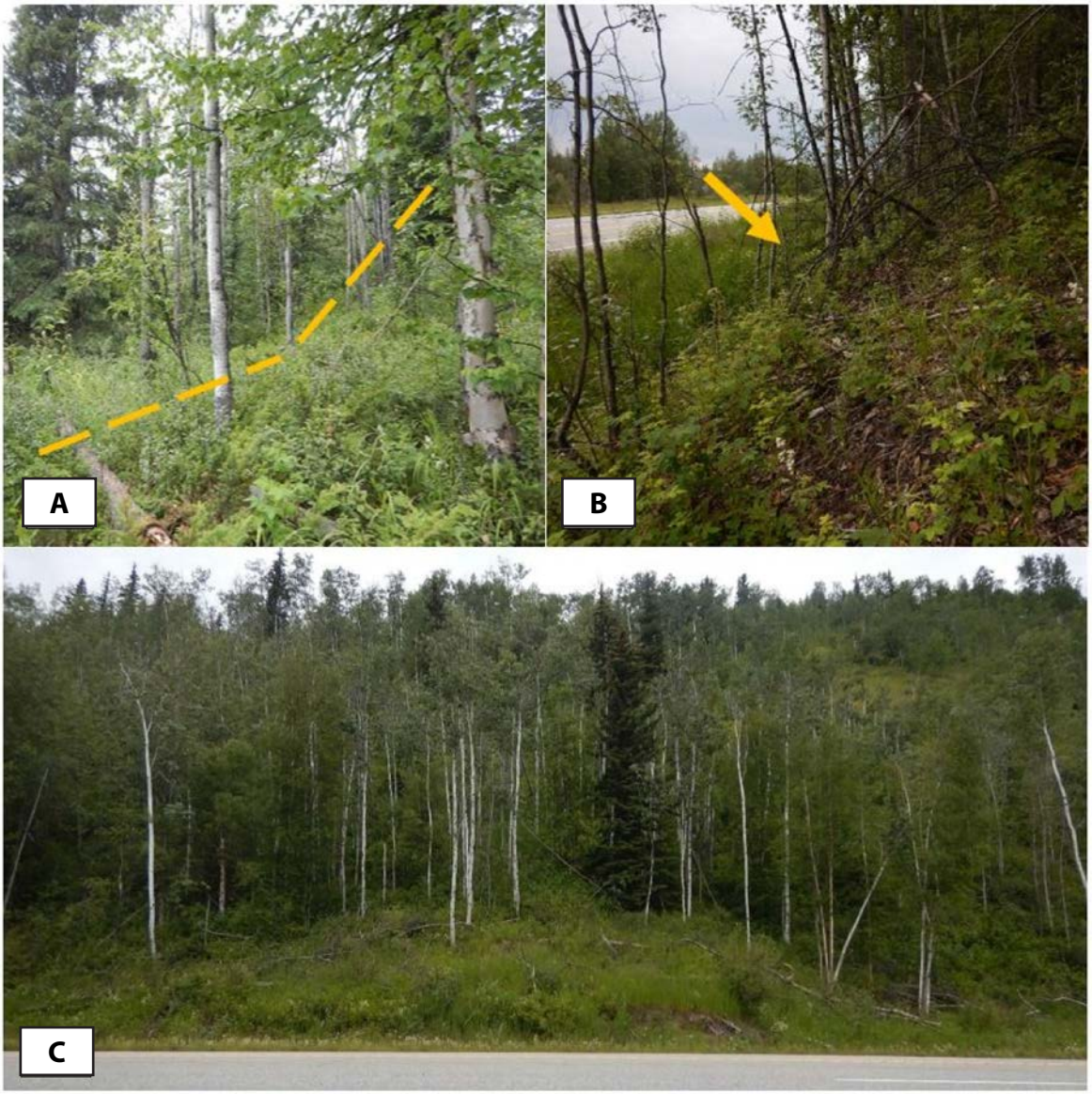

Figure A51. Images of BigB5_7S_6E_24_SE1 from July 2, 2020. **A.** View of the head scarp region with a slope break (indicated by dashed line), (**B**) the landslide toe deposit (indicated by arrow), and (**C**) looking straight upslope at the landslide from the toe. Photographs taken by MD.

APPENDIX B: MAPS OF FIELD EVALUATED LANDSLIDES

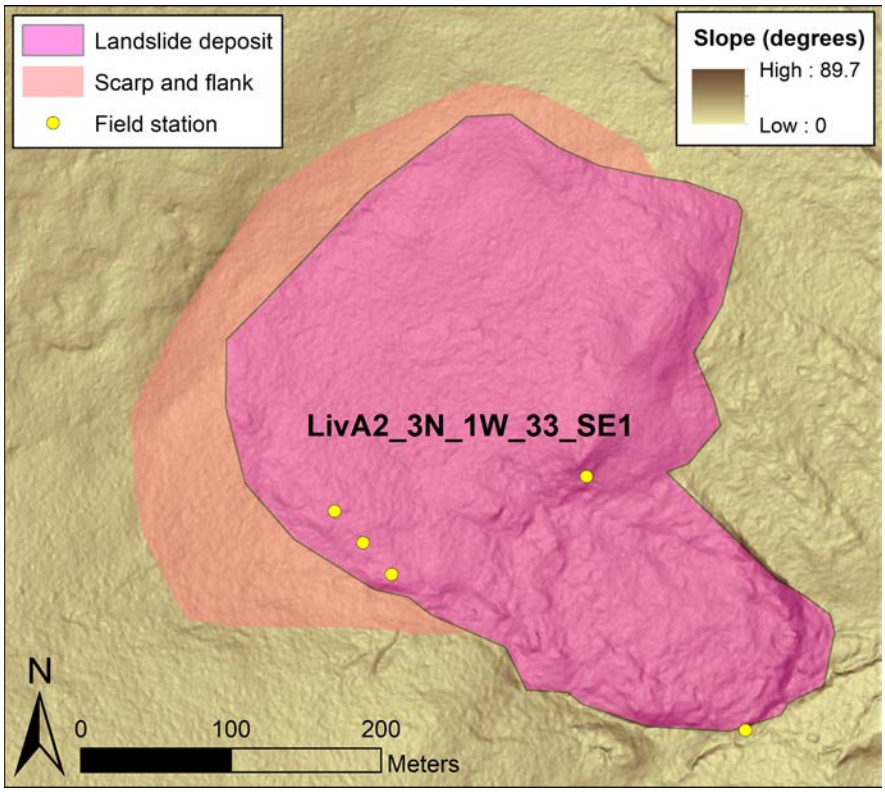

Figure B1. Mapped landslide and field stations from May 15, 2020. The background is QL2 lidar-derived slope map (FNSB, 2020).

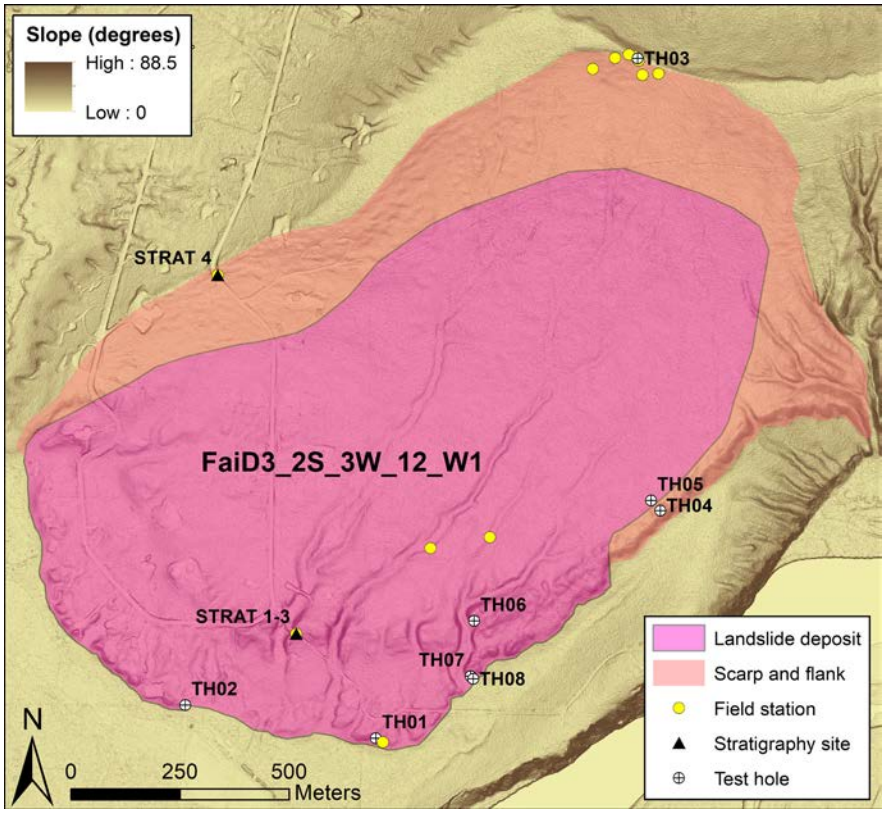

Figure B2. Mapped landslide and field stations from May 28, 2020. Stratigraphy sites and test hole locations, surveyed July 6-9, 2020, are also shown. The background is QL1 lidar-derived slope map (FNSB, 2020).

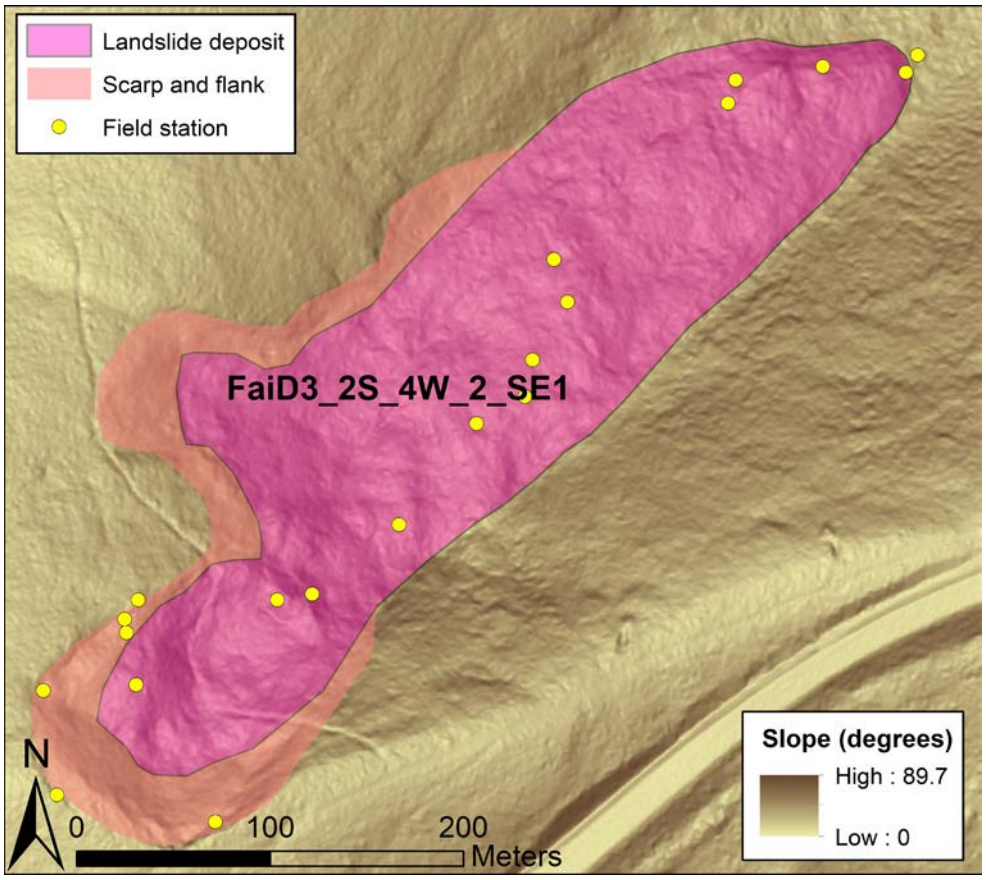

Figure B3. Mapped landslide and field stations from May 29, 2020. The background is QL2 lidar-derived slope map (FNSB, 2020).

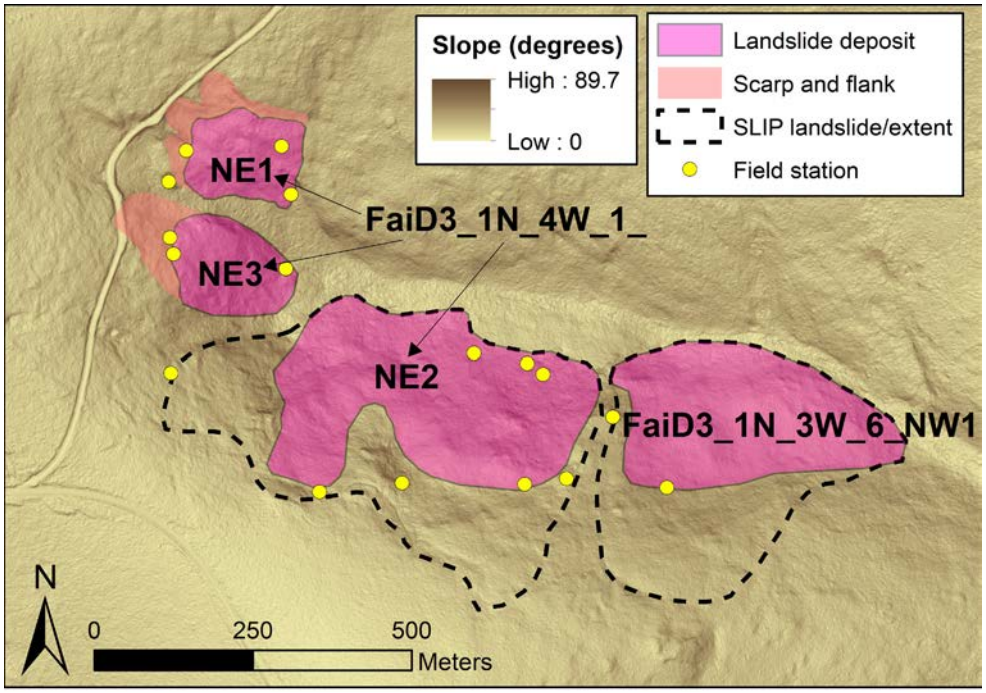

Figure B4. Mapped landslides and field stations from June 2, 2020. The background is QL2 lidar-derived slope map (FNSB, 2020).

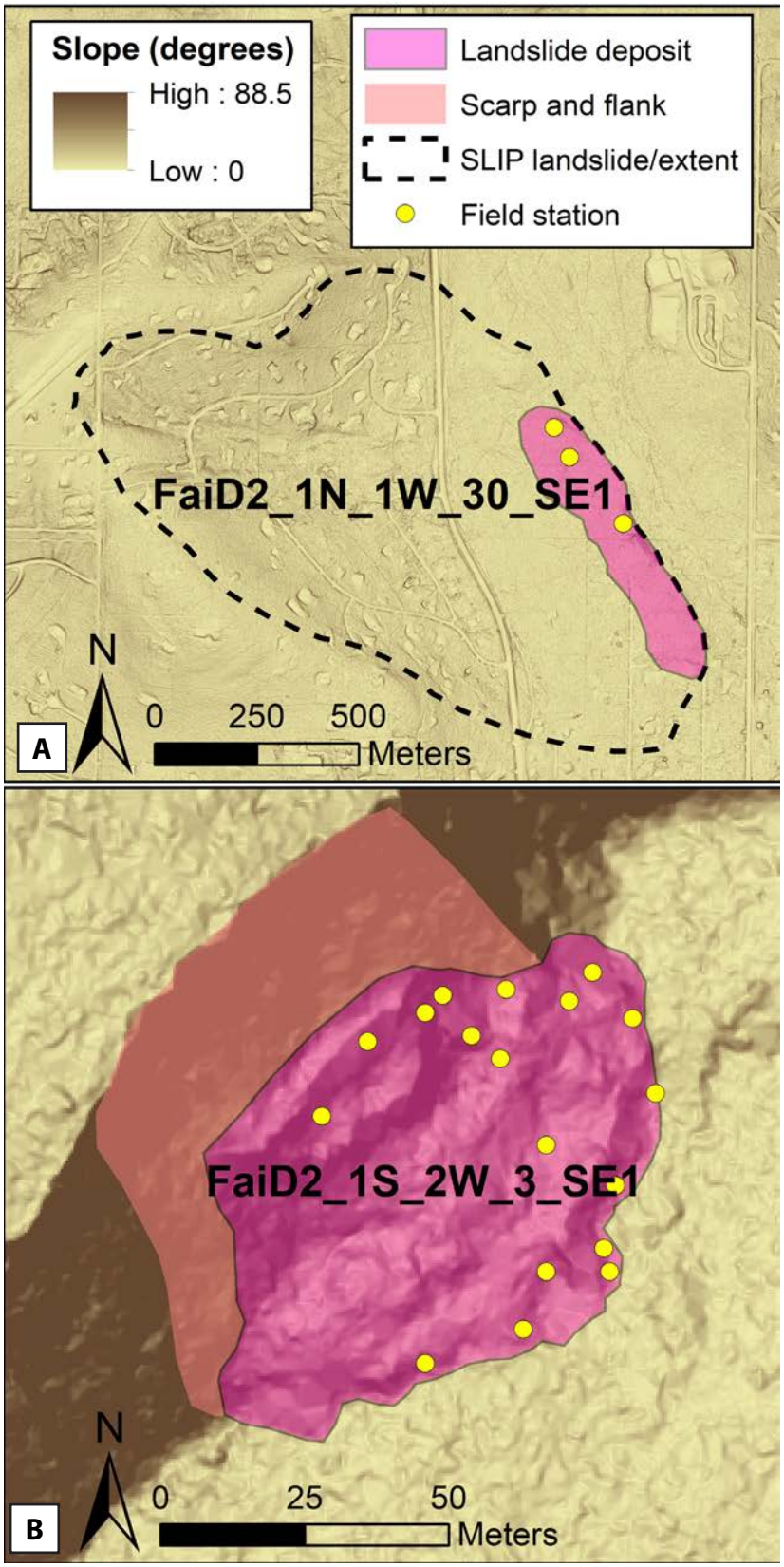

Figure B5. Mapped landslide deposits and field stations from June 5, 2020. **A.** Pearl Creek landslide and (**B**) Gold Hill landslide. The background is QL1 lidar-derived slope map (FNSB, 2020).

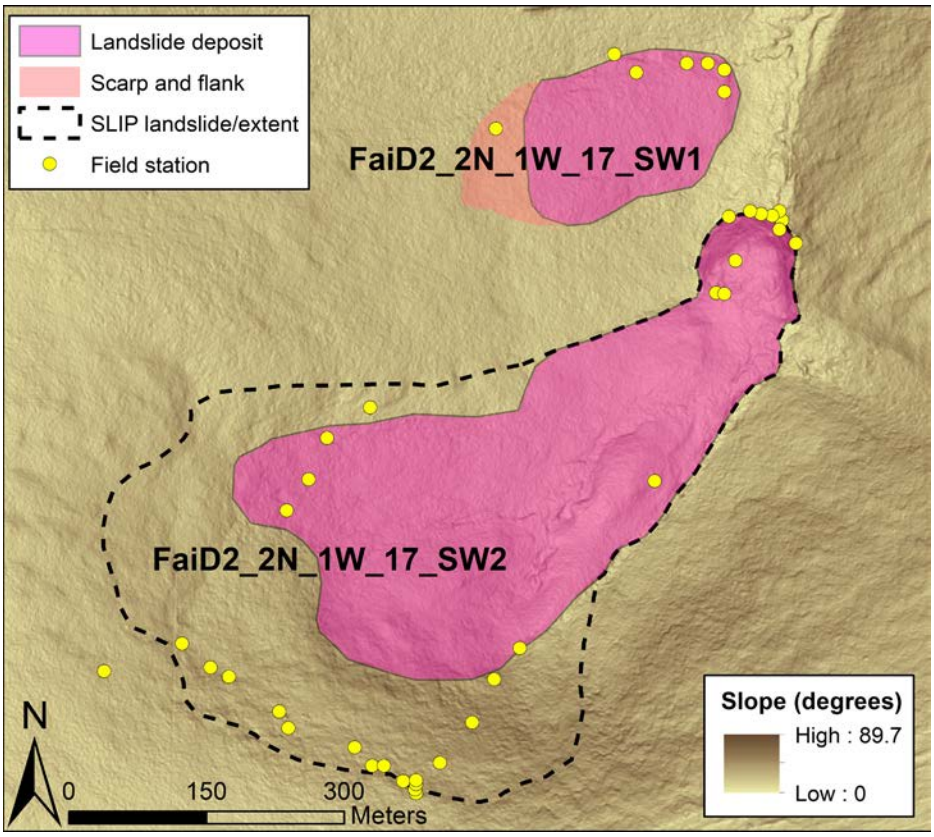

Figure B6. Mapped landslides and field stations from June 8, 2020. The background is QL2 lidar-derived slope map (FNSB, 2020).

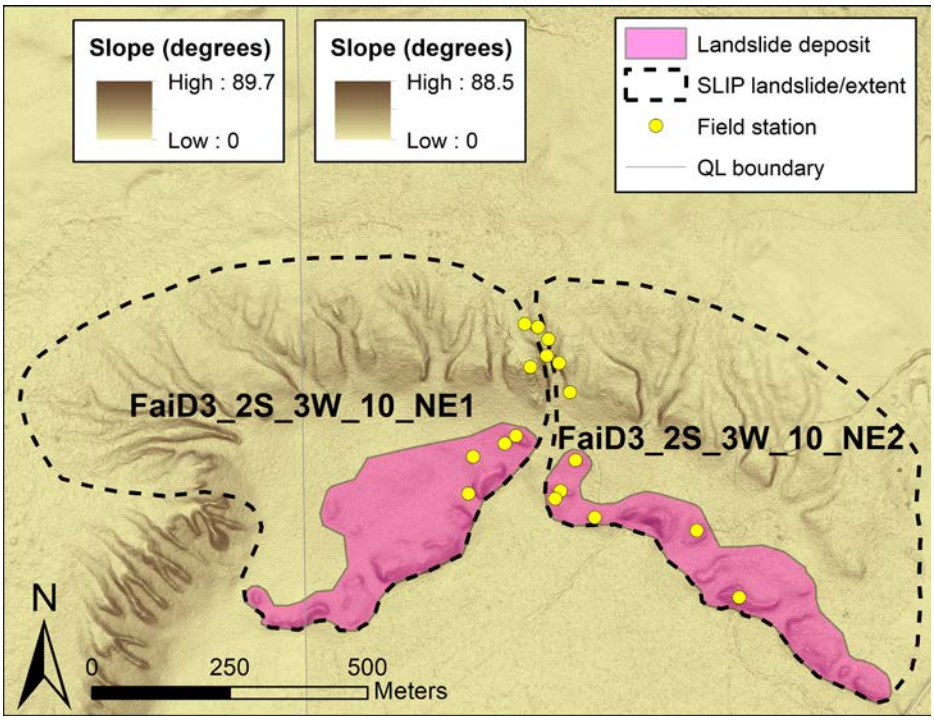

Figure B7. Mapped landslides and field stations from June 11, 2020. The backgrounds are QL1 (right-side of the figure) and QL2 (left-side of the figure) lidar-derived slope maps (FNSB, 2020), with the vertical boundary (indicated by light gray line) cutting across the western landslide body.

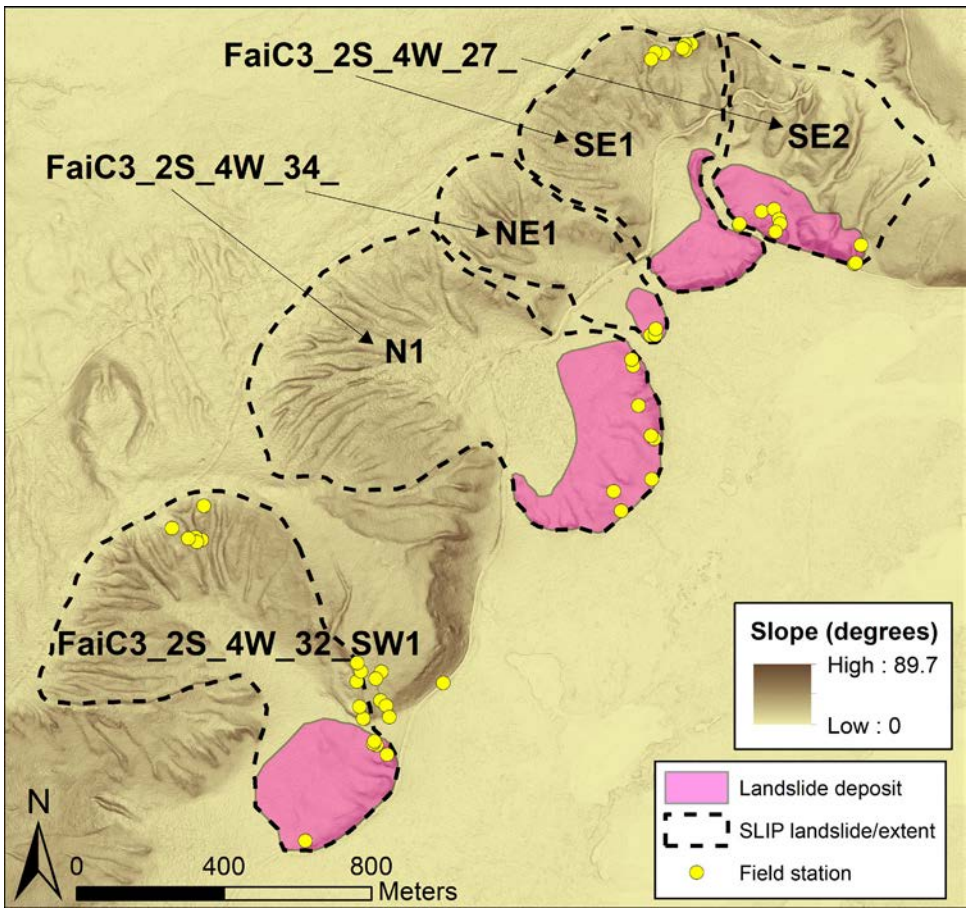

Figure B8. Mapped landslides and field stations from June 12, 2020. The background is QL2 lidar-derived slope map (FNSB, 2020).

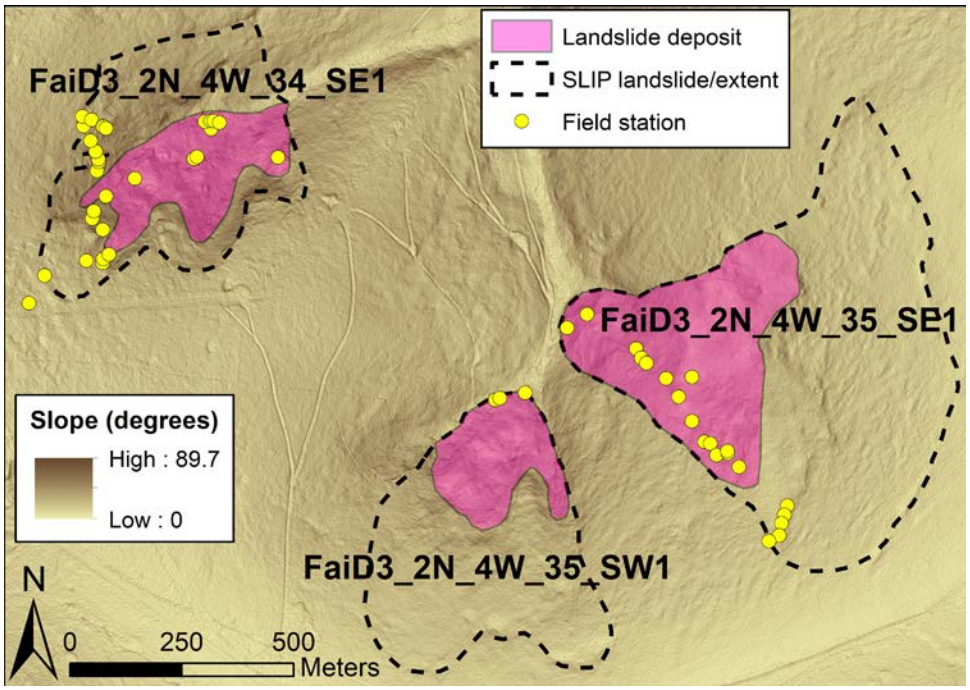

Figure B9. Mapped landslides and field stations from June 15, 2020. The background is QL2 lidar-derived slope map (FNSB, 2020).

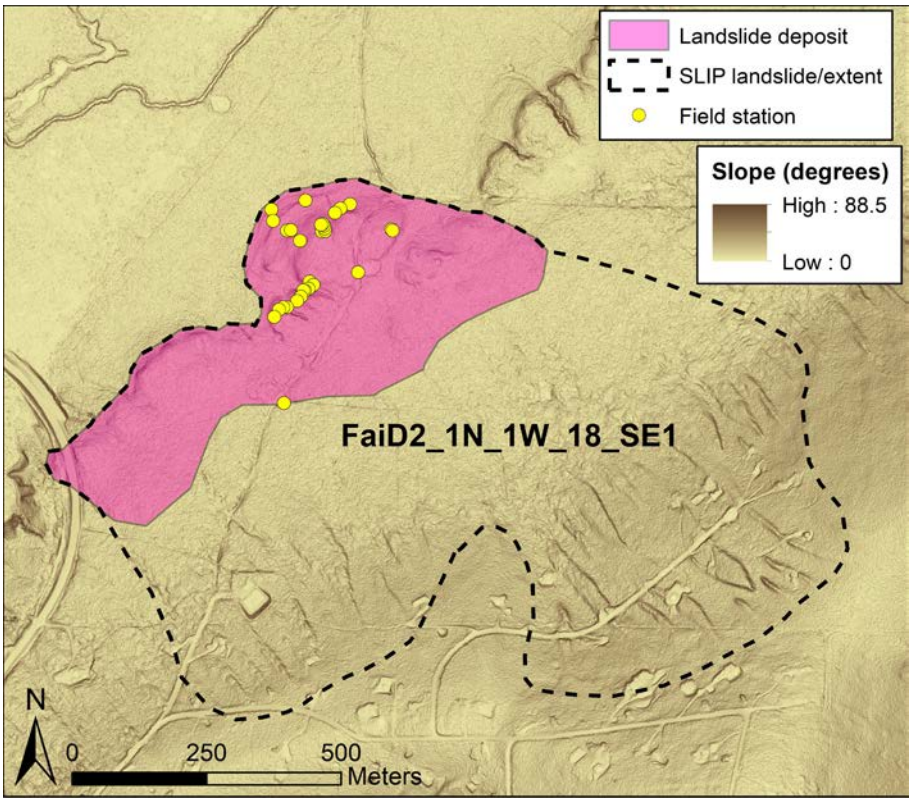

Figure B10. Mapped landslide and field stations from June 18, 2020. The background is QL1 lidar-derived slope map (FNSB, 2020).

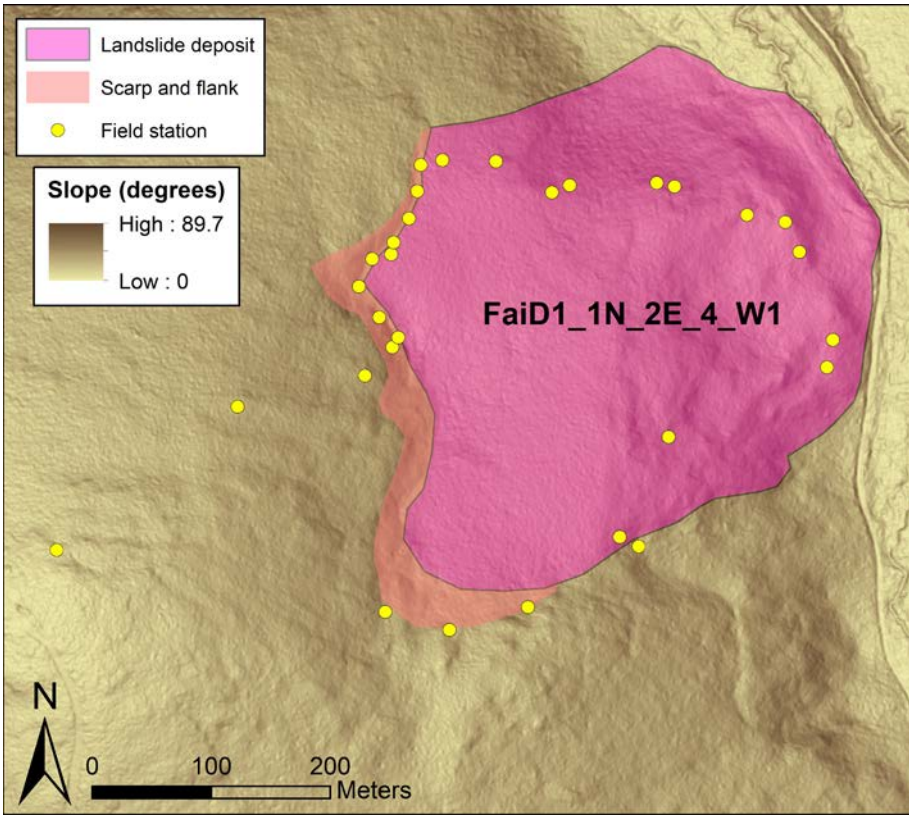

Figure B11. Mapped landslide and field stations from June 19, 2020. The background is QL2 lidar-derived slope map (FNSB, 2020).

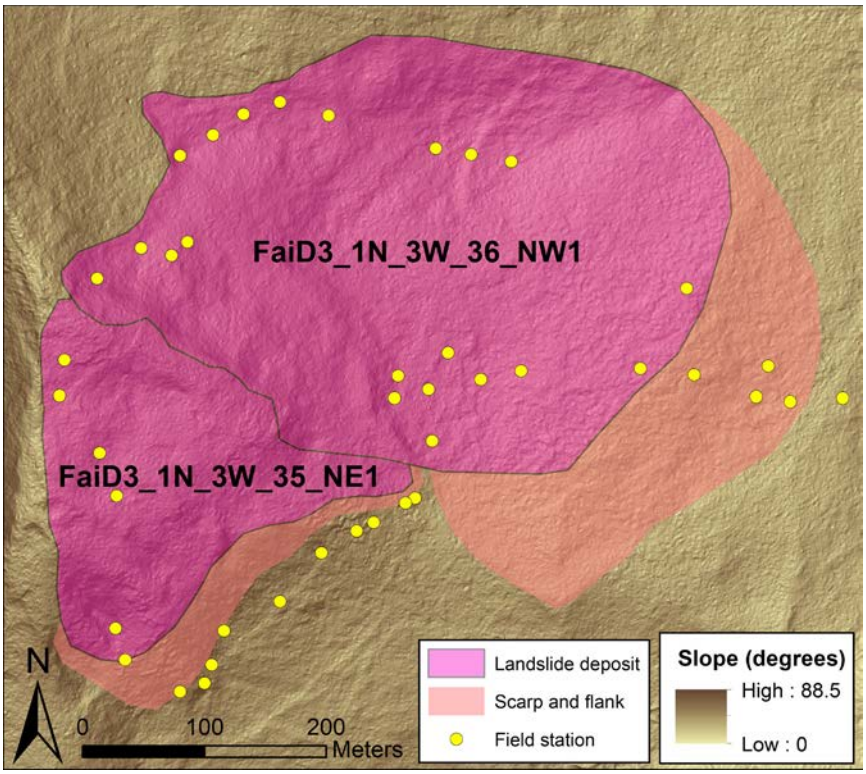

Figure B12. Mapped landslides and field stations from June 24, 2020. The background is QL1 lidar-derived slope map (FNSB, 2020).

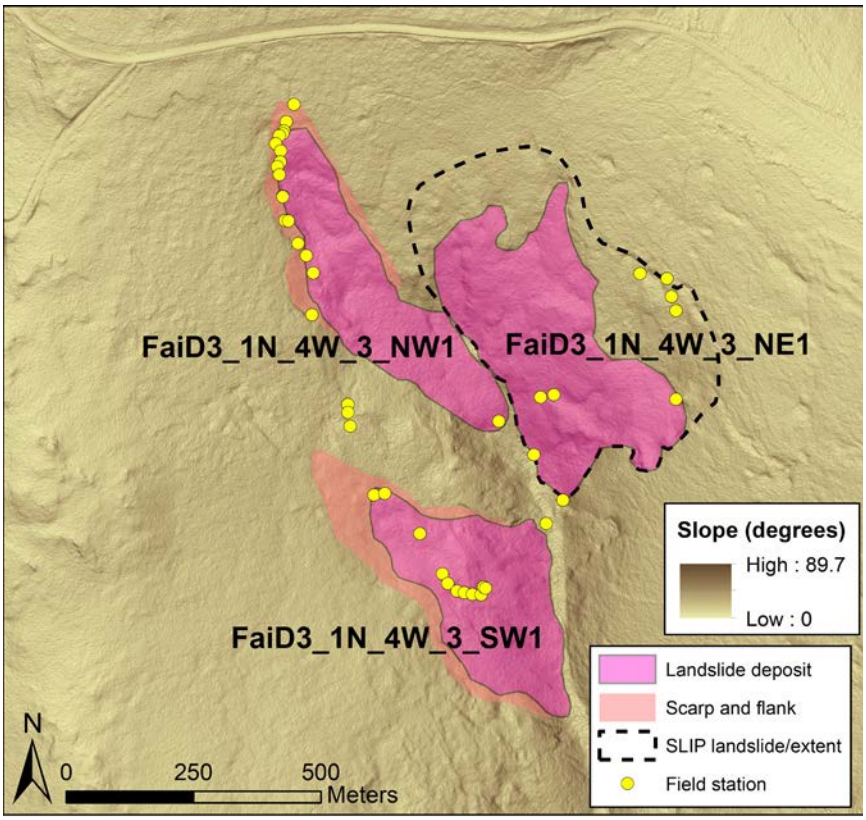

Figure B13. Mapped landslides and field stations from June 25, 2020. The background is QL2 lidar-derived slope map (FNSB, 2020).

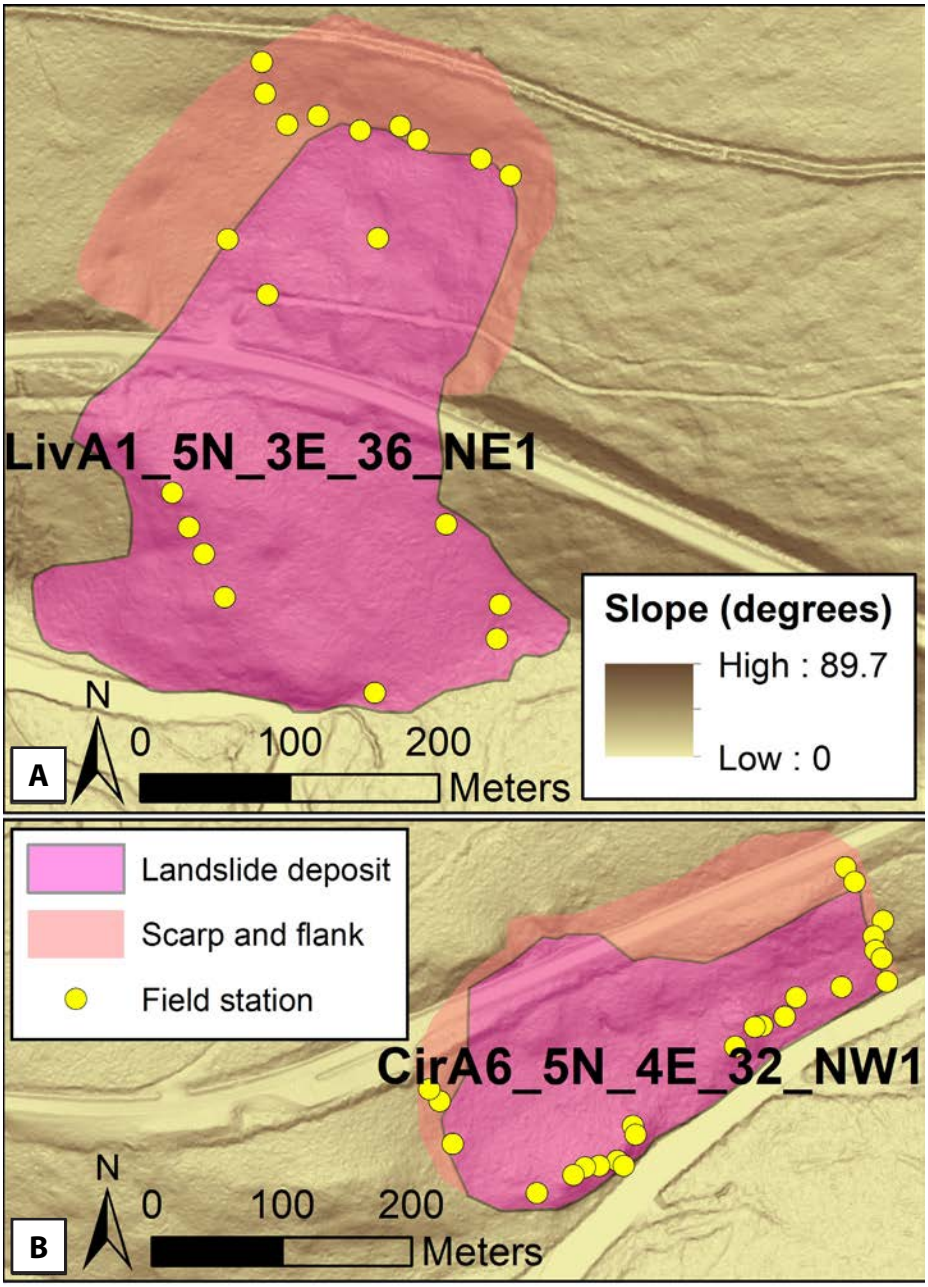

Figure B14. Mapped landslides and field stations from June 26, 2020. **A.** Bear LS (LivA1_5N_3E_36_NE1) and (**B**) Sampled LS (CirA6_5N_4E_32_NW1). The background is QL2 lidar-derived slope map (FNSB, 2020).

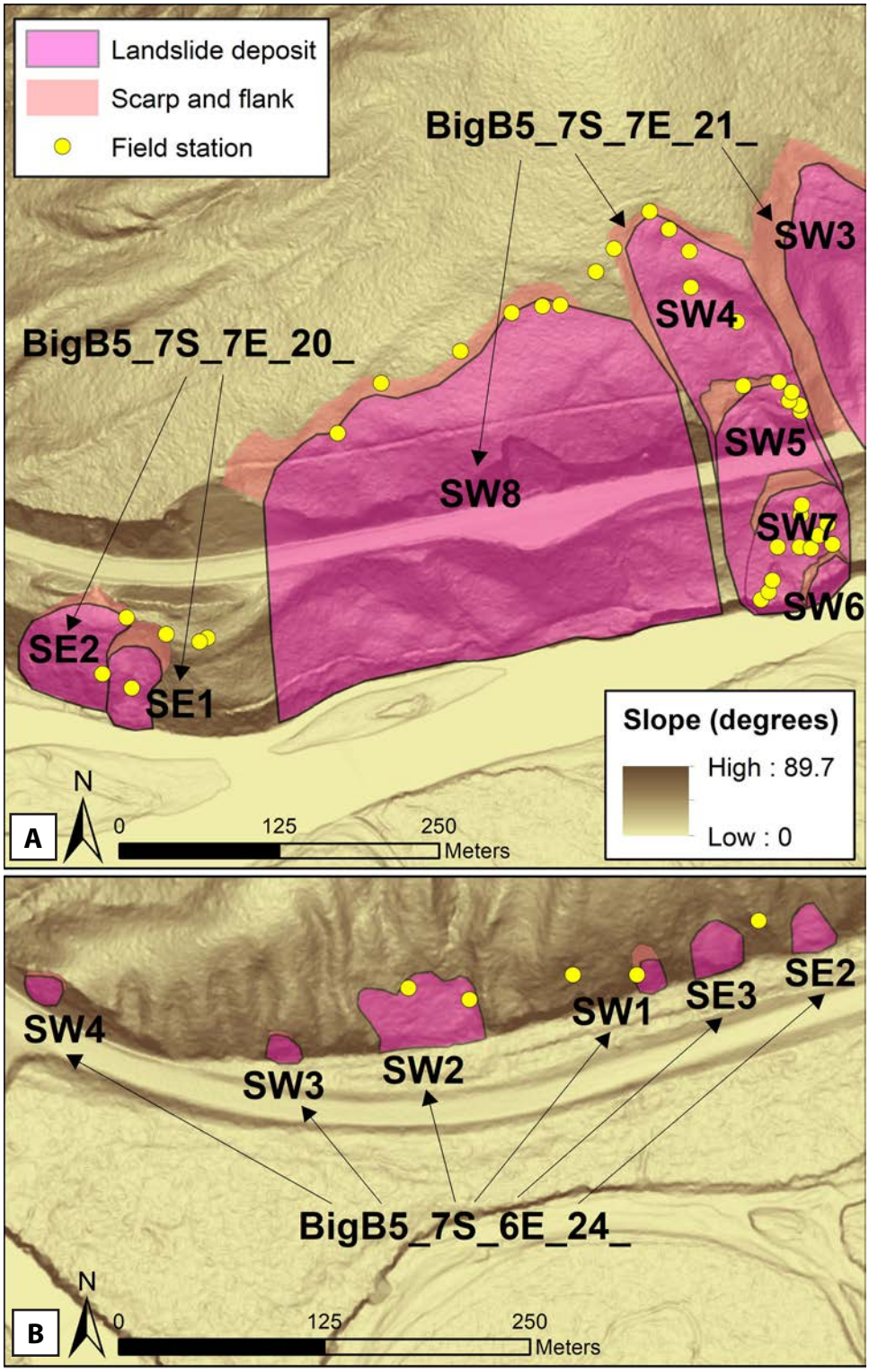

Figure B15. Mapped landslides and field stations from July 1, 2020. **A.** Landslide complexes and (**B**) small landslides along the Richardson Highway. The background is QL2 lidar-derived slope map (FNSB, 2020).

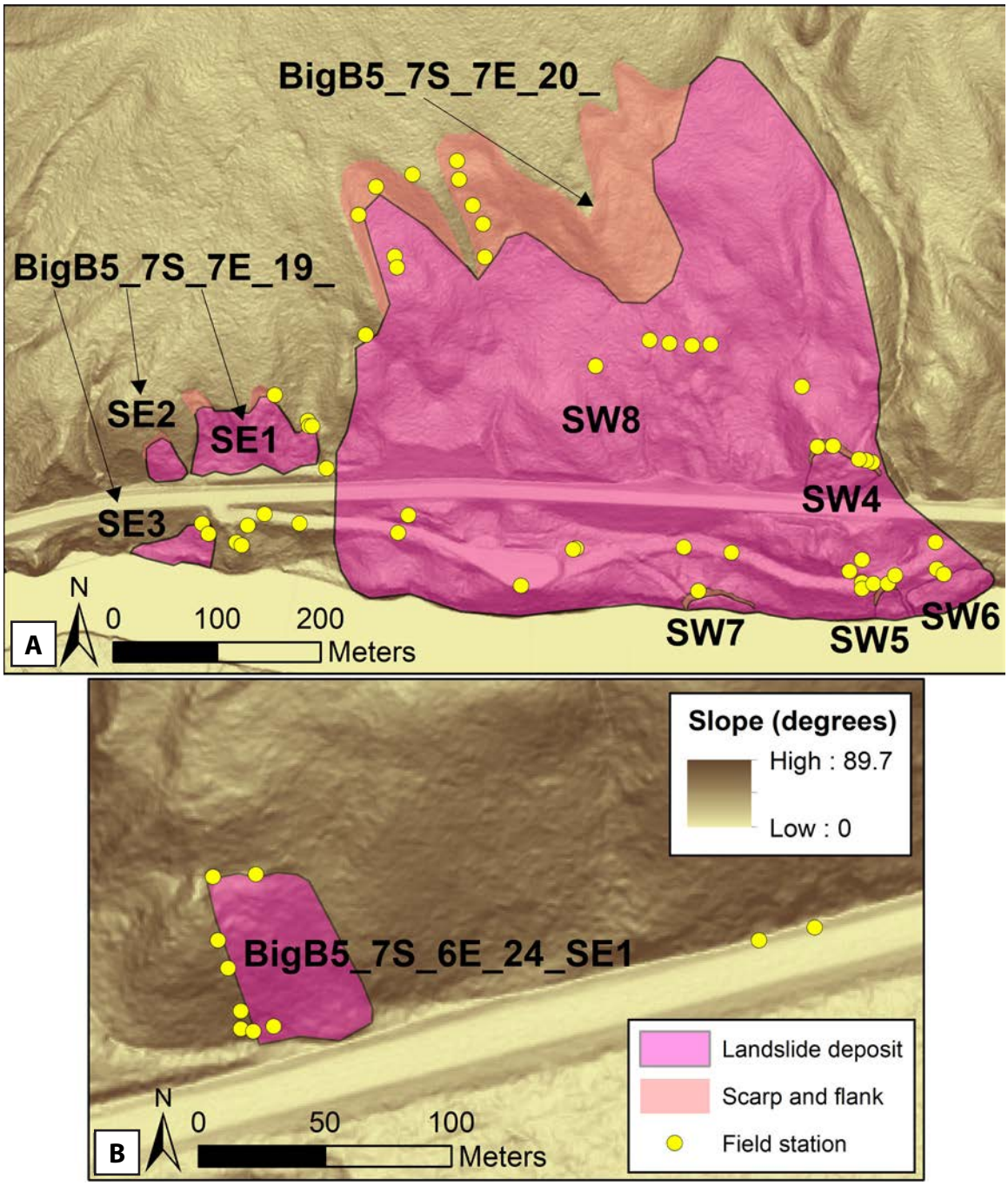

Figure B16. Mapped landslide deposits and field stations from July 2, 2020. **A.** Landslide complexes and (**B**) small landslide along the Richardson Highway. The background is QL2 lidar-derived slope map (FNSB, 2020).

APPENDIX C: TANANA 440 LANDSLIDE—BOREHOLE SAMPLES

Table C1. Samples collected and tests performed from the stratigraphy sites on the Tanana 440 landslide (refer to fig. 3 for locations). The "X" indicates that the test or analysis was completed for a given depth.

Borehole	Depth (m)	Sedimentation Analysis (Hydrometer)	Atterberg Limits	Direct Shear	Natural Moisture Content	Volumetric Moisture Content	Specific Gravity
STRAT2	1.90	X		X			
STRAT2	3.00			X	X		
STRAT2	3.80	X					X
STRAT3	2.75	X				X	
STRAT4	1.7			X	X		
STRAT4	2.3			X		X	
STRAT4	3.6	X	X	X	X		

Table C2. Collected samples and tests performed from test holes 1–4 on the Tanana 440 landslide (refer to fig. 3 for locations). The "X" indicates that the test or analysis was completed for a given depth.

Borehole	Depth (m)	Dry Sieve Analysis (Gradation)	Sedimentation Analysis (Hydrometer)	Atterberg Limits	Direct Shear	Natural Moisture Content	Radiocarbon Date	Specific Gravity
TH01	1.24					X		
TH01	2.40					X		
TH01	3.00						X	
TH01	3.60		X	X		X		
TH02	0.91					X		
TH02	0.91	X	X	X				X
TH02	2.95	X	X					
TH02	2.95					X		
TH02	3.34					X		
TH03	1.33		X			X		
TH03	1.33		X	X				
TH03	1.71				X			
TH03	2.55						X	
TH03	2.90					X		
TH03	3.37		X			X		
TH04	1.42					X		
TH04	2.33		X			X		
TH04	2.59						X	

Table C3. Collected samples and tests performed from test holes 5–8 on the Tanana 440 landslide (refer to fig. 3 for locations). The "X" indicates that the test or analysis was completed for a given depth. 1These two samples were combined into one sample for hydrometer analysis.

Borehole	Depth (m)	Sedimentation Analysis (Hydrometer)	Atterberg Limits	Natural Moisture Content	Radiocarbon Date	Specific Gravity
TH05	0.94	X				
TH05	2.18			X		
TH05	3.52			X		
TH05	3.52	X				X
TH06	1.01			X		
TH06	1.73	X	X			X
TH06	2.37				X	
TH06	3.06			X		
TH07	1.66	X[1]		X		
TH07	2.34		X			
TH07	3.34	X[1]		X		
TH08	1.11			X		
TH08	1.40	X				
TH08	1.65				X	
TH08	2.68	X				
TH08	3.43			X		

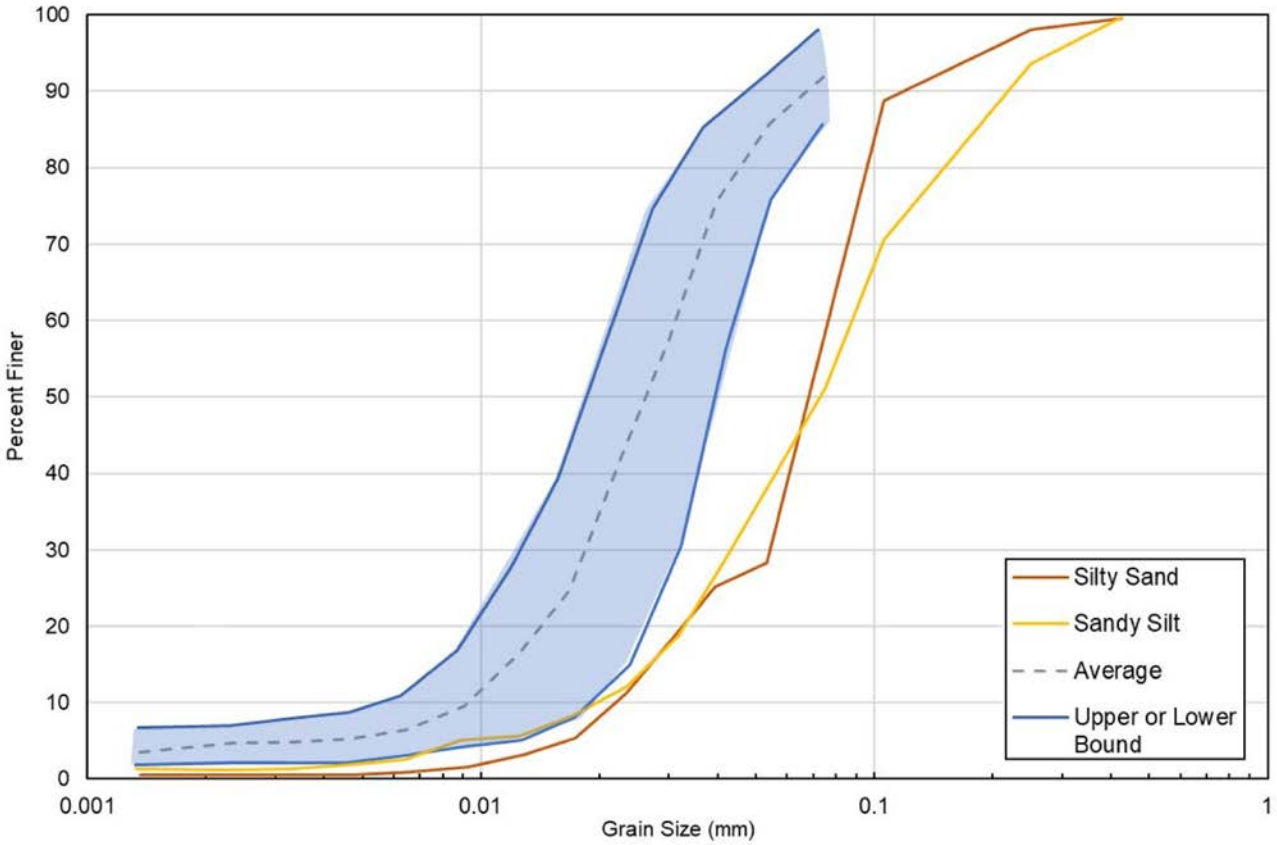

Figure C1. Particle size analysis of the T440 landslide samples. The blue lines indicate the upper and lower boundaries of the grain size distributions of all hydrometer-tested materials (N = 18), and the dotted gray line is the approximate average grain-size distribution within the shaded blue region. There was one discrete sample each of silty sand and sandy silt.